UNCLASSIFIED

AD. 263 440

Reproduced
by the

ARMED SERVICES TECHNICAL INFORMATION AGENCY
ARLINGTON HALL STATION
ARLINGTON 12, VIRGINIA

UNCLASSIFIED

DISCLAIMER NOTICE

THIS DOCUMENT IS BEST QUALITY PRACTICABLE. THE COPY FURNISHED TO DTIC CONTAINED A SIGNIFICANT NUMBER OF PAGES WHICH DO NOT REPRODUCE LEGIBLY.

NOTICE: When government or other drawings, specifications or other data are used for any purpose other than in connection with a definitely related government procurement operation, the U. S. Government thereby incurs no responsibility, nor any obligation whatsoever; and the fact that the Government may have formulated, furnished, or in any way supplied the said drawings, specifications, or other data is not to be regarded by implication or otherwise as in any manner licensing the holder or any other person or corporation, or conveying any rights or permission to manufacture, use or sell any patented invention that may in any way be related thereto.

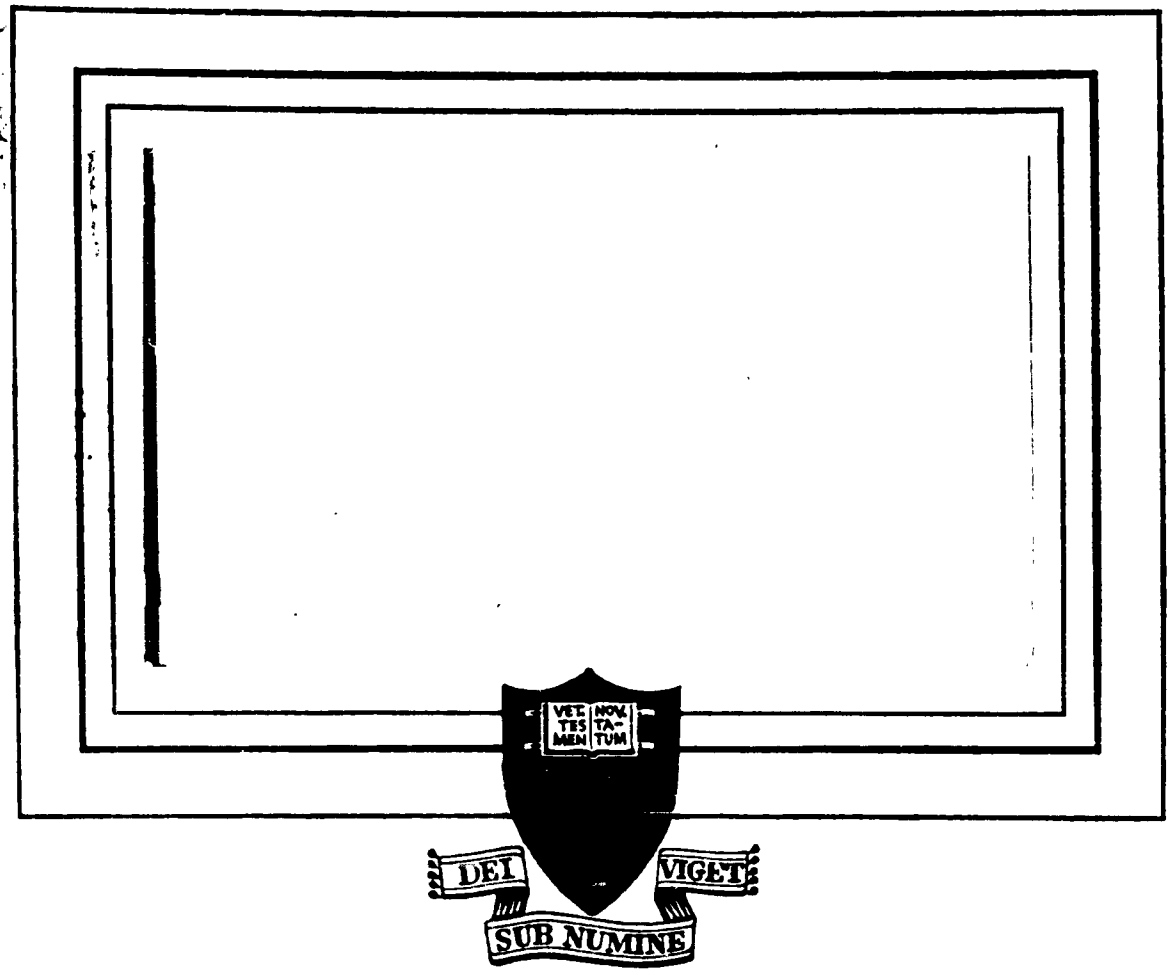

SEP 26 1961

PRINCETON UNIVERSITY

DEPARTMENT OF AERONAUTICAL ENGINEERING

AFOSR 1220

UNITED STATES AIR FORCE
AIR RESEARCH AND DEVELOPMENT COMMAND
AIR FORCE OFFICE OF SCIENTIFIC RESEARCH

A Technical Report on Contract USAF-OSR AF 49(638)-411

THE IGNITION MECHANISM OF COMPOSITE SOLID PROPELLANTS

Aeronautical Engineering Laboratory Report No. 557

Prepared by: Robert F. McAlevy, III
Robert F. McAlevy, III
Research Associate

Approved by: Martin Summerfield 6 KOH
Martin Summerfield
Professor of Jet Propulsion

This research was supported by the United States Air Force through the Air Force Office of Scientific Research of the Air Research and Development Command, under Contract USAF-OSR AF 49(638)-411. Reproduction in whole or in part is permitted for any purpose of the United States Government.

1 June 1961

Department of Aeronautical Engineering
Princeton University
Princeton, New Jersey

ACKNOWLEDGEMENTS

This dissertation was made possible by the assistance and encouragement of many people associated with the James Forrestal Research Center of Princeton University.

First and foremost, my sincere gratitude is extended to Professor Martin Summerfield who suggested the research and whose guidance and encouragement were invaluable to its successful completion.

Messrs. P. L. Cowan and L. H. Sentman were particularly helpful in the calibration of the shock tubes and development of the ignition detection devices employed during the program. Their effort is gratefully acknowledged.

Mr. E. R. Crosby assisted in the mechanical operation of the equipment and produced the fine photographs contained herein. His eager participation is deeply appreciated.

Many other members of the staff of the Jet Propulsion Research Program contributed their time and effort. Mr. Tony Poli and other members of the design group produced the necessary machine drawings of the experimental equipment and many of the illustrations appearing in this document. Miss Frances Allison and the secretarial staff typed the first draft of this manuscript. The author takes this opportunity to thank them all.

The final manuscript was typed by Miss Penny Phelps, a Secretary to the Aeronautical Engineering Department. Her special effort in this matter is gratefully appreciated.

Financial support of this program was provided by the Department of the Air Force, Combustion Dynamics Division (Contract AF 49 (638)-411).

ABSTRACT

This research deals with the investigation of the processes by which a solid propellant ignites. A shock tube technique was employed to experimentally produce ignition by supplying a well-defined surface heating to propellant test specimens. A new theory of ignition is presented which has proven to be successful in its quantitative predictions of the measured ignition time lags.

The designer of ignition systems for practical solid propellant rocket motors currently must perform his task without the fundamental knowledge of the mechanisms by which solid propellant ignition takes place. In lieu of this, he is forced to rely on grossly qualitative concepts such as an arbitrarily defined "ignitability factor", on which to base his design. The current basic research effort was initiated with the objective of revealing the essential nature of the solid propellant ignition process, thereby laying the foundation for the development of igniter design criteria. Of the various means by which the practical igniter can supply the required ignition energy to an exposed propellant surface, conduction from a hot gas was selected for detailed study.

Previous elementary studies of the solid propellant ignition process employed a full spectrum of surface heating techniques (e.g., from embedded hot wires, to exposure to a detonation wave). Most of these suffered from imprecisely defined heating exposure conditions. When rational correlations of these experimental data were attempted, they were based on various versions of a theory whose essential feature was that ignition occurred due to a chemical heat generation in the solid phase. However, a great body of evidence points to gas phase heat evolution as the controlling mechanism for the steady-state deflagration process of solid propellants. Since the transition from the solid phase heat release of the ignition process to the gas phase heat release of the steady-state process is obscure and, in particular, since there is no known mechanism by which significant solid phase heating can take place (especially for the composite type propellants of interest), a new formulation of the ignition problem was proposed, based on a gas phase chemical heating. Indications of the importance of a gas phase chemical reaction in the solid propellant ignition process can be found in the data produced by some of the previous elementary experiments. Generally, this takes the form of a measured decrease of the ignition time lag with increasing oxygen concentration of the ignition gas. The present work was centered on the study of this effect in the ignition of ammonium perchlorate composite propellants.

The shock tube was selected as the basic tool for this research since it can be used to produce a very well-controlled heating exposure of correctly mounted test specimens. Two different shock tubes were employed during the program. A large one, (6" I.D., 75' long) designed to produce a convective heating exposure of 5 milliseconds and a small one (1.6" I.D., 18' long) designed to be rapidly and cheaply operated. The latter was used to develop the necessary instrumentation and phototube ignition detection techniques as well as to investigate the previously mentioned effect of ignition time lag reduction with increasing chemical reactivity (oxygen concentration) of the surrounding atmosphere. All of the quantitative experiments, designed to verify the gas phase ignition theory reported herein, were executed by exposing small specimens of propellants to an instantaneous, controlled, heat input. This was accomplished by reflecting impinging shock waves from their exposed, flat, surfaces when they were mounted in the end wall of the small shock tube. As the igniting gas composition was vitiated with nitrogen the measured ignition time lags increased from a few hundred microseconds in a mixture of 100% O_2, 0% N_2, to 5 milliseconds (the useful testing duration of the small tube) in a mixture of 40% O_2, 60% N_2. Pure fuel specimens exhibited about the same ignition time lags as propellant formulations which incorporated the fuel material as a binder component. This evidence led to an ignition mechanism based on a gas phase heat release due to the reaction between the vaporized fuel component of the propellant and the oxygen component of the ignition gas.

The mathematical theory which was developed to describe the process depends on the determination of the site at which the heat produced by exothermic gas phase chemical reaction first overcomes the local heat loss. The interval between the commencement of the heating exposure and this instant was defined as the ignition time lag. Experimentally, the instant of ignition was defined by the instant of first detectible radiation from the incipient ignition flame, as measured by a scanning phototube. The theory predicted the data remarkably well considering the degree of uncertainty in the values of the chemical kinetic, thermodynamic and transport parameters employed in its evaluation.

This new understanding of the fundamental mechanisms by which a solid propellant ignites suggests improvements that can easily be incorporated into existing practical ignition systems and forms a rational basis for the design of future systems. The shock tube technique can be employed to investigate the ignition of other types of propellants currently being developed. The newly proposed gas phase ignition theory should be applicable to these results with little, if any, modification. A new shock tube technique for the study of chemical kinetics evolved from this work.

TABLE OF CONTENTS

LIST OF FIGURES

FIGURE

FIGURE

LIST OF TABLES

SYMBOLS AND NOTATIONS

A	Arrhenius Equation pre-exponential factor
C	Concentration - mass per unit volume
C_p	Heat capacity per unit mass at constant pressure
C_v	Heat capacity per unit mass at constant volume
D	Mass diffusivity
d	Diameter
E	Arrhenius Equation "activation energy"
e	Internal energy per unit mass
f	Arbitrary function
g	Arbitrary function
i	Direct current
K	Kinetic constant
M	Mach number
$\dot{m}$	Mass flow rate per unit area
P	Static pressure
Q	Heat generation rate per unit mass
q_f	Chemical heat release per unit mass of fuel
R	Universal gas constant
r	Electrical resistance
T	Temperature
t	Time
U	Velocity

V	Voltage
X	Distance
y	Arbitrary variable
Z	Weight fraction
α	Heat diffusivity
β	Coefficient of thermal resistivity
γ	Specific heat ratio
δ	Thickness
λ	Thermal conductivity
ν	Volumetric fraction of fuel component in composite solid propellant
π	Numerical constant (3.14159..)
ρ	Density - mass per unit volume
τ	Ignition time lag
ϕ	Dimensionless distance

SUBSCRIPTS

1,2,...5	Quasi-steady uniform states of basic shock tube flow
f	Fuel
g	Gas
ℓ	Lean Combustion limit
o	Oxygen
p	Propellant
s	Surface
w	Wall

SECTION I

INTRODUCTION

The current ascendency of solid propellant rockets for military applications is a direct consequence of their superior reliability compared to liquid propellant rockets of similar mission capabilities (Reference 1). Possibly the least reliable aspect of the operation of solid propellant rockets is that of the ignition process. For example, a mission failure could result if an uncontrolled ignition delay time introduced a trajectory discrepancy too large to be corrected by the missile's guidance system. Further, the role of solid propellants in near space probes might well be limited by the ignition system's precision and reliability under space conditions (Reference 2).

In general, a correctly designed ignition system should result in (1) reproducible ignition delays, (2) controlled chamber pressure history during ignition, (3) suitable ignition of aged propellants, (4) suitable ignition of propellants at both low and high temperatures, etc. Unfortunately, the only dependable knowledge available to guide design in this sensitive area is that a sustained heating of an exposed propellant surface produces ignition. Consequently, in the absence of any general formulae for designing ignition systems empirical approaches and past performance records of other igniters must necessarily be employed.

This approach has led to the evolution of the several systems currently employed (Reference 3). Typically, they consist of an integral package, installed at the head end of the loaded rocket, which produces a flame after receiving an electrical impulse. The flame is directed at the propellant grain surface and causes ignition in a small fraction of a second. Different igniters vary in the temperature and pressure level of the igniting gases they produce, concentration of condensable substances, chemical reactivity, etc. Therefore, it is possible for the exposed propellant surface to simultaneously receive energy by: (1) heat transfer by forced convection or simple conduction; (2) diffusion of condensable metallic vapors or of energetic radicals from the igniter flame to the cool propellant surface, a process actually joined to (1); (3) transport of heat by hot refractory particles that impinge on the surface and create local centers of ignition; (4) thermal radiation absorption; (5) photochemical absorption. The action of a practical igniter system is indeed complex.

Quantitative knowledge of the response of the exposed propellant surface to these stimuli has been unobtainable up to now. In order to arrive at a rough estimate of a propellant's relative susceptibility to an igniter, referred to as the propellant's "ignitability factor", some grossly qualitative techniques have been generated, even though this factor has never properly

been defined. Obviously, it is a utilitarian rather than scientific concept since it pertains not to the phenomena of ignition per se, but to some measure or value which characterizes the ignition of the propellant in such a way that this value might be used in other connections, such as the design of an igniter for a rocket. Of the several techniques employed, the most prevalent is the use of a small closed bomb containing a test sample of propellant and a measured quantity of specified igniter material. The "ignitability factor" is generally an assigned value based on the reciprocal of the weight of the igniter powder needed to reproducibly ignite the propellant test sample. Recently, to make this work more meaningful, an effort has been made to standardize on a particular piece of equipment and operating technique (Reference 4). It seems doubtful that results so obtained could materially improve the current state of the art of solid propellant igniter design. Certainly such a blind technique could not reveal the detailed mechanism by which a solid propellant ignites, but the acquisition of this very knowledge must necessarily precede the establishment of a scientific basis for igniter design.

In the past, the more fundamental approach to the ignition problem has generally been to consider the solid propellant as a substance capable of producing significant solid phase chemical heating. It was argued that, if the temperature of the solid could be raised to a certain level, then the solid phase heating would become sufficiently great to produce ignition. This physical model has been the basis of several fully developed mathematical analyses leading to the dependence of ignition lag on the physicochemical properties of the propellant and the heat exposure conditions. However, it seems improbable that a significant amount of heat release can occur by means of a solid phase chemical reaction. Therefore, this solid phase ignition theory was regarded at the outset of this research with some degree of suspicion, and an alternate theoretical approach is proposed herein which depends on a gas phase heat release mechanism. This question, solid phase vs. gas phase heat release, was at the heart of the present research.

On the experimental side, some basic ignition studies have previously been performed by subjecting the propellants to a single ignition stimulus. Usually, these elementary experiments consisted of varying the rate of energy input to an exposed propellant surface and measuring the interval (ignition delay time, ignition time lag, or ignition time) between the start of heating and the subsequent ignition (usually indicated by light evolution). In some cases environmental conditions such as ambient temperature, pressure, and chemical reactivity of the surrounding atmosphere were also varied. Generally, this interval has been found to decrease with increasing energy input rate, pressure, and reactivity of the surrounding atmosphere. Most efforts have suffered from imprecisely defined exposure conditions and/or instant of ignition. Those which do not produce ignition within a small fraction of a second are not of practical interest.

The following examples are presented to illustrate the great variety of techniques employed in these more basic studies. One experimental approach (Reference 5) was to employ an electrically heated wire as the ignition source. By virtue of the well defined boundary condition, the experimental results could be correlated by a mathematical solution to the linear heat diffusion equation incorporating the notion of "ignition temperature". In this work no effort was made to vary the temperature, pressure, or chemical reactivity of the surrounding atmosphere (air). For the ammonium perchorate oxidized composite propellant examined, the "ignition temperature" was found to be about 390°C over the range of testing times (1 to 20 seconds) observed. Another, used to study the ignition of homogeneous nitrocellulose-type propellants initially at room temperature in a flowing stream of hot gas (up to 1000°K) at atmospheric pressures, produced slightly reduced ignition times (lowest was 100 msec) (Reference 6). The experimental boundary conditions were rather poorly defined so that it was necessary to rely on dimensional analysis to determine that the product of a heat transfer term and chemical reaction term sufficiently described the ignition time decrease with increasing temperature and heat transfer rate. A mild decrease of ignition time with increasing oxygen concentration was noted. A more precisely controlled exposure situation is possible by employing radiant energy as the ignition stimulus (Reference 7). A rapid shuttering system permitted, within a few msec after triggering, the constant heating of an exposed propellant surface over a range of selected initial temperatures and atmospheric pressures. The presence of oxygen in the surrounding atmosphere was found to reduce the measured ignition times (Reference 8), which for high energy fluxes, were as short as a few msec.

Hydrodynamic techniques produce a heating exposure which can be triggered in less than 1 μ sec. This provides an excellent control of the temporal boundary condition (or initial condition). In a "shot tube" technique (Reference 9) the heating was due to the hot (up to 4000°K), high-pressure (up to 10,000 psi) gases generated at the propellant surface by the arrival of a hydrogen-oxygen detonation wave. Although the heating was rapidly initiated it was not well defined. Also, the detonation wave luminosity obliterated that of the incipient ignition flame with the result that the ignition times were obtained with poor accuracy. They were calculated by the devious means of measuring, from the start of heating, the total time required for the igniting propellant surface to burn a measured distance, and then subtracting the estimated steady-state propellant burning time for this distance. However, even by this crude technique, it was still possible to observe a decreased ignition time when excess oxygen was present in the detonated gas.

Recently, a "shock tube" technique has been developed which has proven to be a most useful tool for solid propellant ignition research (References 10, 11, 11a, 12). It also generates hot gas at the propellant

surface within a fraction of a μ sec. Here, however, the heating gas is produced by an aerodynamic compression to a precisely controlled, constant level of temperature (up to a few thousand ^{o}K) and pressure (1000 psi or more, depending on tube strength). When the aerodynamic shock wave is reflected from the end wall of the shock tube it is possible to allow the doubly compressed gas to flow at a pre-selected velocity to produce (for periods up to 50 msec) controlled convective heating of a propellant sample positioned in the flow (Reference 11, 11a). Using this technique, numerous experiments were performed on several composite propellants over a wide range of exposure conditions. The experimental ignition time lags could be correlated by a semi-theoretical method based on the surface temperature of the solid surface being heated to an "ignition temperature" (about $600^{o}K$) at which time a solid phase heat generation rapidly carries the propellant to full scale burning. Although the presence of oxygen in the heating gas resulted in an order of magnitude decrease of the ignition time, it was impossible for this effect to be explained within the framework of a method depending on solid phase reaction only. Further, this entire theoretical approach to the ignition problem was originally developed for a double-base-type propellant (Reference 13), which might be capable of significant solid phase heat generation (Reference 14), but is, in general, inappropriate for the composite type which is not (Reference 15).

Two different shock tubes were employed during the present program. One, designed to produce ignition by convectively heating a propellant sample during the short duration (5 msec) flow (2000 ft/sec) of hot ($800^{o}K$), high pressure (150 psi), shocked gas following the incident shock wave was, necessarily, quite large (6 in. I.D., 75' long). The other, used to produce a conductive heating of a propellant sample mounted in the end wall of the shock tube from the very hot ($1400^{o}K$), high pressure (750 psi), stagnant gas behind the reflected shock wave could be much smaller and was therefore more simply and rapidly operated. Instrumentation necessary to measure the precise heating exposure and to detect the instant of ignition (by measuring the radiation from the incipient ignition flame) was developed on the small tube.

Even without instrumentation, the small shock tube was used to produce valuable qualitative information about propellant ignitability. The effect of chemical reactivity on ignitability was also studied in this way.

The instrumented shock tube produced quantitative ignition data which could be correlated on the basis of a new theory of composite solid propellant ignition. The theory focusses attention on the gas phase nature of the ignition reaction, and consequently can explain the effect of chemical reactivity of the surrounding atmosphere on the ignition time, a phenomenon which has been so vexing to previous investigators. It also explains the apparent dependence of "ignition temperature" on exposure conditions (e.g., exposure to conductive heating in the shock tube produces ignition with a surface temperature of $425^{o}K$ or so. This is about $200^{o}C$ below any

value previously reported in the literature). It explains the observed nature of the propellant ignitability threshold exposure conditions in the shock tube.

A new concept of propellant ignitability can be evolved from this. Also, a means of improving practical igniters, enhancing the ignitability of propellants, and establishing scientific design criterion for ignition systems are suggested on the basis of the new understanding of the solid propellant ignition mechanism evolved during the present fundamental study.

SECTION II

SHOCK TUBE PERFORMANCE

1. Introduction

The shock tube is a device which generates gas flows for very short periods of time. It was first employed by Vieille in France (Reference 50) at the end of the last century, but then neglected for a period of 40 years until resurrected for a study of the flow process by Payman and Shepherd in England (Reference 51),and calibration of crystal pressure gauges by Professor Bleakney and his associates at Princeton University (Reference 52). The latter also used it for the study of the shock reflection process and other fluid dynamic phenomena (References 53, 70). Lately, the tool has been used in a seemingly unending variety of studies. These include the driving of intermittent wind tunnels, the study of wave phenomena, shock loading of structures, relaxation and imperfect gas phenomena, chemical reaction kinetics studies of very fast reactions, combustion and flame propagation, condensation effects, unsteady boundary layer studies, dissociation, ionization, electrical conductivity, radiation, heat transfer, spectra, magneto-hydrodynamic studies, and many others. This research has led to the publication of a great volume of literature, but since most of it does not directly apply to the present study, only a few recent review articles are cited (References 54-57) as background literature. Recently, it has proven to be a useful tool for solid propellant ignition research (References 10, 11, 11a, 12). The principles of simple shock tube operation necessary to understand its application to this rather limited task are described below.

The simple shock tube consists of two constant area sections of pipe separated by a burst diaphragm (Figure 1). Generally the test section is filled with a test gas at or below atmospheric pressure (P_1) and the other is pressurized with a driving (or working) gas to a predetermined level (P_4). When the driving gas pressure exceeds the failure pressure of the burst diaphragm it rapidly ruptures (1/10 msec), and the high pressure driving gas rushes into the test section, compressing and producing a shock wave in the test gas, while a rarefaction wave propagates into the driving gas. Actually the shock wave is not fully developed until it reaches a point about 10 diameters from the diaphragm section (Reference 57), but to facilitate theoretical description both the shock wave and a centered rarefaction fan are usually assumed fully established immediately after the diaphragm ruptures.

The flow situation produced in a shock tube during its operation has classically been represented by means of a "wave diagram". This is a

diagram whose abscissa represents the distance along the length of the shock tube while the ordinate is time following rupture of the diaphragm. Therefore, wave phenomena of constant propagation velocity are represented by straight lines on such a plot (Figure 2). For example, the line separating the unshocked (region 1) and shocked (region 2) gas is identified as the initial shock wave, S. Similarly, the dot-dash lines separating regions (3) and (4) represent the expansion fan of the centered rarefaction wave, the head of the wave is designated by R, the foot by F. The dashed line separating the shocked test gas (2) and fully expanded driving gas (3) is defined as the contact surface, (the interface between expanded driving gas and shocked test gas which supports no pressure or velocity discontinuity). When the initial shock wave reaches the end of the tube it reflects and propagates back up the tube, re-compressing the once compressed gas of region (2) to a still higher level of temperature and pressure, region (5). Ideally, all of these numbered regions are of a quasi-steady uniform state.

The pressure profiles drawn above the "wave diagram" depict the state of the gas within the tube at three successive times. Before the diaphragm is ruptured ($t = 0$), it supports a large pressure difference. Following its rupture ($t = t_1$), the shock wave produces a step increase of test gas pressure and temperature while impulsively imparting to it a certain velocity; the high pressure driving gas expands through the rarefaction wave to match this pressure and velocity condition at the contact surface. Eventually, at ($t = t_2$), the initial shock runs into the end of the tube and the onrushing shocked gas "piles up" against the end wall. This results in another sharp compression by means of a reflected shock wave which propagates back upstream. At still later times, more complicated interactions between the reflected shock waves, contact surface, rarefaction wave, etc., will take place. The theory governing these events is well established (58 and 59), and provides a useful guide for the design of a particular shock tube to perform a given experimental task (Reference 60).

2. The Ideal Shock Tube

When the shock tube gases are assumed ideal and perfect, with constant specific heat values, it is possible to obtain an algebraic relationship between the initial pressure ratio across the diaphragm (P_4/P_1) and the flow quantities in the two sections after the diaphragm ruptures (References 58-65). This results from matching the velocities, $U_2 = U_3$, and pressures, $P_2 = P_3$, at the contact surface; the state of region (3) is given by an isentropic expansion from condition (4) and that of region (2) can be computed from the conditions in region (1) by the Rankine - Hugoniot shock wave relations. The resulting equation, relating the diaphragm pressure ratio (P_4/P_1)

to the pressure ratio across the shock wave (P_2/P_1), as developed in Reference 65, where it is referred to as equation 1.66, is

$$\frac{P_1}{P_4} = \frac{P_1}{P_2}\left[1 - \left(\frac{P_2}{P_1} - 1\right)\sqrt{\frac{\left(\frac{\gamma_4 - 1}{2\gamma_4}\right)\frac{c_1}{c_4}}{\left(\frac{\gamma_1 + 1}{\gamma_1 - 1}\right)\frac{P_2}{P_1} + 1}}\right]^{\frac{2\gamma_4}{\gamma_4 - 1}}$$

This relation suggests that for a fixed level (P_4/P_1) an increase of shock strength (P_2/P_1) is possible if the internal energy per unit mass of the driving gas is greater than that of the driven gas. Since $e = C_vT$ and it would be both expensive and complicated to create a temperature difference across the diaphragm, then gases with favorable values of specific heat per unit mass must be employed to extract this advantage. In the present work the test gas is generally a mixture of oxygen and nitrogen, $C_v = 0.172$ (cal/gm^oC), so a very light driving gas is required if this gain is to be achieved. Unfortunately, if the lightest gas, hydrogen, $C_v = 2.42$ (cal/gm^oC), were employed, a detonation might occur at the contact surface where it is in contact with the oxygen of the test gas. Therefore, helium, $C_v = 0.746$ (cal/gm^oC) was selected as the standard driving gas and was used exclusively in the present study. Figure 13 is a plot of the above expression (re-plots of Figures 18 and 19 of Reference 64) and clearly shows the advantage of using helium as the driving gas.

These and other theoretical results are so completely covered in the literature, that rather than re-copying or re-deriving well known relations, the author will simply reproduce those which are pertinent, as necessary. The vast majority of shock tube work has employed air as the test gas and the experimental results have verified the theory very well for this gas. Further, the results for oxygen and nitrogen, when used as a testing gas, are almost identical for shock waves below a Mach number of about 6 (Reference 71) due to their similar molecular structure. Therefore, the published results for air will be assumed valid for the other mixtures of oxygen and nitrogen as well (i.e., the test gas mixtures employed in the present work).

3. The Real Shock Tube

For shock waves traveling at velocities greater than a $M_S \cong 2$, the specific heats of the gases become temperature dependent and the simple algebraic relations between the parameters, which were developed on the basis of constant specific heats, are no longer valid. More complicated iterative, numerical methods must then be employed.

The fundamental work in this area was performed by Bethe and Teller (Reference 66) and has undergone considerable development since then (References 64, 67, 69). The many different numerical approaches have been reviewed, with the presentation of considerable data, in References 54, 68, and 69. Table 2 (taken from Table 4, Reference 64) lists the flow quantities on the high pressure side of shock waves in air computed for temperature dependent specific heats.

When the initial shock wave reaches the end wall and reflects from it, the conditions behind the reflected wave can be determined simply by applying the boundary condition of zero particle velocity in state (5) and rewriting the shock wave relations in the reflected shock wave coordinate system (Galilean transformation). Temperature-dependent specific heats necessitate numerical iterative procedures for realistic determination of the reflected shock parameters for $M_s \cong 1.5$, or so, since the temperatures behind the reflected shock are higher than those behind the incident shock wave. Figure 4 shows the variation of flow parameters in air behind a normal reflected shock wave with the incident shock wave Mach number for variable specific heat as presented in Reference 54, Figure 36.

Above $M_s \cong 5$ the effects of dissociation and then ionization become important and must be accounted for in the calculation of shock conditions. The techniques for doing this are well established (References 71-74) and Reference 74 has a particularly useful set of graphs showing the results of such calculations. However, it has been found that the shock tube operating conditions required to ignite solid composite propellants (Section IV) lie in a regime where dissociation and ionization are unimportant, but where temperature-dependent specific heats must be considered. Therefore, Figure 4 and Table I are sufficient to predict theoretically the propellant exposure conditions, throughout the range of operation, which are capable of producing ignition in the present shock tubes.

4. Experimental Comparison of the Performance of the Real Shock Tube with the Ideal

The small shock tube was calibrated so that the actual exposure conditions of the quantitative ignition experiments (Section VI) could be exactly determined. The calibration consisted of the measurement of the propagation velocity of the generated initial shock wave and the pressure behind the reflected shock wave for a range of diaphragm pressure ratios, P_4/P_1, using helium as the driving gas and air as the test gas.

Figure 5 is a picture of the small (1.6" I.D.) shock tube. The 10' long driving section in the foreground is partially hidden by the control panel. The diaphragm holding flanges, the 8' test section, and electronic instrumentation are clearly visible in the background. To operate the tube, after the diaphragm has been inserted, the pressure in the test section, P_1, is drawn down to a predetermined level by means of a vacuum pump and measured by a mercury monometer; then the driving section is charged with helium until the diaphragm fails. The diaphragm burst pressure is measured by means of an 8" dial gauge and recorded as P_4.

Successful shock tube operation depends on obtaining suitable burst diaphragms. Unfortunately, very little data on diaphragm characteristics has been reported. Most of the pertinent information available has been gathered and reviewed in Reference 55, but it is insufficient for exact design purposes. Therefore, it is necessary to undertake a diaphragm development program in conjunction with each new shock tube which is built.

Ideally, the rupture should take place instantaneously, with the diaphragm splitting cleanly, without splinters or metal particles, and with the petals folding back against the tube wall so as not to obstruct the flow. Too long an opening time and flow constriction at the diaphragm section inhibit the formation of the generated shock wave, and therefore the full shock strength capabilities from the pressure ratio initially across the diaphragm are not realized. Also, if pieces of diaphragm are torn loose during a solid propellant ignition test, there is a possibility that ignition might be prematurely triggered by a hot diaphragm particle impinging on the test sample. Finally, a reproducible rupture of the diaphragm will allow the operating condition of the tube, and therefore, the propellant exposure condition to be readily and accurately pre-selected; thus, it is desirable.

It was decided to develop a diaphragm which would allow a precise rupture without initial scoring, and further, would not require an intricate rupturing mechanism (e.g., piercing by a sharp tool, spark discharge, etc.). Commercially available safety discs were evaluated first but proved unsuccessful for a number of reasons and were eventually abandoned. Finally, by machining a carefully rounded corner (1/4"R) on the downstream diaphragm holding flange, it was found that very soft aluminum makes an excellent diaphragm material and at 1/10 the price of the unsatisfactory, commercially available product. The details of the development program are presented in Reference 30.

By assuming that the diaphragm distorts to approximately a hemispherical shape as the burst pressure is approached, and applying the results

of stress analysis of a spherical shell smoothly supported at the rim, it was possible to obtain the following relationship which correlated the experimental data quite well.

$$P_4 = 4 \frac{\delta}{d} S_{ult}$$

where: P_4 is the burst pressure
d is the tube diameter
δ is the diaphragm thickness
S_{ult} is the ultimate tensile strength

Figure 6 is a plot of this relation and the values actually determined are also indicated. The harder aluminum (3003-H14, S_{ult} = 21,500 psi) exhibited a higher burst pressure for a given diaphragm thickness than the more ductile (3003-0, S_{ult} = 16,000 psi). The standard deviation is remarkably small and found to range from 10 to 20 psi (when P_4 varied between 600 and 1,1000 psi) for a given nominal thickness of commercially available aluminum sheet. No material was lost from the diaphragm due to rupture and a consistent petal formation pattern was always in evidence. Attesting to the reproducibility of the rupture process is the fact that during the velocity calibration the quantities affecting shock strength formation (e.g., burst pressure, diaphragm opening time, constriction, etc.) did not vary enough to cause more than a 3% change (the limit of resolution of the experiment) of measured shock velocity in the several calibration runs made for each diaphragm thickness and material, as described below.

The shock strength calibration was conducted by measuring the time necessary for the initial shock wave to propagate a known distance. The measurement was made at the very end of the shock tube where the propellant ignition test samples are mounted so that the actual propellant exposure conditions would be accurately known. Thin film heat gauges were used to sense the instant of shock wave passage. The amplified outputs of these gauges were also used to trigger various electronic devices employed during the program.

The thin film heat gauge has found wide application in the measurement of transient heating phenomena (References 82-86). The temperature sensitive platinum film is usually made quite thin (1/10 micron) to reduce "thermal inertia" so that its instantaneous temperature is essentially the surface temperature of the glass backing material and the characteristic response time (time necessary to reach 94% final value) will be about 1/30 microsecond (Reference 84).

In the present work the thin film was formed by painting the surface of a pyrex (type 7740 borosilicate) element with a suspension of platinum

IN THIS DOCUMENT WAS OF POOR QUALITY. BEST POSSIBLE REPRODUCTION FROM COPY FURNISHED ASTIA.

in an organic liquid (Hanovia Liquid Bright Platinum, Hanovia Chemical and Manufacturing Company, Newark, New Jersey), and baking the element at a temperature close to the pyrex softening temperature (to drive off the organic component and leave behind a metallic platinum film bonded to the pyrex).

The element is then placed into a carefully machined slot in a Kel-F housing plug and the ends of the film are soft soldered to brass screws which run through the plug and act as electrical lead-ins. Since the shock tube has a curved wall, the glass elements are cut from pyrex tubing of the same I.D. as the shock tube. The end surface of the plug is also machined to this radius so that the guage will conform to the shape of the tube and not disturb the gas flow when mounted in the side wall. A completely assembled heat transfer gauge is shown in Figure 7.

The body of the Kel-F gauge housing plug is machined to be compatible with one of the identical multi-purpose instrumentation housing ports located at nine positions along the shock tube. When correctly adapted to these standard housings, pressure gauges, observation windows, etc., can then be mounted at any of these positions. Also, it is through these access ports that the tube is evacuated or pressurized and pressure levels are measured. Figure 7a is a scale drawing of one of these, showing a heat gauge mounted in position.

As the shock wave passes over one of these heat transfer gauges, the flowing, shocked gas impulsively heats the gauge (as it does the rest of the wall) in a way which causes the heat transfer rate to vary as the inverse square root of time (Reference 85). This produces a step increase of the film temperature, causing a jump in its level of electrical resistance. When a constant current of 12 milliamperes is flowing through a platinum element of 50 ohms initial resistance, the jump of resistance level typically produced by normal shock tube operation results in a small (10 millivolt) step voltage rise across the element. This signal gives a very precise indication of the arrival of the shock wave.

The time interval between voltage pulses was measured with 1 microsecond accuracy by means of a Hewlett Packard Model 523B Electronic Interval Counter. It was found necessary to amplify the small output voltages from the thin film gauges by a factor of 1,000, by means of high frequency (10 mc.) amplifiers, in order to bring the voltages to a level sufficient to actuate the counter (5 volts). The accuracy of the time interval measurement was checked for each run by simultaneously displaying the unamplified gauge outputs on a Textronix type 531 oscilloscope with a 53/54 plug-in preamplifier and photographing the trace with a DuMont type 2620 oscilloscope camera. The interval between pulses recorded in this way agreed to within 3% (the calibrated scope's accuracy) of the time measured by the time interval meter.

A schematic representation of the instrumentation system is shown in Figure 8. A total of three thin film heat gauges were employed during a shock velocity calibration run. The upstream gauge first sensed the oncoming shock wave and its amplified output was used to trigger the oscilloscope. The second gauge, whose amplified output signals the time interval meter to commence counting, was located downstream about 3 inches. The third gauge, which signals the time interval meter to cease counting, was located 3 inches further downstream. The unamplified outputs of each of the last two gauges were fed directly into the scope, while the amplified outputs were fed to the time interval meter.

The measured shock velocities, reduced to Mach numbers, were plotted against the ratio of helium pressure in the pressure chamber to air pressure in the test section, which existed across the diaphragm at rupture. (Figure 9). Also shown is the theoretical curve based on instantaneous and perfect opening of the diaphragm and frictionless fluid flow, but taking into account variable specific heats and dissociation (re-plot of Figure 24, Reference 65). All experimental points are based on measurements of time intervals which did not vary by more than 1 microsecond, the limit of resolution of the counter. At least seven runs were made at each operating point. Deviation from the theoretical curve is seen to increase with increasing shock strength. This was caused by wall friction and turbulent mixing at the contact surface, which increase in severity with diaphragm pressure ratio. The small run-to-run fluctuations in diaphragm burst pressure as indicated in Figure 6, and diaphragm rupture times were apparently too small to produce a measurable variation of the shock strength. This was a result of the excellent performance of the pressure ruptured soft aluminum diaphragms employed.

The pressure history behind the reflected shock wave was measured over a range of incident shock wave velocities ($2 > M_s > 5$). The Rankine-Hugoniot shock wave relations successfully predict the pressure level immediately following reflection of the incident shock wave. However, as the reflected shock wave begins to propagate back up the tube, it overtakes a nonuniform (due to attenuation) slug of once-shocked test gas, the contact surface, expansion wave, etc., and its interactions with these produce reflected waves which propagate back to the end wall to produce pressure fluctuations. Consequently, the pressure history at the end wall is very difficult to predict theoretically. Therefore, in order to know the test gas pressure during an ignition run, it had to be experimentally determined.

It is most desirable to conduct the ignition testing at a constant test gas pressure level. This situation can be realized only if the reflected

shock wave passes through the contact surface smoothly, without creating a reflected wave. Both the driving and test gases must finally be brought to equal pressure and velocities by the passage of the reflected shock wave for this to occur. A wave diagram for the condition of nonreflection at the contact surface is shown in Figure 10.

By imposing this matching condition on the shock tube equations, it is possible to calculate, for any reflected shock in a testing gas, the initial temperature and pressure of driving gas necessary to produce the condition of nonreflection at the contact surface (References 86, 87, 88). It can be demonstrated that when both gases are initially at room temperature (as in the present work), then for a given testing gas there is a unique relation between the desired shock Mach number and the composition of the driving gas which will produce this condition. In particular, if the driving gas is helium and the testing gas is air, then there is only one diaphragm pressure ratio (i.e., M_S) which satisfies the relation. For constant specific heats this is calculated to be $M_S = 3.8$ (Reference 88) is obtained. The complete theoretical development of Reference 87 indicates that the nonreflecting condition is quite insensitive to the actual M_S value as long as it is near the critical value.

The experimental results of Reference 87 indicate that the critical condition occurs at $M_S = 3.4$ on the basis of optical observations of the wave interaction patterns. However, actual measurement of the pressure histories (Reference 88) demonstrated that the contact surface was effectively nonreflecting over the entire range tested ($3.4 < M_S < 4.2$). Pressure histories obtained during the present program indicate this to be true down to $M_S \cong 3.0$, which verifies the theoretical result of Reference 88.

Experimental pressure histories of the shock reflection process were obtained by means of a pressure gauge mounted in an instrumentation port located 2.5 inches from the end wall. The pressure was sensed by a fast response (5 μ sec) quartz crystal piezo-electric shock tube pressure gauge (type PZ-6-S, Kistler Instrument Corporation, North Tonawanda, New York). The output signal from this gauge was amplified by a Kistler PC-6 Amplifier-Calibrator and displayed on a Tektronix 531 oscilloscope. In addition, a type 1P39 vacuum phototube was mounted to peer through a quartz window located directly opposite the pressure pickup. By employing the Tektronix 53/54 dual beam plug-in preamplifier it was possible to simultaneously display both the pressure and luminosity histories for each test (Figure 11). The radiation produced by the shock reflection process was measured so that it might be possible to later separate it from the incipient ignition flame radiation during an ignition run. (This turned out to be unnecessary as indicated in Section V).

Two distinct types of pressure histories, depending on whether the Mach number of the generated shock wave was greater or less than that required for nonreflection at the interface, were observed. Each type became more accentuated as the tube was operated at conditions farther removed from the nonreflecting condition. At Mach numbers less than the critical value, the shock wave would be somewhat absorbed as it was refracted at the interface, a situation resulting in reflected rarefaction waves which decreased the end wall pressure. On the other hand, stronger-than-critical level shock waves would be amplified when refracted at the interface, and compression waves would be reflected, producing a gradual pressure rise. The left hand trace of Figure 12 illustrates the former condition ($M_S = 2.7 < 3.4$) while the other shows the latter ($M_S = 4.76 > 3.4$). At $M_S = 3.4$ the pressure trace seemed most level.

The propagation of the reflected wave through the nonuniform test gas produced a gradual pressure rise for operation below $M_S = 4$. This was terminated by arrival of the interface reflected wave system. The net effect was a pressure peak of level P_5^*, which is slightly above the Rankine-Hugoniot value, a few hundred microseconds after reflection. Finally, there was a period of constant pressure. Above $M_S = 4$ this peaking was not in evidence and there was only a continuous pressure rise from the Rankine-Hugoniot value to the final constant "equilibrium" pressure level. The "equilibrium" pressure level, P_5, persisted until arrival of the reflected rarefaction wave which produced a sharp drop in pressure level (about 5 milliseconds following shock reflection in the small tube when $M_S \cong 3$). Shock tube operation between $3.0 < M_S < 4.0$ resulted in values of P_5 and P_5^*, which did not differ by more than 10%, at $M_S = 3.4$ they were equal. These criteria were used to determine respectively, the nonreflecting interface range of operation and the exact value at which it occurs.

Figure 13 is a plot of the experimentally determined pressure ratios P_5/P_1 and P_5^*/P_1 as well as the Rankine-Hugoniot values, against incident shock Mach number. It may be noticed that the value of the "equilibrium" pressure ratio does not follow the Rankine-Hugoniot value. This demonstrates that it is a phenomenon which is not governed by the shock reflection process, but is a peculiarity of shock tube operation. Its nature is at present little understood, but actively being investigated (Reference 89) as a means of better controlling the operation of the hypersonic shock tunnel.

A curious aspect of the equilibrium pressure is that it always reaches a constant level which is a certain fraction of the driving gas pressure level; Figure 14 demonstrates this experimental fact. Here, the ratio of equilibrium pressure, P_5, to helium driving gas pressure, P_4, is plotted against the

incident shock M_S, for various P_4 values. The solid curve represents values predicted on the basis of ideal shock tube operation; the dashed curve is calculated using the Rankine-Hugoniot relations and experimentally determined P_4/P_1 (M_S) values (Figure 9); the dash-dot curve characterizes the actual operation. The ratio is found to be remarkably constant at about 0.75. Others have observed this effect although different ratios were reported: 0.80 (Reference 89), 0.92 (Reference 11). The value seems to depend on the geometry of the tube, wall roughness, etc., and must be determined for each individual shock tube.

The surface temperature of the end wall was measured during the process of shock reflection. This quantity exhibits a step increase at the moment of reflection (Appendix A) and a thermometer capable of a very rapid response is necessary to sense the change. Therefore, a calibrated thin film resistance thermometer of the type employed to indicate the instant of shock passage was used to make the measurement.

It was mounted in a flange which was used as the small tube's end wall, so that its surface would be flush with the end wall surface. That is, the surface of the gauge was flat, whereas previously, when mounted in the side wall, it was curved. (See above.) Therefore, there were no protrusions to disrupt the normal shock reflection process, and the heating of the integral surface was by pure conduction from the stagnated test gas column behind the reflected shock wave.

The electrical resistance of the platinum element, r, at a given temperature, T, can be related to its resistance, r_o, at some initial temperature, T_o, by,

$$r = r_o + r_o \beta (T - T_o)$$

where β is the coefficient of thermal resistivity of the platinum film. When a constant current, i_o, is passed through the element, a change of temperature results in a voltage change across the gauge. Therefore, the temperature change is related to the voltage change by,

$$T - T_o = \frac{V - V_o}{i_o r_o \beta}$$

The particular gauge employed had a resistance of 49 Ω and a β of 0.0020 (1/°C) (a value different from the handbook value for bulk platinum - 0.0038 (1/°C)). The energizing current was kept at 16.7 milliamperes by means of a large ballast resistance in series with the element.

A series of measurements were made with the helium driving gas held at 980 psi while the downstream air pressure was varied to produce shock waves of different strengths. The voltage output from the gauge was displayed on an oscilloscope (the sweep started by the passage of the shock over a similar gauge mounted upstream) and photographed for a permanent record. Figure 15 shows a temperature history recorded for the condition P_4 = 980 psi He, P_1 = 1 atm. air. The temperature history was found to exhibit two distinct jumps: the first, to its theoretically predicted level (Appendix A); the second, to about twice this value. This behavior has been noticed by others (Reference 11a) and is thought to be caused by the density change of the gas layer near the wall as it is cooled. (The theoretical values were determined for the case of a constant gas density level.)

SECTION III

THE SHOCK TUBE AS A TOOL FOR SOLID PROPELLANT IGNITION RESEARCH

1. Model Location and Heating Exposure

The shock tube can be employed to study the ignition of solid propellants produced by conductive heating from a stagnated gas, convective heating from a flowing gas, or a combination of the two. The geometry of the shock tube and the location of the propellant test sample in the tube determine the nature of the exposure for any particular case. Once a standard test configuration is adopted, the shock tube can be used to study the relative ignitability of different propellants or the effect of test gas reactivity on ignitability in a very simple manner. For this qualitative work, only the pressure levels of the driving and test gases need be recorded. The ignition threshold exposure conditions can be uniquely expressed in terms of these two shock tube variables.

Three different propellant sample geometries have been employed for ignition testing in the small shock tube. They were the flat surface, the cone, and the sting mounted cone (Figure 19); the last two are essentially the same, varying only in degree. These were all mounted in, or from, the end wall from which the incident shock wave was reflected. That is, they were bathed in the doubly compressed stagnant gas behind the reflected shock wave of region (5) at some time during the testing period. Some early experiments performed in the large shock tube exposed conically shaped models to convective heating only. This situation was achieved by allowing the incident shock wave, when it reached the end of the tube, to pass into a large volume reservoir (dump tank) attached to the end of the tube (Figure 17a). In this way the reflected shock wave was eliminated and the model was heated only by the steady high velocity flow of the singly shocked, hot test gas of region (2). After a few milliseconds, the contact surface arrived and the model was rapidly cooled by the flow of the cold, driving gas. The arrival of this cold gas at the model terminated the useful ignition testing period, as the cooling had been demonstrated to be sufficiently strong to quench an incipient ignition flame. In fact there was some experimental evidence (e.g., lack of luminosity) indicating that a normal flame could not be initiated at all in this configuration (Section IV). It was therefore abandoned in favor of more fruitful approaches.

It was then conclusively demonstrated that positive ignition of a solid propellant could be achieved in a shock tube when the end of the tube was

closed with an end wall so that the propellant would be bathed in the very hot stagnated gas, following the reflected shock wave (Reference 10). Figure 17b shows the wave diagram for this shock tube operation. When the sample was flush mounted in the end wall, it experienced only the conductive heating from the stagnated testing gas left behind by the reflected shock wave in region (5). When a conical model was mounted on a 2-1/2" long sting, a small fraction (about 1/20) of the total exposure time was given to the strong convective heating of region (2) before arrival of the reflected shock wave. It is important that the sting must not be too long or it will position the test sample so far from the end wall that the contact surface will arrive before the reflected shock and the incipient flame will be extinguished before it really gets started.

The sting mounted cone produces a somewhat more vigorous heating of the propellant surface, and, therefore results in a more prompt ignition than is possible if the sample were exposed only to the conductive heating behind the reflected shock. This is a useful technique for extending the range of shock tube heating exposure conditions which will produce ignition, although the exposure is more difficult to describe analytically than in the case of pure conductive heating. Consequently, it is useful only for qualitative testing. All of the quantitative work was performed with the test sample mounted in the end wall. In this configuration, the useful testing period is terminated by the arrival of the reflected rarefaction wave, which rapidly decreases the temperature and the pressure and terminates the useful testing period.

2. Model Preparation Techniques

Before the ignition detection instrumentation was developed many ignition tests were carried out in the large (6" I.D., 75" long) shock tube on a go-or-no-go basis to obtain the threshold exposure conditions necessary to produce ignition of an end wall mounted propellant. A disturbing fact evolved from these tests, that is, the propellant was found to ignite for almost any exposure condition. These results seemed incredible since theoretical analysis predicted only a modest temperature rise of the propellant surface when heated by conduction (as low as 20°C for some conditions which produced ignition). It was obvious that an additional heating occurred during these tests. Further investigation (Reference 46) showed that improper mounting of the propellant produced uncontrolled local heating, causing local hot spots, which resulted in spuriously easy ignition. The heating was due to the convection of hot gases through the crack between the unsupported edge of the propellant sample and its mount. At this juncture, the small tube became operative and was used exclusively for the development of adequate mounting techniques, instrumentation, etc., since it could be operated at 10 times the frequency and 1/50 the cost of the large tube.

The structurally weak edge was eliminated by making a strong chemical bond with a surrounding resinous compound. This "potting" of the propellant before mounting in the end wall was the key to the successful ignition testing of the end wall samples. The composition of the inhibiting potting compound is given in Table 2. In order to shield the organic base potting compound from attack by the oxygen in the testing gas, an event which could possibly cloud the propellant ignition, it was covered with a very thin layer of inorganic insulating cement. A mixture of water-glass and fine asbestos was developed which had sufficient strength to withstand the sharp impact of the incident shock wave without breaking and was used exclusively for this purpose.

The end wall propellant test mount configuration consists of a 1/4" diameter strand of propellant surrounded by and bonded to a 1/8" thickness of inhibitor, which was glued in a 3/8" deep recess in a stainless steel housing. The surface of the propellant was carefully machined to be even with the surface of the plug, and the thin layer of inorganic insulating cement was applied. The housing is then mounted in a stainless steel plug which became the end wall of the tube when it was inserted (Figure 18).

The standard sting on which a propellant test sample was mounted was 5/32" in diameter and 2-1/4" long. A small pin, 1/4" long and 3/64" in diameter protruded from the forward end of the sting. The propellant sample was mounted on this pin. Propellant test samples, drilled to fit the pin, were glued on to it and machined to their final shape (1/2" long with a 38° included angle conical nose). A thin layer of the inorganic cement was applied to the interface between the propellant and sting to prevent the test gas from entering the crack or reacting with the organic glue. Figure 19 shows a prepared sting mounted in the flange which becomes the end wall of the shock tube when bolted on. All sting mounted conical samples tested in the small tube were prepared in this way.

3. The Shock Tube as a Qualitative Tool for Solid Propellant Ignition Research

The simple shock tube, without instrumentation, is itself a useful tool for solid propellant ignition research. If only the pressure levels of the driving and testing gases are known, and the occurrence of ignition recorded on a go-or-no-go basis, it is possible to obtain readily the qualitative ignitabilities of various propellants and the effect on ignitability of testing gas chemical reactivity, by comparing the threshold exposure conditions for ignition.

Sting mounted propellant samples prepared as described above were employed for a series of these qualitative tests since they were found to

ignite over a broader range of shock tube operating conditions than the end wall mounted samples, due to their more vigorous heating exposure. Only Batch #6 propellant (see Table 3 for composition) was completely tested by this qualitative technique, as the main objective of the experimental program was to obtain quantitative ignition information to verify the newly developed theory. Two different test gases (80%N_2, 20%O_2 and 50%N_2, 50%O_2) were employed, so that the effect of chemical reactivity could be studied. The results of these tests are shown in Figure 20. At each operating condition of the shock tube tested (completely described by P_4/P_1 and P_1), if ignition occurred, a cross was plotted; if ignition did not occur, a triangle was plotted. The boundary between the crosses and triangles defines the ignition threshold of the propellant and the data points resulting from tests made with the 0.50 wt. fraction oxygen test gas are circled. The threshold exposure necessary to obtain ignition in this gas was quite a bit lower than for the 0.20 wt. fraction oxygen test gas, indicating the strong effect of surrounding gas reactivity on propellant ignitability.

The threshold ignition conditions depend on the geometry of the particular shock tube in which the experiments are performed. A larger tube, by virtue of an extended testing duration, would allow exposure conditions, which were previously found insufficient to cause ignition, to act for a longer time; ignition would then take place. A shorter tube, on the other hand, would reduce the exposure duration, and conditions previously just sufficient to produce ignition in the original tube would now become inadequate due to the shorter exposure period. Changes in the relative lengths of the driving and testing section, which vary the testing duration, would produce the same effect for a tube of fixed length. Therefore, ignitabilities of various propellants expressed in terms of ignition thresholds can be compared only if they are all obtained in shock tubes of the same geometry.

The mechanical strength of the shock tube determines the strongest exposure which the tube can produce. The uppermost curve in Figure 20 represents the operating limit of the small shock tube. Exposure conditions above this curve would require a driving gas pressure level greater than the safe operating pressure (1050 psi) of the tube. A weaker tube would have a lower limiting curve and, for example, could not ignite the propellant with a 0.20 oxygen testing gas at all if it were sufficiently weak. On the other hand, a stronger tube would produce ignition in a testing gas with an oxygen concentration below the present limit, and over a wider range of exposure conditions. Again, this applies only to a shock tube of fixed geometry.

The ignition response of a propellant to a given heating exposure depends on its chemical kinetic, thermodynamic and physical properties.

Indeed, these are the very quantities which determine a propellant's ignitability. A certain grouping of these parameters, which has been found significant in predicting quantitatively the results of ignition testing when only the conductive mode of heating is operative, can be employed to form a basis for the explanation of these qualitative results. This is justified, a priori, on the basis that the convective period represents only about 5% of the total testing time in the sting mounted cone configuration; during the other 95% of the testing time, the conductive mode is operative.

The quantity of interest is,

$$\left[\frac{(T_5 - T_s)\, C_{pg}\, \alpha_g^{1/2}}{2 g_f \sqrt{\rho_f}\, A_f \exp\left(\frac{-E_f}{R T_{sf}}\right) A_g \exp\left(\frac{-E_g}{R T_5}\right) Z_o}\right]^{2/3} \qquad \text{Eq. (V.1)}$$

The various terms are defined in Section V. It has the units of time but is not the measured "ignition time". It must be multiplied by an additional factor, which reflects the ignition mechanism, to obtain this. Still, since the quantity reflects the important chemical reaction factors which actually produce ignition, it might be advantageous to employ the value of this quantity as an index to characterize the relative ignitability of various propellants. The smaller the quantity, the greater the ignitability of the propellant.

The variation of this quantity with shock tube operating condition can account for the shape of the experimentally determined ignition threshold in the P_4/P_1, P_1 plane. This is due to the shape of the exponential dependence of this quantity on T_5 and T_{sf}, and the fact that T_5 depends only on P_4/P_1 while T_s depends on both P_4/P_1 and P_1 (Appendix A). Therefore, certain combinations of P_4/P_1 and P_1 will produce values of T_5 and T_{sf} sufficient to reduce the quantity below a certain level while others will not. The quantity Z_o is, of course, independent of shock tube operation and can be varied at will.

Ignition will occur when a sufficient quantity of fuel is vaporized from the propellant and reacts with the oxygen already in the test gas to produce a flame, according to the new gas phase ignition theory (Section V). The rate of fuel vaporization depends on T_{sf} (Appendix B), that is, both P_4/P_1 and P_1 while the rate of chemical reaction in the gas phase depends on P_4/P_1 only.

If a propellant is subjected to an ignitability test, conducted so that the tube operates as a fixed value of P_4/P_1 (horizontal line in Figure 20),

then the level of T_5 is held constant. If P_1 is too low, then T_{sf} will be too low to vaporize the critical amount of fuel required for ignition and the sample will fail to ignite. However, as the P_1 level is increased, it will become possible to produce ignition within the time available. That is, an ignitability threshold will be reached. Further, an increase in P_4/P_1 produces a higher T_g, so that the critical quantity of fuel can be accumulated for a reduced level of P_1. Conversely, a reduced P_4/P_1 level would require a higher value of P_1. This behavior of the threshold ignitability conditions has been experimentally observed (Figure 20).

According to the gas phase ignition theory, an increase of test gas oxygen concentration will permit ignition to occur at a reduced level of fuel vapor concentration. This means that lower levels of the fuel evaporation rate (e.g., lower T_s) should be sufficient to produce ignition, as the oxygen concentration level of the test gas is increased. Therefore, for a constant level of $T_5(P_4/P_1)$ the T_{sf} required for ignition will be reflected by a lower ignition threshold level of P_1. This predicted reduction of the P_1 ignition threshold with increased oxygen concentration in the test gas is verified by the experimental results presented in Figure 20.

If the oxygen concentration in the test gas is sufficiently reduced, then a level of T_{sf} will be required which, for a given value of P_4, can not be reached simply by increasing P_1 because, eventually, a P_4 level would be necessary (if the ratio P_4/P_1 is to be kept constant) which exceeds the pressure limit of the tube. Therefore, in a shock tube with a limited P_4 capability, the propellant will fail to ignite below a definite level of test gas oxygen concentration which is different for each value of P_4/P_1. Experimentally, this effect is observed by termination of the fixed oxygen concentration ignitability limits at the curve of P_4 limited shock tube operation. (Figure 20).

The successful explanation of the experimentally determined ignitability limits of a sting mounted propellant on the basis of a grouping of terms, which is important in describing quantitatively the ignition process in the case of an end wall mounted model heated by pure conduction, indicates that the sting mounted configuration is quite similar to the end wall mounted model in its overall ignition behavior. Further, it is proposed that the value of this quantity, evaluated at some arbitrary exposure condition, might be a useful index of relative propellant ignitability.

SECTION IV

MEASUREMENT OF IGNITION TIME LAG

The aim of this program was the fundamental understanding of the process by which solid propellants ignite. A theory capable of predicting quantitatively the ignition time of propellants as a function of their heating exposure conditions was developed. Quantitative measurements of the ignition time lags of various composite propellants were made in order to verify this theory. Both photographic and photoelectric techniques were employed in making these measurements.

Initially, conically shaped sting mounted propellant samples were tested in large shock tube (6 in. I.D., 75' long). A dump tank was attached to the downstream end to eliminate the reflected shock wave. During a test, the propellant was first heated by the hot, flowing test gas, and then cooled by the flow of the cold, expanded driving gas. This cycle was described in the last section. Models tested in this way were visually inspected following removal from the tube after such an exposure. In general, no change from their appearance before testing could be detected; however, in some instances, a slight discoloration near the tip of the cone was noticed. It could not be determined whether this alteration was due to a chemical change, produced by the incipient ignition reaction, or merely erosion from exposure to the high velocity gas flow.

1. Ignition Detection by Photographic Means

High speed photography (5000 frames/second) was employed in an attempt to detect the flash of an incipient ignition flame, if it occurred. The results were indecisive since in many cases there would be no noticeable exposure of any sort for one run, but the very next run, at the same exposure condition, would exhibit an exposed frame or two. The exposures were quite "thin" and they could have very well been produced by the luminous shock or some spurious marking of the film during development. In order to capture all of the light produced within the tube during a test, a nonframing high speed strip camera was employed. This also produced inconclusive results.

When the end wall of the shock tube replaced the dump tank, definite ignition was produced. A photographic study of the ignition and burning process was made (Reference 10). However, since the large tube (6" I.D., 75' long) was designed to study ignition produced by pure convective heat transfer, and it was found impossible to ascertain if ignition was possible in this configuration, it was decided to temporarily abandon

this tube. The remainder of the experiments were conducted in the small shock tube (1.6" I.D., 18 long), which could be operated much more easily and cheaply, but still was capable of producing ignition when operated in the end wall configuration.

This change permitted suitable burst diaphragms and test models, as well as wave speed and photoelectric instrumentation, to be swiftly developed at a small fraction of the cost which would have been incurred if the large tube were employed for the purpose. Photographic techniques proved invaluable in the development of the models and interpretation of the ignition results.

The high speed camera employed for this work was a Wollensak 16 mm Fastax. A special double lens system, consisting of Wollensak 50 mm f.2 inner lens and a Schreider-Krenynach 80 mm f.4 outer lens, allowed the camera to be positioned with the forward lens only 1/2" from the quartz observation window of the small shock tube. This technique produced an image of the propellant test sample which filled almost the entire frame. A small neon light within the camera flashed once every millisecond. This produced an exposure pattern on the edge of the film which provided a means of timing events.

Figure 21 illustrates the use of the photographic technique in the development of suitable propellant models for ignition testing. These were taken as various propellant model geometries were being evaluated as possible alternates to the conical shape, since it was difficult to reproducibly machine the sharp tip of the cone, due to the inhomogeneous nature of the composite propellants. It was postulated that a rounded nose contour could be more easily machined, or that a model with an inert tip might eliminate the problem altogether. Unfortunately, neither of these proved successful. The round nose models ignited on the cylindrical afterbody rather than on the nose (Figure 21a). The ignition lag data from these rounded models exhibited more scatter than the conical models and were abandoned. The inert tip model was also unsuccessful, as the joint between the aluminum tip and the propellant could not be adequately insulated without disturbing the flow about the model. When the insulated models were tested, a great deal of scatter appeared in this data. When the crack was left uninsulated (Figure 21b), ignition would prematurely occur at that position. This type of model was also abandoned.

Figure 22 shows two examples of the photographic records obtained when the conically shaped models were tested. The propellant formulation which contained no iron oxide ignited at the tip and spread rearward as the burning progressed (Figure 22a). This behavior was typical of the conical models. The addition of iron oxide to a formulation resulted in a propellant which was characterized by a rough surface, after machining. This probably resulted in the occasional ignition in the region somewhat behind the tip of the cone (Figure 22b). However, when this modified propellant was tested

in the flat end wall configuration, its behavior is no different from the unadulterated formulation. A typical ignition run for an end wall mounted sample is shown (Figure 22c). Since there is no preferred ignition site with this flat geometry, as opposed to the tip of the conically shaped models, ignition sites usually appear at several random surface locations simultaneously.

It was noticed quite early in the program that test gas mixtures containing a high percentage of O_2 (i.e., greater than 65%) produced a great deal of radiation upon passage of the reflected shock wave. In some cases, it was sufficient to obscure the radiation from the incipient ignition flame of the solid propellant. It was the focus of considerable attention until its cause was finally uncovered and eliminated. The use of high speed color photography greatly aided this effort.

The film strips reproduced in Figures 20 and 21 are all black and white Kodak Tri-X, with a nominal ASA tungsten rating of 250. Since only the light from phenomena within the tube (which is not too great during the ignition process) was used to expose the film, and the framing rate was so fast, it was necessary to develop the film for 9 minutes in straight Dektol. This process was found to increase the graininess somewhat, but it was necessary to bring out the image. Several types of color film were employed during the program, but the best results were obtained from Kodak color 16 mm Reversal film with a standard ASA rating of 120. The normal development by the Kodak Company was found to be adequate. The color photographs were generally superior to the black and white, but unfortunately cannot be reproduced here.

2. Ignition Detection by Photoelectric Means

It was found quite difficult to assign an accurate time of ignition when only the photographic technique was employed. The phenomenon of ignition could, of course, always be recognized, but a definite number had to be assigned to each ignition test if the quantitative theory was to be verified. Therefore, the first response of a scanning vacuum phototube was arbitrarily selected to signal the instant of ignition.

At first, one, and later, two, photocells were employed to view the igniting propellant samples. The quartz windows through which the photocells peer are located 3" from the end wall of the shock tube. The sting length was chosen (2-1/2") so that the entire length of mounted propellant was visible through either window. The length of the end wall plug (2-13/16") permitted the entire end wall mounted propellant surface to be scanned. When two photocells were employed, both sides of the sting mounted sample could be viewed simultaneously.

The initial measurements were made by means of a single photocell mounted directly on the tube. This proved unsuccessful since vibrations due to the firing of the tube would produce electrical "noise" which obscured the instant of ignition. The next development was to isolate the photocell from the tube by mounting it on a sturdy camera tripod. This eliminated the noise, but introduced the possibility of spurious ignition measurements due to run-to-run misalignments between the photocell and propellant model. Finally, a permanent mount for two photocells was constructed.

A photograph of the end of the testing section of the tube, showing the two photocell units mounted on a precisely aligned optical bench, is presented as Figure 23. The optical bench was securely fastened to a metal frame and bolted to the floor. Therefore, its position was always fixed relative to the nonmoving testing section. Small vertical and horizontal adjustments of the photocell mounts were possible, but once accurately positioned, they were tightly secured. Each phototube housing contained a cathode follower at the output of the phototube. When a 4' coaxial cable was used to carry the output from the cathode follower to the oscilloscope, the rise time of the system was found to be less than 10 microseconds.

For both the sting and end wall configurations, apertures were designed, which, when placed between the photocells and propellant sample, would limit the field of view of the photocells to the propellant sample itself. This was necessary to reduce the high level of background radiation, produced by the reflected shocks of high oxygen concentration, which sometimes obscured the ignition phenomena. Even after this radiation was effectively eliminated, the apertures were left in place as a matter of good practice. The window apertures and photocell geometry for both the sting mount and end wall are shown in Figures 24 and 25 respectively.

By placing a filter in the optical path between the photocell and propellant sample, a further reduction of background radiation was possible. After several selected filters were evaluated, in combination with both type 935 and type 1P39 vacuum phototubes, it was found that the combination of a Kodak Wratten 18-A filter with the type 935 phototube gave the best ratio of ignition signal-to-background noise. The spectral response sensitivities and other considerations which led to the selection of this particular combination are discussed in Reference 49.

A schematic diagram of the instrumentation setup used to make the time-to-ignition measurements is shown in Figure 26. A thin film gauge, mounted 6 inch upstream of the testing position, was used to sense the arrival of the onrushing shock wave. Its amplified output triggers the oscilloscope sweep. Eventually, the shock wave reaches the propellant position,

and at some later time the luminous incipient ignition flame is detected by the photocells (if ignition occurs). This signal produces a vertical deflection of the oscilloscope trace. The trace is photographed to produce a permanent record of the event.

Figure 27 shows four typical traces obtained in this way. Figure 27a is a trace obtained from a contaminated tube containing 79% 0_2 in the testing gas, with no propellant in place. The deflection of the trace was caused by the flash produced by reflected shock wave when the tube was contaminated. Careful cleaning of the tube with a damp, lint-free rag followed by a second cleaning with trichloroethylene (a degreasing agent), reduced the radiation to a level which could not be detected (Figure 27b). An indisciminately handled model, inserted in an otherwise clean tube, would cause about the same level of background radiation for the same operating condition. Occasionally, this would die out before the first ignition radiation was detected, and it was deduced that this luminosity was caused by the flashing of oil, inadvertently deposited on the surface of the model during its normal handling. By carefully preparing the models and wiping their surfaces with trichloroethylene before inserting in the tube, this spurious radiation was completely eliminated. Figure 27c is a trace obtained when an inert model, which was carefully cleaned before mounting in the tube, was tested at the same exposure. A carefully cleaned propellant model and tube produced the ignition trace presented as Figure 27d. Here, the only radiation detected was from the incipient ignition flame. The instant of ignition is marked by an arrow labeled I.

SECTION V

THE THEORY OF SOLID PROPELLANT IGNITION

1. Previous Ignition Theories - Solid Phase Heat Release

Previous theoretical treatment of the solid propellant ignition problem focussed on heat release phenomena which took place only in the solid phase. Although this approach had limited success in correlating some experimental data, the solid phase model has yet to be verified experimentally. Its most obvious defect is the inability to incorporate the well-established (References 6, 8, 9, 11, 12) reduction of ignition time lag with increasing oxygen concentration in the surrounding atmosphere. In this section, a brief review of the previous solid phase ignition theories will be made. Then, a theory which is based on a gas phase heat release will be presented, which results in a quantitative agreement with experimental findings.

A correct mathematical statement of the ignition problem must incorporate, in some form, the basic equation for describing the nonsteady flow of heat in a medium capable of heat generation. For the particular case of one-dimensional heat flow in a homogeneous medium, the equation is,

$$\rho C_p \frac{\partial T}{\partial t} = \lambda \frac{\partial^2 T}{\partial x^2} + Q \qquad \text{Eq. (1)}$$

This is the standard Fourier diffusion equation. It is a linear (if Q is a linear function of T) partial differential equation of the second order. In the linear form it is susceptible to relatively straightforward mathematical treatment, and analytic solutions for a variety of boundary conditions have been obtained (References 16, 17); a solution is a mathematical relation between the temperature, T, the dependent variable, and the two independent variables, x, linear distance, and t, time, for a particular set of boundary conditions. If the heat release term is a nonlinear function of T, then the solutions are more difficult to obtain. In particular, for the ignition problem, the dependence of chemical heat release rate on temperature is exponential in nature, most frequently written as $Q \sim \mathcal{E}^{-\frac{E}{RT}}$ (where: E, the "activation energy", is a constant for a particular reaction, and R is the universal gas constant). This function is so strongly nonlinear that an exact analytical solution to a thermal problem with chemical heat generation has never been obtained. However, modern computational machines make it possible to generate complete solutions of any desired accuracy for a sufficient expenditure of effort.

An alternate, less exact, approach to the problem has been to neglect the nonlinear term so that the classical solutions to the equation can be obtained (Reference 5). These analytic solutions are valid only below a certain temperature level. When the propellant temperature exceeds this "ignition temperature", the chemical heat is assumed to be generated discontinuously, due to its powerful temperature dependence, and the runaway of the temperature to complete ignition and burning occurs "instantaneously" compared to the time required to reach this "ignition temperature". Therefore, the term which is removed from the equation itself is inserted in the boundary conditions by establishing the maximum temperature of the substance for which the linear equation is applicable. The time necessary to reach this "ignition temperature" is defined as the ignition delay time. Both the ignition delay and "ignition temperature" must be experimentally determined.

For special applications, other approximations can be made by neglecting either the rate of temperature change with time or the presence of temperature gradients, as the particular physics of a given situation dictates. Analytic solutions to these reduced equations become possible only if the nonlinear chemical heat generation term is suitably approximated. The first mentioned situation describes the "stationary thermal explosion" (References 18, 19), and the second, the "nonsteady thermal explosion" (20, 21). Recently, more sophisticated approximations have resulted in refinement of these approximate solutions (Reference 22).

Neither the "stationary thermal explosion" nor the "nonstationary thermal explosion" approximations can be employed to describe the short time delay ignition of solid propellants produced by vigorous surface heating. The former could predict, for example, the largest tolerable mass of propellant at a given initial temperature, or the maximum initial temperature for a given mass of propellant, before "spontaneous ignition" would take place. However, when the critical quantity of mass is exceeded, it would be incapable of describing the companion increase of temperature with time during the ignition process, as this term was eliminated from the basic equation for which the solution was obtained. On the other hand, the latter treatment could adequately describe, for example, the ignition of well-mixed reactable gases after rapid adiabatic compression. That is, when the entire mass is uniformly heated it is reasonable to neglect the conduction of heat, as no temperature gradients will exist. Clearly, this approach is also inapplicable to the problem of interest, where the heat conducted from the surface of the solid propellant to the interior determines the surface temperature for any given surface heating rate; however, it might be useful if the entire mass of the solid could be uniformly heated by, for example, electromagnetic radiation.

Complete numerical solutions of equation (1) were made by Hicks (Reference 13) for a zero order chemical reaction (i.e., reaction rate independent of reactant concentrations). Q could then be represented as:

$$Q = q A e^{-\frac{E}{RT}}$$

where:

q is the heat release per unit mass

A is the "frequency factor"

E, R, & T are defined above

The heat flow equation was then numerically integrated throughout a semi-infinite, exothermically reactive solid, at arbitrary initial temperatures, for a range of surface heating rates. The mathematical form of the heating rate boundary condition was a step function application of the heating at t = 0. These thorough solutions are of theoretical interest since they show the quantitative behavior of thermal ignition based on this simple model. By comparing the exact numerical solutions with analytical solutions of the linear equation (Q = 0), when using as an ignition criterion the time at which the ratio of heat production rate by the chemical reaction becomes a certain fraction at the surface of that supplied by external heating, it was found that this linear approach was accurate in its prediction of ignition times to at least 10% of the values given by the complete numerical solutions in most cases. Further, the time to ignition was found to be relatively insensitive to the value of the fraction selected, due to the exponential nature of the heat release term.

This mathematical agreement represents the best justification, to date, for neglecting the exponential term in the integration of equation (1), a step previously based on physical argument and intuition. An example of the intuitive approach is the method of Altman & Grant and Altman & Nichols (Reference 5). Here the ignition criterion was based on the level of the local absolute temperature reaching an "ignition temperature" rather than a heat balance. Justification of their approach is based on its proven ability to correlate ignition data for a composite solid propellant over a limited range of well defined exposure conditions produced by an electrically heated hot wire. The heat balance criterion of Hicks was employed by Ryan and Baer (References 11, 11a) to correlate the ignition data obtained by subjecting a particular composite propellant to a wide range of convective heating exposure situations. The correlation was successful if, and only if, the oxygen concentration in the surrounding atmosphere was held constant during the tests. The method was apparently less successful for other propellants they tested.

There has not appeared in the literature, except for the present work (Reference 12), any other theoretical description of the ignition of solid propellants. Other workers in the field were content either to rely on empirical dimensional analysis to correlate their data (Reference 6), or simply to present the experimental data without a well-defined scheme of correlation (Reference 9). This is not surprising in the light of the forementioned fundamental difficulties in obtaining a theoretical solution to the basic equation.

The two correlations discussed above, which have been made on the basis of the theoretical solutions, do not verify the model employed (i.e., the solid phase heat generation model). The experiments were performed on composite propellants which are incapable of producing the level of solid phase heat generation due to chemical reaction (Reference 15) required by the theory. Explosives (Reference 27) and nitrocellulose-nitroglycerin double-base propellants (Reference 14) do possess this capability and should be more likely candidates on which to test the solid phase ignition theory. However, there is a more fundamental reason for doubting the model based only on solid phase reactions. That is, it has been well established on the basis of both theoretical and experimental investigations, that in the steady-state deflagration of solid propellants the bulk of the heat release occurs in a gaseous reaction zone adjacent to the solid surface (References 14, 23, 24, 25). Further, the above theory cannot explain the required transition from the initial exothermic reaction to the ultimate steady-state burning structure. This is essential to a complete statement of an ignition theory.

Perhaps the most serious shortcoming of the solid phase theory is its failure to account for the sensitive dependence of the ignition time lag on the chemical reactivity of the surrounding atmospheric environment. It seems certain that the observed effect of pressure level and oxygen concentration in the surrounding atmosphere in speeding up the ignition process of both composite (References 11, 12) and double base propellants (References 6, 9, 28), as well as the initiation of primary explosives (Reference 26) must be explained on the basis of important gas phase reactions, and cannot be incorporated in a theory that depends on solid phase reactions alone. The new theory is developed on the basis of a gas phase ignition reaction. It allows a quantitative prediction of the ignition time lags of composite solid propellants to be made. The results of experiments designed to test the theory verify its predictions. The previously inexplicable results of other experiments (References 11, 11a) producing different boundary conditions can be explained qualitatively (Section VII) on the basis of this theory.

2. New Ignition Theory - Gas Phase Heat Release*

The theory treats the case of composite solid propellant ignition caused by instantaneous exposure to conductive heating from a stagnant gas. This situation can be achieved experimentally if the propellant to be tested is mounted in the end wall of a shock tube, so that its exposed surface is flush with the wall, and the normal shock wave which propagates through the test gas, which fills the downstream section of the tube, reflects from this flush, flat,surface. Then, heat will instantaneously start to flow into the propellant in a way which produces a step increase of the surface temperature. However, due to differences in their thermal properties, the temperature of the oxidizer crystal surface will not be the same as the binder surface temperature; it will be, in general, lower (Appendix A).

It is assumed that the propellant decomposition products, vaporized from the heated surface, will react in the gas phase very near the propellant surface, to produce a chemical heating. Theoretically, the ignition delay is defined on the basis of a balance between the chemical heat generation and the heat loss to the surroundings. Experimentally, it was recorded as the time from the moment of reflection of the impinging shock wave to the moment of first detectable light from the incipient ignition flame at the propellant's surface.

Experimental evidence indicates that, for surface temperatures below about 600°K (i.e., the shock tube end wall temperatures which can be produced by the heating due to reflection of a normal shock wave (Figure 28)), the fuel component of an ammonium perchlorate oxidized composite propellant vaporizes much more rapidly than the perchlorate crystals. That is, when the measured surface temperature of a hot plate is varied as various fuel-type substances and inorganic perchlorates are pushed against it, the former generally have a far greater linear decomposition rate below 600°K. (References 29, 40). In particular, this is true of the two fuel binders employed in the present study (Figure 29). This fact results in a considerable simplification of the following analysis.

During a test, as the surface of the propellant is continuously heated, a corresponding cooling-off of the test gas takes place. Immediately after reflection the gaseous layer adjacent to the surface starts to cool down, and a "cooling wave" propagates upstream at a rate governed by the laws of heat conduction (Appendix A). Simultaneously, the fuel-rich propellant vapors generated at the surface are also propagating upstream at a rate governed by the laws of mass diffusion (Appendix B). At some later time the "fuel wave"

---

*In the development of this new theory., the physical model was suggested by Professor M. Summerfield in 1959. The mathematical development is the result of joint work of R. F. McAlevy,III and M. Summerfield, and was presented for the first time in 1960 at the A.R.S. Conference in Princeton (Reference 12).

overtakes the "cooling wave", fuel vapor penetrates into the zone of hot oxygen, and ignition occurs, if sufficient oxygen exists in the igniting test gas (Figure 30). Ignition must take place within the available useful testing time of the tube (about 5 msec) or it will not take place at all, since the arrival of an expansion wave, which signals the end of this period (Figure 10) will cool the reacting gases below the ignition conditions.

This period is much too short for sufficient oxygen to be liberated by means of the extremely slow decomposition of the oxidizer crystals to affect the ignition phenomenon. Therefore, only the exothermic reaction between the vaporized fuel binder decomposition products and oxygen contained in the test gas atmosphere will be considered in the formulation of the following theory. The presence of the oxidizer crystal in the igniting propellant's surface is taken into account only as an obstruction to fuel vaporization. That is, increasing the amount of oxidizer in the propellant will result in less exposed fuel surface area available for vaporization.

Some additional assumptions will be made:

(1) Heat flow is by pure conduction in a stagnant gas, that is, no convection. Also, the heating starts instantaneously upon shock reflection.

(2) Thermodynamic and transport properties are independent of temperature. Gas properties will be taken to be their values at the reflected shock conditions. That is, evaluated at P_5, T_5.

(3) The density of the gas near the propellant does not change during the cooling process.

(4) The diffusion of heat and mass can be represented by the one-dimensional form of the equations.

(5) The pressure remains uniform in the gas zone of interest. This is true only for nonreflecting interface shock tube operation.

(6) The outflow of fuel vapor by diffusion into the stagnant gas does not modify the temperature distribution, or oxygen concentration, in the test gas. This means that the mass flow from the surface must be small.

(7) The rate of vaporization of fuel from the surface is controlled by an Arrhenius type rate law, and is not limited by the rate of heat flow from the hot gas to the surface.

(8) The chemical heat generation by the incipient ignition reaction does not modify the temperature distribution during the ignition delay period.

(9) The oxidation reaction consumes so little fuel during the ignition delay that it does not modify the fuel concentration distribution in the gas phase.

(10) The gaseous oxidation of the vaporized fuel is by a second-order reaction.

(11) The rate of heat absorption at the surface by the endothermic pyrolysis of the fuel binder to form the fuel vapor can be neglected in comparison with the rate of heat input by conduction.

The equation governing the heat flow in the gas near the propellant surface is the one-dimensional, unsteady Fourier Equation.

$$\rho_g C_{p_g} \frac{\partial T_g}{\partial t} = \lambda_g \frac{\partial^2 T_g}{\partial x^2} + Q$$

For the postulated second order exothermic reaction between the vaporized fuel and oxygen in the igniting gas the chemical heat generation rate may be expressed as:

$$Q = q_f C_f C_o A_g \exp\left(\frac{-E_g}{R T_g}\right)$$

where: q_f is the heat of combustion of the fuel/unit mass.

C_f is the fuel concentration in units of mass/unit volume.

C_o is the oxygen concentration in units of mass/unit volume.

A_g is the pre-exponential factor for the gas phase reaction.

E_g is the "activation energy" for the gas phase reaction.

T_g is the gas temperature.

R is the universal gas constant.

A_g, E_g, and q_f are all unalterable physical constants which depend only on the chemical nature of the vaporized fuel. C_o depends on the density behind the reflected shock wave and the oxygen mass fraction of the test gas

mixture, and therefore is independent of both time and position in the stagnant test gas column during the useful testing interval. However, neither C_f or T_g are steady or uniform during this period. Therefore, Q is a function of both time and position. By comparing this chemical heat generation term with the conductive heat loss term, which also varies with both time and position, both the site of ignition and the ignition time lag will be obtained.

Figure 31 is a plot of both the gas temperature and fuel concentration profiles at two different times following shock reflection, calculated on the basis of analyses appearing in Appendices A and B. The heat conduction rate can be determined from the curvature of the temperature profile; that is, net rate of heat conduction = $\lambda_g \partial^2 T_g / \partial x^2$, a quantity which is always negative but of an ever-decreasing magnitude for the temperature profiles produced by the reflected shock heating process. Conversely, the chemical heat generation is always a positive quantity whose magnitude depends on the local temperature and the local fuel concentration, that is, on time and position. The temperature dependence, being exponential in nature, is much more powerful than the linear fuel concentration effect, so that the site of maximum chemical heat generation will always be near the "head" of the "cooling wave", where T_g is still almost equal to T_5. The magnitude of the heating at that point increases as the local fuel concentration builds up due to the outward diffusion of fuel vapor from the propellant surface. Therefore, ignition will first occur in this region.

Some insight into the nature of the problem is gained if attention is focussed at the point on the temperature profile where $T_g \cong .97\ T_5$. This can be taken as the "head" of the "cooling wave", since the temperature profile becomes extremely flat past there (Figure 31), and the temperature dependent term of the reaction rate expression is already about 2/3 of its value at $T_g \cong .97\ T_5$. The absolute magnitude of the chemical heat generation rate at this point increases continuously, as more and more fuel accumulates. For example, notice in Figure 31 that the fuel concentration at $T_g \cong .97\ T_5$ at 1 msec after reflection, has increased by a factor of 4 over its level at 1/10 msec. Eventually, sufficient fuel will diffuse out to this point to create a lean combustion limit mixture, and the heat generation will reach a level such that ignition can first occur. Qualitatively, the process can be thought of as a lean combustion limit concentration fuel vapor "wave" overtaking a "cooling wave" which advances as $t^{1/2}$ while the "concentration wave" has a velocity nearly proportional to t. An analytical statement of the situation follows below.

The mathematical statement of the ignition criterion is that $\partial T_g / \partial t = 0$ at the ignition site when ignition takes place. Using this criterion in conjunction with the Fourier Equation for the situation of interest:

$$0 = \rho_g C_{\rho_g} \frac{\partial T_g}{\partial t} = \lambda_g \frac{\partial^2 T_g}{\partial x^2} + Q$$

Therefore, at ignition, we have the relationship:

$$Q = -\lambda_g \frac{\partial^2 T_g}{\partial X^2}$$

That is, ignition will occur when the chemical heat generation first becomes equal to the conductive heat loss.

In order to arrive at an analytical expression for the ignition time lag certain approximations have been made. They are essentially the approximations of negligibly small perturbations to both the linear temperature and concentration profiles due to the nonlinear chemical heat generation. Then, the analytic solutions obtained in Appendices A and B can be inserted into this relation in order to obtain an analytic expression for the ignition time lag. This can be considered a zeroth order approximation.

It is recognized that at the moment of ignition the chemical heat generation can no longer be considered small, but due to the nature of the term it is reasonable to assume it small for all times before ignition. Indeed, it cannot be small after this, if full ignition is to take place.

Now, the $\lambda_g \frac{\partial^2 T_g}{\partial X^2}$ term can be evaluated by twice differentiating the gas phase temperature distribution of Appendix A, thus

$$\lambda_g \frac{\partial^2 T_g}{\partial X^2} = \lambda_g (T_s - T_\infty)\, erf'' \frac{X}{2\sqrt{\alpha_g t}} \times \frac{1}{4\alpha_g t}$$

or

$$\lambda_g \frac{\partial^2 T_g}{\partial X^2} = \frac{\rho_g C_{pg} (T_s - T_\infty)}{4t}\, erf'' \frac{X}{2\sqrt{\alpha_g t}}$$

The chemical heat generation rate can also be evaluated by employing the linear temperature and fuel concentration expressions. That is,

$$T_g(X,t) = T_\infty + (T_s - T_\infty)\, erf \frac{X}{2\sqrt{\alpha_g t}}$$

and

$$C_f(x,t) = \frac{\nu_f \rho A_f \exp\left(\frac{-E_f}{R T_{sf}}\right)}{D_{fg}^{1/2}} \times t^{1/2} \times 2\,\mathrm{ierfc}\,\frac{x}{2\sqrt{D_{fg}t}}$$

so that,

$$Q(x,t) = q_f C_o \frac{\nu_f \rho A_f \exp\left(\frac{-E_f}{R T_{sf}}\right)}{D_{fg}^{1/2}} \times t^{1/2} \times 2\,\mathrm{ierfc}\,\frac{x}{2\sqrt{D_{fg}t}} \times A_g \exp\left(\frac{-E_g/R}{T_s + (T_s - \bar{T}_s)\,\mathrm{erf}\,\frac{x}{2\sqrt{\alpha_g t}}}\right)$$

The ignition condition $Q = -\lambda_g \frac{\partial^2 T_g}{\partial x^2}$ can then be represented as

$$\frac{\rho C_{pg}(T_s - \bar{T}_s)}{4t}\,\mathrm{erf}''\frac{x}{2\sqrt{\alpha_g t}} =$$

$$q_f C_o \frac{\nu_f \rho A_f}{D_{fg}^{1/2}} \exp\left(\frac{-E_f}{R T_{sf}}\right) \times t^{1/2} \times 2\,\mathrm{ierfc}\,\frac{x}{2\sqrt{D_{fg}t}} \times A_g \exp\left(\frac{-E_g/R}{T_s + (T_s - \bar{T}_s)\,\mathrm{erf}\,\frac{x}{2\sqrt{\alpha_g t}}}\right)$$

, or, $t^{3/2} =$

$$\frac{(T_s - \bar{T}_s) C_{pg} \rho D_{fg}^{1/2} \frac{\mathrm{erf}''\frac{x}{2\sqrt{\alpha_g t}}}{2}}{2 q_f C_o \nu_f \rho A_f \exp\left(\frac{-E_f}{R T_{sf}}\right) \times 2\,\mathrm{ierfc}\,\frac{x}{2\sqrt{D_{fg}t}} \times A_g \exp\left(\frac{-E_g/R}{T_s + (T_s - \bar{T}_s)\,\mathrm{erf}\,\frac{x}{2\sqrt{\alpha_g t}}}\right)}$$

We seek a solution to this equation which results in the minimum value of t. For time less than this minimum value, no solution can exist

since the heat loss will always be greater than the chemical heat generation. When they first become equal, then the chemical heating will rapidly accelerate and a flame will be generated. After this instant, the heat generation can no longer be considered a small perturbation and the approach ceases to be valid. Therefore, only the solution which results in the minimum time is physically meaningful, and this is defined as the ignition time lag, τ .

Before solving the equation it is convenient to define a few parameters. They are:

$L_{fg} \equiv \frac{D_{fg}}{\alpha_g}$, a mixed Lewis-Semenov Number

$Z_o \equiv \frac{C_g}{\rho_g}$, the mass fraction of oxygen in the igniting gas

$\epsilon \equiv \frac{\exp\left(\frac{-E_g}{RT_g}\right)}{\exp\left(\frac{-E_g}{RT_5}\right)}$, a quantity which represents the chemical kinetic rate at any gas temperature, T_g, referred to that at the shocked gas temperature, T_5.

$\phi \equiv \frac{X}{2\sqrt{\alpha_g t}}$, a dimensionless distance, which is the natural independent variable for solutions to the Fourier Equation.

Rewriting the equation for t in terms of these quantities,

$$t = \left[\frac{(T_5 - T_s)\, c_{pg}\, \alpha_g^{1/2}}{2 q_f Z_o \sqrt{\rho_f}\, A_f \exp\left(\frac{-E_f}{RT_{sf}}\right) A_g \exp\left(\frac{-E_g}{RT_5}\right)}\right]^{2/3} \times \left[\frac{\frac{erf^{-1}\phi}{2}}{\epsilon \times 2\, i\,erfc\left(\phi, L_{fg}^{1/2}\right)}\right]^{2/3} \quad (V.1)$$

All of the terms in the first bracket are recognized to be independent of time and position. This group is primarily a function of the chemical kinetics of the fuel binder, and condition of the test gas, but independent of the diffusional ignition mechanism. It is defined as 1/K and has the units of time.

The second term contains the factors which express the competition between the diffusion of heat and the diffusion of mass. It also contains the term $\epsilon = \epsilon(\phi, T_5, T_s, E_g)$. However, it has been found (Reference 44) that the second order gas phase hydrocarbon oxidation reaction generally has an activation energy which is reasonably independent of the specific nature of the hydrocarbon fuel. Therefore ϵ is considered independent of E_g for propellants containing binders which produce hydrocarbon vapors when heated. Also it is only weakly dependent on T_5 and T_s for $2 \leq M_s \leq 4$.

Therefore, ϵ will be considered a function of ϕ only, for the purpose of the following analysis; a situation which is exactly true for the testing described in Section 7, and nearly true for most other conditions found necessary to produce ignition in a shock tube (Section III, 3). Note that the condition $\epsilon = \epsilon(\phi)$ is not necessary to obtain a solution, since a solution is readily obtained for the most general case with only a bit more computational work. It does, however, lead to a conceptually simpler statement of the ignition situation. That is, the second term of the equation becomes a function only of ϕ , defined as $F(\phi)$

Then:

$$t = \frac{1}{K} F(\phi)$$

Remembering that $\tau \equiv t_{min}$, this implies that the ignition condition is given by the minimum value of the function $F(\phi)$. That is,

$$\tau \equiv t_{min} = \frac{1}{K} F_{min}(\phi) = \frac{1}{K} F(\phi^*)$$

where ϕ^* is defined as the solution to

$$\frac{dF(\phi)}{d\phi} = 0$$

and X^* is the ignition site.

This has been done numerically, and the results are presented in Figure 32, which is a plot of $F(\phi)$ vs. ϕ for a series of L_{fg} values. The minimal values of F, and corresponding ϕ^* value for any value of L_{fg} can readily be obtained from this curve. As this expression reflects the competition between the diffusion of mass and the diffusion of heat, and since this competition is the essential element which determines the ignition time lag, the strong influence of L_{fg} on the solution (as evidenced in Figure 32) is as expected.

3. Illustrative Example of New Ignition Theory

It is now possible to rapidly compute the X^* and τ for any selected composite propellant when ignited by means of conductive heating produced by reflecting a normal shock wave from its surface, if the chemical kinetic parameters of the propellant are known. However, if the useful testing time of the shock used to produce ignition is less than the ignition time lag of

the test propellant, the propellant will not ignite. Therefore, the following example will illustrate a theoretically predicted ignition time of a test propellant which can be ignited experimentally in a time less than the tube's useful testing time, for the exposure conditions selected, thus allowing the theoretical result to be experimentally verified.

Unfortunately, the exact physical and chemical properties for the selected formulation are, in general, not known. Therefore, the computation will be based on those values obtainable (Reference 44) from the literature for similar materials. The gas phase kinetic parameters are taken to be the same as those experimentally determined from the rates of combustion of a gasoline-type fuel in air in a homogeneous reactor (A_g is altered to account for the difference of molecular weight). The values of A_f and E_f were taken from unpublished experimental work (Reference 43) on the linear pyrolysis rate of a P-13 fuel-type substance when pushed against an electrically heated plate. The experiments were conducted in the region $T_{sf} > 700^{\circ}K$ so that it was necessary to extrapolate these results in order to obtain values at temperatures comparable to those produced by normal shock reflection (e.g., about $425^{\circ}K$). The extrapolation formula used was merely to extend the experimentally determined straight (solid) line in Figure 29 to the desired temperature region (dashed); this implies that the values of the chemical kinetic parameters are independent of temperature.

In the calculation the test propellant is taken to be a sample of Batch #6. (See Table II for composition). It is assumed that the vaporized decomposition product of the pyrolysis of the large solid fuel molecule is equivalent to propane in molecular weight, diffusivity, heat of formation and reactivity with oxygen. The shock tube operation is taken to be that actually produced by 980 psi helium in the driving section and 14.7 psi of pure oxygen in the test section, both initially at $300^{\circ}K$. This produces a $M_s = 3.1$ (actual) when the diaphragm ruptures. (Figure 9).

Some values of the quantities necessary to calculate τ already have been determined in Appendices A and B. Others can be found from various charts and calibration curves presented herein. The calculation is based on the actual exposure conditions.

$T_5 = 1370\ (^{\circ}K)$ - Figure 7

$P_5 = 51$ (atmos) - Appendix A

$\rho_5 = 1.31 \times 10^{-2}$ (gm/cc) - Table I

C_{pg} = .290 (cal/gm °K) - Table III

λ_g = 0.00019 (cal/cm sec °K) - Table III

α_g = 0.050 (cm^2/sec) - Appendix A

T_s = 432 (°K) - Appendix A

D_{fg} = 0.133 (cm^2/sec) - Appendix B

L_{fg} = 2.65 = D_{fg}/α_g

Z_o = 1 (pure oxygen case)

ρ_f = 1.122 $\frac{gm}{cm^3}$ - Table III

ν = 0.30 - Appendix B

q_f = 12,000 (cal/gm) - Reference 45

A_f = 24.0 (cm/sec) - Reference 43 and Figure 29

E_f = 11,200 (cal/gm mole) - Reference 43 and Figure 29

E_g = 40,000 (cal/gm mole) - Reference 44

A_g = 1.0×10^{15} $\left(\frac{cm^3}{gm.sec}\right)$ - Reference 44; adjusted for difference in molecular weights and in order of reaction (from 1.8 to 2.0)

Therefore, the ignition time lag can be immediately evaluated:

$$\frac{1}{K} = \left[\frac{(0.290)\ (938)\ (0.224)}{2\ (12{,}000)\ (0.30)\ (1.122)\ (5.52 \times 10^{-5})\ 10^{15}}\right]^{2/3}$$

$$= 47 \times 10^{-6} \text{ sec.}$$

$L_{fg} = \frac{D_{fg}}{\alpha_g} = 2.65$ from Figure 32, $F(\phi^*) = 55$; $\phi^* = 0.94$

Therefore, $\tau = (55)\ (47)\ (10^{-6}) = 2.6 \times 10^{-3}$ sec.

and $$X^* = \phi^* 2\sqrt{\alpha_g \tau}$$

$$= (0.94)\ (2)\ \left[(0.05)\ (0.0026)\right]^{1/2}$$

$$= 0.214 \text{ millimeters}$$

The fuel concentration at any position and time is given by,

$$C_f(X,t) = \frac{\nu_f \rho_f A_f \exp\left(\frac{-E_f}{RT_{sf}}\right) \times t^{1/2}\, 2\, \text{ierfc}\, \frac{X}{2\sqrt{D_{fg}t}}}{D_{fg}^{1/2}}$$

$$= \frac{(0.30)\ (1.122)\ (5.52 \times 10^{-5})}{(0.133)^{1/2}} \times t^{1/2}\, 2\, \text{ierfc}\, \frac{X}{2\sqrt{D_{fg}t}}$$

$$= 5.1 \times 10^{-5} \times t^{1/2}\, 2\, \text{ierfc}\, \frac{X}{2\sqrt{D_{fg}t}}$$

Therefore the fuel concentration at the wall, x = 0, at t = τ is

$$C_f(0,\tau) = 5.1 \times 10^{-5} \times 5.1 \times 10^{-2} \times 2\, \text{ierfc}\,(0)$$

$$C_f(0,\tau) = 26 \times 10^{-7} \times 1.1284$$

$$= 29.3 \times 10^{-7} \left(\frac{gm}{cm^3}\right)$$

at the ignition site, $x = x^*$, at t = , it is 3.12×10^{-7} $\frac{gm}{cm}$

The respective wt. fractions are found by dividing by the density, ρ_s.

$$Z_f(0,\tau) = \frac{29.3 \times 10^{-7}}{1.13 \times 10^{-2}} = 25.9 \times 10^{-5}$$

$$Z_f(x^*,\tau) = \frac{3.12 \times 10^{-7}}{1.13 \times 10^{-2}} = 2.76 \times 10^{-5}$$

The mixture ratio at which ignition first occurs is only about $\frac{1}{1000}$ of those which are normally reported in the literature for lean limit gas phase ignitions. This is due to the vast physical differences between the two situations.

The rate of temperature rise, due to chemical heating at the ignition site, can be expressed as,

$$\left.\frac{\partial T}{\partial t}\right|_{x^*,\tau} = \frac{g_f Z_f Z_o \rho_s^2 A_g \exp\left(\frac{E_g}{RT_g}\right)}{\rho_s C_{pg}}$$

$$= \frac{(1.2 \times 10^4)(2.76 \times 10^{-5})(1.13 \times 10^{-2})(10^{15})}{(0.290)(2.22 \times 10^6)} = 5.8 \times 10^6 \left(\frac{^\circ C}{sec}\right)$$

which is a fast run-away condition.

The assumption that the heat being carried away from the vaporizing fuel surface, due to the endothermic vaporization process, is a negligibly small fraction of the heat transferred to the surface, as a result of the shock wave reflection process, will eventually be violated. The solution will be assumed valid until the heating falls, from its initially infinite value, to be only 1000 times the vaporization heat loss rate.

The time at which this occurs is calculated thusly,

$$\dot{q}_w = \frac{(\lambda \rho C_p)_w^{1/2}}{\pi^{1/2}} \times \bar{T}_s \times \frac{1}{t^{1/2}}$$

and

$$\dot{q}_{evap} = \dot{m}\, \Delta h_{evap.}$$

and we are seeking the time at which

$$\frac{\dot{q}_w}{1000} = \dot{q}_{evap.}$$

Therefore,

$$\frac{(\lambda \rho C_p)_w^{1/2}}{\pi^{1/2}} \times \frac{\bar{T}_s}{1000} \times \frac{1}{\dot{m} \Delta h_{evap.}} = t^{1/2}$$

For the problem of interest: M_S = 3.1; P = 1 atm; Batch #6 test propellant: assume $\Delta h_{evap.} = 500 \left(\frac{cal}{gm}\right)$

So, $$\frac{1.36 \times 10^{-2}}{1.78} \times \frac{1070}{1000} \times \frac{2}{1.86 \times 10^{-5} \cdot 10^{3}} = t^{1/2}$$

t = .94 sec.

The heat being carried away from the surface by evaporation is always a very small percentage of the surface heating rate for the useful testing times available in the shock tube. Therefore, the assumption that T_S is unaffected by the fuel evaporation process is quite good, even for very extended testing durations.

The ignition time of a model of P-13 binder, which contains no oxidizer, can be calculated using the above expression when ν_p =0.30 is replaced by ν_f =1.0. Since there is no "blockage effect" of oxidizer crystals in the case of a pure fuel, so it should ignite sooner, other factors held constant.

$$\tau_f \nu_f^{2/3} = \tau_p \nu_p^{2/3}$$

$$\tau_f = \tau_p \left(\frac{0.30}{1.0}\right)^{2/3} = 2.6 \times .45$$

= 1.16 msec.

The experiments performed on both the P-13 and Batch #6 models showed that pure fuel does indeed ignite in a time of this order, demonstrating that the crystalline oxidizer does not participate in the ignition reaction at low surface temperature levels. However, instead of igniting sooner than the oxidized propellant, the reverse was true (Section VI). That is, the pure fuel ignited more slowly than the propellant. This was due to the fact that the fuel binder in the Batch #6 propellant possessed properties which were different from the P-13 fuel strands tested to obtain the pyrolysis data. The reason for this is explained in Section VI. Therefore, the apparent paradox was due to using inexact pyrolysis data when evaluating the theoretical prediction of the propellant's ignition time lag. A new means of obtaining the pyrolysis data, making use of radiant heating (Section VII) should allow a more exact evaluation of the theory to be made.

SECTION VI

RESULTS AND CONCLUSIONS

This section contains a description of the results of the experiments which were performed in order to verify the newly developed gas phase theory of composite solid propellant ignition. It is demonstrated herein that the theory leads to a successful correlation of these results, as well as the previously inexplicable results of others. A new means of performing solid propellant "ignitability" tests, based on consideration of the factors demonstrated to be important in the gas phase ignition process, is presented.

The present investigation of the solid propellant ignition process was prompted by certain, apparently anomolous, results reported by others working in the field. The prevailing theory of the ignition process was one that rested on the concept of a solid phase exothermic reaction as being the underlying cause of ignition. It was postulated that if the surface temperature of a propellant test specimen could be brought to a certain "ignition temperature" level, then the heat released by the solid phase chemical reaction would rapidly bring it to complete ignition and full scale burning. According to this theory, the surrounding atmosphere could have no effect on the ignition process. Experimental results which tended to refute this corollary were thought to be spurious, or were treated as special cases of solid phase ignition (References 11, 11a). The present work centered on the exploration of the role of the chemical reactivity of the surrounding atmosphere on the ignition of solid propellants.

A shock tube technique was employed for this study. When a test specimen of solid propellant was flush mounted in the end wall of a shock tube its surface temperature would immediately jump to a higher level (by about 125°C) at the instant the shock wave reflected from its surface. The impulsive application of surface heating was by means of conduction from the stagnant gas left behind by the retreating reflected shock wave. The pressure level of the gas was constant for the entire duration of an ignition test (5 msec). The temperature level of the gas depended on both time and position since it was continuously being cooled as it heated the wall. The test gas was composed of varying mixtures of oxygen and nitrogen.

Ammonium perchlorate composite propellants were selected for ignition testing. Other experiments have demonstrated that for identical surface temperature levels the fuel component of an ammonium perchlorate composite propellant would vaporize at a rate many times that of the oxidizer, in the rather low temperature (425°K) range of interest (Reference 40). Therefore, it was reasoned that the exothermic chemical reaction, which leads to ignition, must take place between the vaporized fuel component of the propellant and

the oxygen already contained in the test gas. A balance between the local rates of heat generation and loss led to the analytic description of the ignition time lag as a function of exposure condition which is given by equation (V.1). On the basis of this result, quantitative predictions of the ignition time lags of a propellant and of a pure fuel were made. These were verified by the experiments which are described below. Since the basic premise of this new approach to the theory of composite solid propellant ignition was that the exothermic heat generation took place in the gas phase, the chemical reactivity of the surrounding atmosphere was selected as the principal experimental variable for the quantitative testing. The theory predicts an inverse dependence of ignition time lag on the oxygen weight fraction of the test gas, other factors held constant.

Three different series of experiments were performed in the small shock tube, following the initial exploratory work conducted in the large tube. First, the qualitative go-or-no-go series was performed which resulted in the isolation of the ignition domain of a typical propellant as a function of the shock tube's operating conditions. Then, qualitative ignition time lag measurements of sting mounted propellant samples were made, after a phototube detection system was installed. Finally, after refinement of the experimental technique, the accurate measurement of the ignition times of end wall mounted specimens was made. These results verified the newly developed gas phase ignition theory.

The following technique was used in order to insure that for each run the chemical reactivity of the test gas would be known exactly. In advance of each series of tests, several selected test gas mixtures of oxygen and nitrogen were prepared and stored in separate pressure vessels adjacent to the tube. Their exact compositions were determined by means of a Beckman Model D-2 Oxygen Analyzer, which depends on the measurement of the magnetic susceptability of the gas sample for its operation. The actual oxygen content was determined to within 1% in this way. In order to charge the tube with a selected test gas, the testing section of the tube was first evacuated below 1 mm. pressure, then the test gas was bled in. This cycle was twice repeated before the test gas pressure was brought to the desired P_1 level.

As discussed in Section III, 3, the uninstrumented shock tube can be used to obtain qualitative ignitability data of various propellants, or the effect of test gas reactivity on ignitability. Figure 20 shows the results of such testing of the Batch #6 propellant. A propellant ignitability obtained in this way can be compared to the ignitabilities of other propellants only if they are tested in the same tube (or one having the same geometry), have the same model geometry, and are located in the same position. When all of these conditions are fulfilled, then the shock tube appears to be an excellent tool for the determination of relative ignitabilities of solid propellants. Since the shape of the ignition threshold in the plane can be explained on the basis

of the gas phase ignition theory, propellant ignitabilities obtained in this way would be more meaningful than those obtained by a device which produces a poorly defined stimulus, and without knowledge of the ignition mechanism which is operative (e.g., by the S.P.I.A. closed bomb "ignitability" tester). Furthermore, if the A_f and E_f for the fuel decomposition process were known (e.g., from independent measurements of the linear pyrolysis rates), then it would be possible to evaluate the grouping of terms which evolved from the gas phase ignition theory (Equation V.1) at some standardized exposure condition. This could be based on current practice and, therefore, be selected to be typical of that which a practical igniter produces at the surface of a propellant in an operational rocket. In this way a more meaningful index of ignition or "ignitability factor" can be obtained. For example, one approach could be merely to determine the minimum test gas pressure (of a standard test gas composition) which will produce ignition at a certain diaphragm pressure ratio (selected as the standard ignitability testing exposure condition). A propellant with a calculated low "ignitability factor" should be readily ignitable, and, therefore, exhibit a low ignition threshold pressure. One with a high "ignitability factor" should be more difficult to ignite, and, therefore, exhibit a high ignition threshold pressure. It is recognized that there might be some difficulty in comparing the ignitabilities of propellants with different oxidizers in inert or nearly inert atmospheres, since the principal source of oxygen, which participates in the gas phase ignition reaction, must be supplied by the oxidizer crystal decomposition. However, expansion of the present concepts should allow this situation to be treated, as well.

The first quantitative ignition time measurements were made on sting mounted, conically shaped, propellant test specimens. The mounting procedure is described in Section III. 2, the ignition detection system in Section IV. 2. A 1P39 phototube was mounted on a photographic tripod, and viewed the sample through a Wratten 18-A filter, and an aperture system (Figure 24). This technique reduced the background radiation which generally accompanied the arrival of the reflected shock wave in test gases of high oxygen concentration. The rise time of this old phototube circuit was about 200 μ sec. During this series, the shock tube operating condition was held constant; P_4 = 980 psi He, P_1 = 1 atm test gas, which produced a M_s = 3.1 initial shock wave. The contact surface was stagnated about 8 in. from the end wall of the shock tube, and, therefore, the cold helium did not interact with the test sample of propellant, located about 3 in. from the end wall. The oxygen concentration of the test gas was employed as the independent variable. An example of the ignition time lag data obtained with the Batch #23 propellant is shown in Figure 33.

The scatter of the data could have been due to a variety of reasons. Some of these were: run-to-run variation of alignment between propellant samples and the photocell, nonreproducibly machined tips on the conical models, difficulty in interpreting the precise instant of ignition due to background radiation, a 200 μsec. time lag of ignition detection system, etc. The last two are

particularly deleterious to the precision of data obtained at higher oxygen concentrations, where the blast of background radiation is most powerful and the ignition time lags the smallest (i.e., a few hundred microseconds).

The ignition time lags were defined in two different ways, in an attempt to eliminate interference produced by the radiation from the reflected shock wave on the measurement of the incipient ignition flame radiation. It was argued that the reflected shock would always produce some radiation. This could introduce an error in the exact measurement of the ignition time lag, when the instant of ignition was defined on the basis of the first detectable light. That is, by the first noticeable verticle deflection of the oscilloscope trace which displays the output of the scanning photocell. Figure 27d illustrates how this "breakaway" ignition time lag is obtained (i.e., by measuring the distance between arrows). An alternate definition, based on the instant of ignition being defined by a one-division deflection of the oscilloscope trace, was also employed. Figure 33 shows a linear plot of the results of ignition testing of the Batch #23 propellant using both definitions. The very strong dependence of ignition time lag on oxygen weight fraction in the test gas is immediately obvious in both sets of data. The scatter of the data seemed to be a bit greater when the 1 cm rise definition of ignition was employed. The values obtained by using this definition are all displaced upward in a systematic way from the ones based on the "breakaway" definition of ignition.

Other propellants tested, in addition to Batch #23, were Batch #6 and Batch #33 (see Table II for compositions). A comparison of the ignition characteristics of Batch #6 and Batch #33 would reveal the effect of the different fuel binders, while any difference between batch #33 and Batch #23 would be due to the presence of Fe_2O_3, a known burning rate accelerator. By plotting the measured ignition time lags against oxygen concentration on logarithmic coordinates, curves similar to those presented in Figure 33 were obtained for each of these propellants. They all exhibited a strong dependence of ignition time lag on test gas oxygen concentration. Further, the presence of the Fe_2O_3 in the Batch #23 formulation allowed the limiting oxygen concentration (for ignition within the useful testing time of the small shock tube) to be reduced from 30% O_2 to 10% O_2.

The gas phase ignition theory (Section V.2) suggests plotting the measured ignition time lags versus the oxygen weight fraction of the test gas on a logarithmic basis for a constant level of heating exposure.

This was done for each of the propellants tested (Figures 34, 35 and 36). Each point on these curves represents the arithmetic mean of several ignition tests. The theoretically predicted inverse relation between the ignition time lags and oxygen concentration was verified for Batch #33 (except for the 100% oxygen point) and Batch #23, but the curve for Batch #6 appeared to exhibit an abrupt break at a mixture of 50% O_2, 50% N_2.

It was impossible to determine if these deviations were real effects or whether they resulted from the aforementioned difficulties in making precise ignition time lag measurements at the higher oxygen concentrations with the primitive ignition detection system which was employed for these experiments. However, later testing demonstrated that they were due to imprecise measurements.

Nevertheless, some tentative conclusions can be drawn on the basis of these unrefined measurements. They are: (1) All of the ammonium perchlorate composite propellants tested exhibited a decrease of ignition time delay with increasing test gas oxygen concentration. (2) The chemical nature of the fuel binder seems to temper this effect. That is, the slope of the $\ln \tau$ vs $\ln Z_o$ curve for the epoxy binder propellants (Batch 23 and Batch 33) is less than that for the polystyrene binder propellant (Batch 6). (3) A known burning rate accelerator, Fe_2O_3, also acts as an ignition promoter. These similarities and differences are apparent when the ignition time lags for each of the three propellants, based on the first detectible light output, are all plotted on the same graph (Figure 37).

Improvements of the model preparation techniques, photocell mounting, ignition detection techniques, and phototube circuitry (all described in Sections III and IV) were made before the final series of experiments was performed. These modifications resulted in the most accurate data which were produced during the course of the program. By permanently locating the phototubes on a rigidly mounted optical bench the run-to-run variations in the measurements of the ignition time lag, due to their misalignment with the test specimens, were eliminated. By cleaning both the models and the tube with a degreasing agent (trichloroethylene), the flash which accompanied the reflected shock wave was greatly reduced. It was further reduced (in fact, almost completely eliminated) by making the measurements by means of a new phototube-filter-aperture combination. A cathode follower reduced the rise time of the photocell circuit from 200 μ sec to less than 10 μ sec. Finally, only the simple to prepare, flat, flush mounted, end wall models were tested. This eliminated the extremely sensitive tip region of the conical models, which was difficult to reproducibly machine. This model geometry, experimentally produces the exposure situation treated by the gas phase ignition theory (Section V.2).

The purpose of the ignition testing of the end wall models was to gather sufficient data to evaluate the gas phase ignition theory. Perhaps the most unusual aspect of the theory is that it predicts that the fuel binder of a propellant would exhibit about the same ignition time lag as the propellant itself, when corrected for the blockage effect of the oxidizer. Of course, it was realized that sustained burning of the binder would be impossible, but still, the time necessary to produce the first incipient ignition flame should be approximately the same for the two (after first compensating for the "blockage" effect of the oxidizer crystals). Therefore, end wall mounted samples of

the P-13 fuel were prepared and tested in the same way as the Batch #6 propellant (P-13 fuel) in order to verify this prediction. The fuel samples tested were from the same batch as those used for the determination of the decomposition kinetics (Figure 29) of the P-13. The ignition times of each type was measured as the oxygen concentration of the test gas was varied, while holding the heating exposure constant (P_4 = 980 psi He, P_1 = 1 atm test gas). The experimental results, based on ignition time lags defined by the first detectible light output, are shown in Figure 38. This linear plot illustrates the magnitude of the effect.

The first thing to be observed was that the pure fuel binder itself could be ignited, as predicted by the gas phase ignition theory. Further, it appeared that the theory could correlate this data on a quantitative basis. For example, the measured ignition time lag of the fuel in pure oxygen (500 μ sec) is remarkably close to the theoretical value (1,160 μsec) predicted by the gas phase ignition theory (Section V.3). The theoretical prediction was evaluated by employing values for parameters which probably were somewhat different from those which described the actual process. For example, the measured ignition time of the Batch #6 propellant was found to be shorter than that of the fuel binder, although the theory predicts the opposite to be true due to the "blockage" effect of the oxidizer crystals. However, the linear pyrolysis kinetic factors (E_f, A_f) used to evaluate the ignition time lags, for both the fuel and the propellant, were taken to be the values obtained from tests conducted on the fuel samples. These samples had to be specially prepared so that they would not buckle when pushed against a hot plate (the technique used to obtain the pyrolysis data). An extra large quantity of a curing agent was added to the fuel sample batch (Table II), and it was cured for a full week at 180°F (as opposed to the normal 24 hour period for the propellant) to produce the required stiffness. This technique allowed the required strength properties to be achieved by increasing the degree of cross-linking between the elements of the styrene monomer. It is known that increasing the cross-linkage decreases the value of the pre-exponential factor, A_f, in the linear pyrolysis rate expression. This means that it becomes more difficult to vaporize (Reference 40). Therefore, the binder component of the propellant, being cross-linked to a lesser degree than the specially prepared fuel samples, will vaporize more readily. The relative ease of propellant binder vaporization is reflected in experimentally measured ignition time lags which are lower than those of the fuel, despite the "blockage effect" of the surface perchlorate crystals.

The average values of the ignition time lags for both the P-13 fuel and Batch #6 propellant were plotted against the weight fraction of oxygen in the test gas mixture on a logarithmic basis (Figure 39). It can be seen that both curves have the same slopes. Indeed, the theory predicts that they would be the same, on the basis that the chemical processes leading to ignition are the same for both. However, the theoretical slope is predicted to be -2/3, whereas, the actual slopes were found to be -2.2. This probably indicates

that the critical reaction does not proceed by means of a simple second order mechanism, as assumed in the theoretical development, but seems to reflect a complicated dependence on the chemical nature of the fuel, as discussed below. Also, the fuel pyrolysis rate depends on oxygen concentration.

Figure 40 is a plot of the average ignition time lags for both the Batch #23 and Batch #33 propellants. The Batch #23 was easier to ignite than the Batch #33 over the range of test gas compositions employed. This demonstrates that the Fe_2O_3 is an ignition promoter as well as a burning rate accelerator (a result previously indicated by the sting mounted propellant testing). The slopes of both curves are about the same. The theory predicts that this would be true if an additive is incorporated in the formulation which acts as a reaction catalyst, that is, if it alters the kinetic "activation energy" terms. Fe_2O_3 is generally assumed to produce a catalytic action. The nature of its behavior in promoting ignition tends to verify this assumption, when the experimental ignition results are interpreted in the light of the gas phase ignition theory. Further discussion of this point is presented in the following section.

The amount of oxygen incorporated in the binder molecule as well as other chemical effects, which vary from binder to binder, would be expected to affect the ignition behavior of the propellants. Intuitively, in order to explain the observed differences of slope between Batch #33 and Batch #6, one might argue that, since the epoxy binder (Batch #33) is already composed of about 1/3 oxygen then a decrease of oxygen concentration in the testing gas would affect it less than it would the P-13 (Batch #6), which is only 1/6 oxygen. However, these chemical effects actually work through paths which are much too devious to be explored or explained within the scope of the present work. As a first step toward an understanding of these pyrolysis measurements of the various binders should be made in the presence of oxygen in order to reveal its role as a decomposition catalyst. Then it might be possible to incorporate into the gas phase ignition theory a more complete description of the chemical action. A chemical analysis of the binder decomposition products would greatly aid this work.

The gas phase ignition theory has been demonstrated to be successful in explaining both the occurrence and the shape of the shock tube ignitability threshold exhibited by a composite solid propellant. It also predicted the experimentally demonstrated effect of oxygen concentration on this limit. Further, it was found possible to correlate the preliminary time to ignition data, obtained with sting mounted propellant samples, on this basis. Finally, quantitative agreement between the theoretically predicted ignition time lags of an ammonium perchlorate solid propellant and those obtained experimentally has been demonstrated. This can also be done for the fuel component of the propellant itself. These results constitute the experimental verification of the theory of composite solid propellant ignition.

The theory was developed to treat the situation encountered when oxygen is present in the test gas. That is, when the ignition reaction occurs between vaporized fuel and the oxygen in the test gas. However, for high enough surface temperatures sufficient oxygen will be liberated from the oxidizer crystals to significantly participate in the gas phase ignition reaction. Eventually, for sufficiently high temperatures (between 550°C and 650°C) it will become the dominant source of oxygen. Indeed, this is the mechanism by which a composite propellant ignites in a completely inert gas. The useful testing time of the present shock tubes was too short, and the heating exposure too mild, for sufficient oxygen to be generated by means of oxidizer decomposition to produce ignition in an inert gas. Therefore, ignition in an inert atmosphere could not be studied during the present program.

These high surface temperature levels have been obtained by means of a different shock tube technique (References 11 and 11a). It employed a nozzle expansion of the doubly compressed gas behind the reflected shock wave to convectively heat samples of propellant which are exposed to the flow. In this way it was possible to produce usable testing times up to 40 msec. Ignition time lags were measured for ammonium perchlorate propellants over a range of surface heating rates in nitrogen, oxygen, and air. These data will be interpreted in the light of the gas phase ignition theory in order to illustrate the nature of the transition of the ignition mechanism from the situation in which the oxygen in the surrounding atmosphere plays the dominant role in the ignition process to where it becomes ineffective.

When propellants are tested by exposing them to the convective heating produced by a flowing gas, ignition will take place when sufficient propellant vapors can penetrate into the boundary layer to reach the station at which the chemical heat generation first overcomes the local heat loss to the surroundings. This situation is analogous to the case of the conductive heating of an end wall mounted propellant sample. Therefore, the concepts which were evolved for that case can be used to qualitatively describe this new situation as well.

The steady convective heating produces a parabolic increase of the surface temperature with time ($T_s \sim \dot{q}_w t^{1/2}$) whereas, the conductive heating produced a constant temperature level. The exponential temperature dependence of propellant vaporization rate therefore results in a different expression describing the path by which the vapors reach the critical concentration at the ignition site. The solution to the problem depends quite strongly on the instantaneous level of the vaporization rate at the surface. Therefore, correlations of ignition time lags, which depend on critical concentration levels being reached at the ignition site, can also be made in terms of critical vaporization rates. This then can be reduced to temperatures since there is a one-to-one correspondence between evaporation rate and surface temperature (Reference 40).

To be more specific, different concentrations of fuel vapor (i.e., vaporization rate) will be required to produce the critical level of chemical heating rate just sufficient to overcome heat losses at the ignition site, for each different level of test gas oxygen concentration employed. Since the vaporization rate depends on the surface temperature, this results in a unique relationship between the heating rate and time required to reach the necessary surface temperature. It is, $-\frac{1}{z}\ln\tau = \ln \dot{q}_w + f(T_{sig})$. Figure 41 (Figure 5 of Reference 11), which is an exponential plot of experimental $\tau^{1/2}$ vs. $\dot{q}_w$ for a series of levels of T_{sig} demonstrates the one-to-one correspondence between the test gas oxygen concentration and surface temperature, which is called for by the gas phase ignition theory. This result was inexplicable by those authors within the framework of the solid phase ignition theory they presented to correlate data.

As the test gas oxygen concentration is reduced, the required fuel vaporization rate, and therefore (T_S), necessary to produce ignition, continues to grow. Eventually, a surface temperature will be reached which will be large enough to vaporize sufficient oxygen from the oxidizer crystal to submerge the effect of test gas oxygen concentration. When this point is reached, there should be little effect of measured ignition time delay on oxygen concentration. The point at which this occurs depends on the relative pyrolysis properties of both the binder and oxidizer crystal and will, in general, be different for different propellant formulations.

Figure 42 shows a replot of the data taken from Figure 41 at a heating rate of 100 Btu/ft^2 sec. Since both the pressure level and oxygen weight fraction were varied, it was necessary to plot the oxygen concentration of the test gas at any data point as a fraction of the maximum oxygen concentration tested. The gas phase ignition theory suggested that the measured time to ignition be plotted against this fraction on a logarithmic basis. When this was done the transition predicted on the basis of the gas phase ignition theory, between the region which is sensitive to oxygen concentration in the test gas and that which is not, is seen to take place at about a 30% oxygen concentration weight fraction level. The gas phase theory predicts a similar behavior for data obtained by exposure to conductive heating. Unfortunately, this could not be verified during the present program, since it was impossible to produce the required level of surface temperature without exceeding the strength limitations of the existing shock tubes.

The results of the gas phase ignition theory suggest some interesting modifications which might be made to the ignition systems of practical composite solid propellant rockets in order to decrease the amount of energy required to produce ignition, and to increase their reliabilities. They are based on the demonstrated decrease of ignition time lag with oxygen

concentration. Therefore, if the surface heating rate were kept at a constant level, then less total energy need be expended to produce ignition if oxygen is present (in excess of a certain level) than if it were not. Also, the probability of successful reproducible ignition should be increased with increasing oxygen concentration since the data exhibited less overall scatter at the higher oxygen concentrations.

Oxygen might be introduced into the rocket motor in place of the air which would normally be entrapped when the end of the nozzle is closed by a burst diaphragm. If the rocket could be pre-pressurized then the gain would be amplified due to the increased oxygen concentration. An alternate means of introducing oxygen at the igniting propellant surface is to employ a gas producing igniter which yields free oxygen when it burns. In fact, the optimum stoichiometric point of such an igniter would seem to be a fuel lean (i.e., oxygen rich) mixture, and not the fuel rich mixtures normally employed.

The gas phase ignition theory suggests a new concept of "ignitability index" which can truly be considered a property of the propellant itself, as previously discussed (Section III.3).

Finally, it should now be possible for an igniter designer to calculate, once a propellant's ignition characteristics have been established, the required heat input to the surface necessary to produce ignition within a specified time. That is, for any ignition energy source and rocket chamber gas composition (i.e., T_g, Z_O) this quantity can be calculated by correctly applying the results of the gas phase ignition theory. For example, the optimum mixture ratio and weight of the igniter could be established. These deductions represent the first step in developing logical design criteria for practical solid propellant rocket ignition systems.

SECTION VII

SUGGESTIONS FOR FUTURE RESEARCH

The shock tube has been established as an important tool for solid propellant ignition research. A gas phase ignition theory has been developed which can quantitatively predict the experimentally determined ignition characteristics of ammonium perchlorate composite propellants.

A logical extension of this work would be to employ the present shock tube technique for the study of other types of solid propellants. For example, the ignition characteristics of ammonium nitrate and nitrocellulose type propellants could be experimentally investigated without alteration to the existing shock tubes. The gas phase ignition theory should apply to these results with little, if any, modification.

On the other hand, the study of solid propellant ignition in an inert test gas could not be studied without some modification of the existing equipment. Participation of the oxygen released by the oxidizer decomposition, in the gas phase ignition reaction, would be necessary to produce ignition in this case. This has been shown to require a propellant surface temperature in excess of 500°K, a condition which cannot be achieved with the present apparatus. However, if the propellant specimen were preheated, or an extended heating duration could be achieved (e.g., by making a shock tunnel modification to the end wall of the tube), then the present tubes could be used for the study of ignition in an inert gas. The gas phase ignition theory would have to be modified in order to apply to this case.

Successful completion of these researches should lead to a unified theory of the solid propellant ignition process.

The fundamental concepts of the nature of the solid propellant ignition process, which evolved from the gas phase ignition theory and are verified by the shock tube experiments, should be subjected to testing in a realistic environment. That is, by means of tests conducted in an actual rocket motor. In this way, both the efficiency of the igniter and the ignitability of the propellants themselves could be evaluated on a practical basis. The predictions of the gas phase ignition theory concerning igniter performance, such as: mixture ratio, generated pressure level in the chamber due to igniter gas production, flame temperature, nature of the combustion products, etc., as well as predictions concerning the factors which affect the response of the propellant itself, such as: initial temperature, initial chamber pressure, propellant composition, surface conditioning, etc., could then be realistically appraised. If the results obtained from these practical experiments

can be adequately described on the basis of our new understanding of the fundamental mechanisms involved, then a rational basis for the design of practical ignition systems will be at hand. For example, rules for the scaling of igniters to produce successful ignition of large solid propellant grains, predictions of igniter requirements in order to produce successful ignition in a space environment, ignition of new propellant formulations, etc., could be evolved. It should be remarked that the ignition of a full propellant grain will not be required for each of these motor tests. That is, since only the surface of the grain responds to the ignition impulse, then a dummy grain with a thin surface layer of propellant will suffice for this limited purpose.

The shock tube technique, as it is presently employed, can be used as a fundamental research tool in the field of chemical reaction kinetics. The reaction rate parameters of interest would be revealed by treating the measured ignition time lags in a manner which is suggested by Equation (V.1).

$$\tau^{3/2} = \left[\frac{(T_5 - T_s) C_{pg} \alpha_g^{1/2}}{2 \rho_f^{1/2} \rho A_f \exp\left(\frac{-E_f}{R T_{sf}}\right) A_g \exp\left(\frac{-E_g}{R T_s}\right)} \right] \times \frac{1}{Z_0} \times F(\phi^*, L_{fg})$$

The evaluation of the "activation energies" for both the fuel pyrolysis process, E_f, and the gas phase ignition reaction, E_g, can proceed by plotting the logarithm of the measured ignition time lags versus the reciprocal of the relevant absolute temperature levels. Therefore, these temperatures represent the experimental variables for this work.

One interesting feature of the present shock tube technique is that it permits both of these temperatures to be independently varied. The temperature level of the gas behind the reflected shock wave, T_5, depends only on the Mach number of the incident shock wave, $M_s(P_4/P_1)$. However, the temperature level which the heated end wall reaches depends on both the temperature, T_5, and pressure, P_5, behind the reflected shock wave. But, since the level of P_5 depends on both the Mach number of the incident shock wave, $M_s(P_4/P_1)$ and the initial pressure level of the tube, P_1; then it is readily understood that it is fundamentally the independence of the diaphragm pressure ratio, P_4/P_1 and the initial absolute pressure level of the tube, P_1, which permits the independent variation of $T_5(P_4/P_1)$ and $T_s(P_4/P_1, P_1)$.

This technique can be employed to investigate the action of the common catalytic additives, which are known to be burning rate accelerators, and/or ignition promoters, such as iron oxide, ferrocine, copper chromite, etc. At the present time even the site of action of these catalysts remains a mystery.

The information which can be obtained by this technique should prove to be an important contribution to the understanding of the steady state deflagration of solid propellants as well as to the ignition problem.

This shock tube technique is only one of the several possible ways that surface decomposition kinetics could be studied. The results of other, independent, studies of this phenomenon, when compared to those obtained by means of the shock tube technique, would provide an interesting corroboration of the gas phase ignition theory. Some method other than the hot plate pyrolysis technique (Reference 40) should be employed to gather this information since the data obtained in this way is inherently inaccurate. This stems from the underlying assumption that the temperature measured on the surface of the hot plate is identical to that existing on the surface of the decomposing solid test specimen. It is inconceivable that the necessary transfer of the exothermic heat of decomposition through the layer of outflowing vapors can take place without benefit of a temperature difference.

Therefore, it is suggested that a radiative source of energy be substituted for the hot plate as a means of controlling the surface temperature of the test specimen. In addition to resulting in a more exact experiment, this technique has a certain practical advantage; that is, the test specimen would not have to be artificially prestiffened to prevent buckling as it is pushed against the hot plate. Therefore, the kinetic measurements could be made on the very same material that appears in the actual propellant formulation which is being evaluated. This should lead to a more accurate numerical evaluation of the gas phase ignition theory than that which is presently possible (Section V.3).

REFERENCES

1. Adelman, B. R., Keathley, A. C., "Reliability Aspects of Solid Propellant Rocket Engines," ARS Preprint No. 1043-60. Presented at the Solid Propellant Rocket Research Conference, Princeton University, Princeton, New Jersey, January 28-29, 1960.

2. Stehling, K. R., "Landing on the Moon," Space/Aeronautics, February, 1960, p. 42.

3. Rabern, J. W., "Systems for Ignition of Solid Propellants," ARS Preprint No. 977-59, presented at ARS 14th Annual Meeting, Washington, D.C., November 1959.

4. "Proceedings of the Third Meeting of the J.A.N.A.F. Ignitability Panel" held at Applied Physics Laboratory, Silver Springs, Maryland, June 19, 1959.

5. Altman, D., Grant, A., "The Thermal Theory of Solid Propellant Ignition by Hot Wires," Fourth Symposium on Combustion, Baltimore, Williams and Wilkins Company, 1950, p. 158.
Altman, D., Nichols, P. L., Jr., "Ignition of Solid Propellants," Jet Propulsion Laboratory Report No. 20-85. California Institute of Technology, Pasadena, California, September, 1959, (CONFIDENTIAL).

6. Churchill, S. W., Kruggel, R. W., Brier, J. C., "Ignition of Solid Propellants by Forced Convection," A. I. Ch. E. Journal, December, 1956, p. 568.

7. Reference 4, p. 56.

8. Remark by N. Fishman at Round Table Discussion. Solid Propellant Rocket Research Conference, Princeton University, Princeton, New Jersey, January 29, 1960.

9. Cook, M. A., Olsen, F. A., "Chemical Factors in Propellant Ignition," A.I. Ch. E. Journal 1, 1955, p. 391.

10. Summerfield, M., McAlevy, R. F., III, "The Shock Tube as a Tool for Solid Propellant Ignition Research," Jet Propulsion, Vol. 28, No. 7, July 1958, p. 478.

11. Baer, A. D., Ryan, N. W., Salt, D. L., "Fundamental Studies of Ignition by Means of a Shock Tube," ARS Preprint No. 1059-60 presented at the American Rocket Society Meeting on Solid Propellant Research, Princeton, New Jersey, January 28-29, 1960.

11a. Baer, A. D., "Composite Propellant Ignition," Ph.D. thesis, University of Utah, March 1959.

12. McAlevy, R. F., III, Cowan, P. L., Summerfield, M., "The Mechanism of Ignition of Composite Solid Propellants by Hot Gases," ARS Preprint No. 1058-60, presented at the American Rocket Society Meeting on Solid Propellant Research, Princeton, New Jersey, January 28-29, 1960.

13. Hicks, B. L., "The Theory of Ignition Considered as a Thermal Reaction," J. Chem. Phy., Vol. 22, No. 3, March 1954, p. 414.

14. Crawford, B. L., Jr., Huggett, C., McBrady, J. J., "Mechanism of the Burning of Double-Base Propellants," J. Phys. and Coll. Chem. 54, p. 854.

15. Huggett, C., "Combustion of Solid Propellants," Vol. II of Princeton Series on High Speed Aerodynamics and Jet Propulsion, p. 567.

16. Carslaw, H. S., Jaeger, J. C., "Conduction of Heat in Solids," Oxford (Clarendon) Press, 1959.

17. Jakob, M., "Heat Transfer," Vol. I, John Wiley & Sons, Inc., New York, 1949.

18. Semenov, N. N., "Some Problems in Chemical Kinetics and Reactivity," Vol. 2, Princeton University Press, 1959, p. 88.

19. Frank-Kamenetskii, D. A., "Diffusion and Heat Exchange in Chemical Kinetics," Princeton University Press, 1955, p. 237.

20. Van't Hoff, J. H., "Etudes de Dynamique Chemique," p. 161, Amsterdam, (1884).

21. Todes, D. M., "Aeta Physicochim," U.R.S.S. 5 (1936) 785.

22. Grey, P., Harper, M. J., "The Thermal Theory of Induction Periods and Ignition Delays," Seventh Symposium on Combustion, London, Butterworths Scientific Publications, 1959, p. 425.

23. Rice, O. K., Ginell, R., "The Theory of the Burning of Double-Base Rocket Powders," Journal of Physical and Colloid Chemistry, Vol. 54, No. 6, June 1950, p. 885.

24. Parr, R. G., Crawford, B. L., "A Physical Theory of Burning of Double-Base Rocket Propellants," Journal of Physical and Colloid Chemistry, Vol. 54, No. 6, June 1950, p. 929.

25. Summerfield, M., Sutherland, G. S., Webb, M. J., Taback, H. J., and Hall, K. P., "Burning of Ammonium Perchlorate Propellants," ARS Preprint No. 737-58, presented at the American Rocket Society's 13th Annual Meeting, New York, November 1958.

26. Erikson, T. A., "Pure Shock Environmental Testing of Condensed-Phase Unstable Materials," ARS Journal, Vol. 30, No. 2, February 1960, p. 190.

27. Bowden, F. P., Yoffe, A. D., "Initiation and Growth of Explosion in Liquids and Solids," Cambridge University Press, 1952.

28. Rideal, E. K., Robertson, A.J.B., "The Spontaneous Ignition of Nitrocellulose," 3rd Combustion Symposium, Williams and Wilkins, Baltimore, 1949, p. 536.

29. Chaiken, R. F., Anderson, W. H., "The Role of Binder in Composite Propellant Combustion," paper presented at the 136th meeting of the American Chemical Society, Symposium on Plastics and Elastomers in Rockets, Atlantic City, New Jersey, September 13-18, 1959.

30. McAlevy, R. F., III, Summerfield, M., "Research on the Ignition of Solid Propellants," Fourth Quarterly Progress Report (Princeton University Aeronautical Engineering Report No. 433-d) June 1, 1959.

31. Morse, P. M., Feshbach, H., "Methods of Theoretical Physics," McGraw-Hill Book Company, New York (1953), p. 171.

32. Hilsenrath, J., et al, "Tables of Thermal Properties of Gases," N.B.S. Circular 564, United States Government Printing Office, Washington, D.C., (1955).

33. Reid, R. C., Sherwood, T. K., "The Properties of Gases and Liquids," McGraw-Hill Book Company, New York, 1958, p. 276.

34. Kennard, E. H., "Kinetic Theory of Gases," McGraw-Hill Book Company, New York (1938), p. 198.

35. "Physical Properties of Plexiglas Sheet," Rohm and Haas Company Bulletin No. 229c, May 1959.

36. Welte, F. E., Plastics Department of Rohm and Haas Company, Personal Communication, December 1959.

37. Reference 11a - p. 124.

38. "Properties of Selected Commercial Glasses" Booklet B-83, Corning Glass Works, Corning, New York (1959).

39. Bloom, M., "Thermal Conditions Associated with Aircraft in Flight," WADC Technical Report 55-169, March 1956.

40. Schultz, R., Green, L., and Penner, S. S., "Studies of the Decomposition Mechanism, Erosive Burning, Sonance and Resonance of Solid Composite Propellants," Selected Combustion Problems, Vol. III, Butterworth's Scientific Publications, London, 1958.

41. Fich, A., Ann. Phys. Lpz. 170 (1855), p. 59.

42. Crank, J., "The Mathematics of Diffusion," Oxford (Clarendon) Press, 1956, p. 31.

43. Chaiken, R. F., Aerojet-General Corporation, Personal Communication, January, 1960.

44. Longwell, J. P., Weiss, M. A., "High Temperature Reaction Rates in Hydrocarbon Combustion," Industrial and Engineering Chemistry, Vol. 47, No. 8, August 1955, p. 1635.

45. McAlevy, R. F., III, Summerfield, M., "Research on the Ignition of Solid Propellants," First Quarterly Progress Report, Princeton University Aeronautical Engineering Report No. 433-a, August, 1958.

46. McAlevy, R. F., III, Summerfield M., "Research on the Ignition of Solid Propellants," Second Quarterly Progress Report, Princeton University Aeronautical Engineering Report No. 433-b, January 1959.

47. McAlevy, R. F., III, Summerfield, M., "Research on the Ignition of Solid Propellants, Third Quarterly Progress Report, Princeton University Aeronautical Engineering Report No. 433-c, April 1959.

48. McAlevy, R. F., III, Summerfield, M., "Research on the Ignition of Solid Propellants," Fifth Quarterly Progress Report, Princeton University Aeronautical Engineering Report No. 433-e, September 1959.

49. Cowan, P. L., "Experiments on the Ignition of Composite Solid Propellants," MSE Thesis, Department of Aeronautical Engineering, Princeton University, January 1960.

50. Vieille, P., Comptes Rendus, Acad. Sc., Paris, Vol. 129, p. 1228, 1899.

51. Payman, W., Sherherds, F., "Proceedings of the Royal Society, A186, p. 293, 1946.

52. Reynolds, G. T., "A Preliminary Study of Plane Shock Waves Formed by Bursting Diaphragms in a Tube," Office of Scientific Research and Development, Washington, No. 1519, 1943.

53. Bleakney, W., Weimer, D., and Fletcher, J. C., "The Shock Tube - A Facility for Investigations in Fluid Dynamics," Rev. Sci. Inst. 20, 807, 1949.

54. Glass, I. I., "Shock Tubes - Part I: Theory and Performance of Simple Shock Tubes," Institute of Aerophysics, University of Toronto, UTIA Review No. 12, 1958.

55. Hall, J. G., "Shock Tubes - Part II: Production of Strong Shock Waves; Shock Tube Applications, Design, and Instrumentation," Institute of Aerophysics, University of Toronto, UTIA Review No. 12, 1958.

56. Dolder, K., Hide, R., "Bibliography on Shock Waves, Shock Tubes, and Allied Topics," AD-127681 (Great Britain: Atomic Energy Research Establishment, 1956).

57. Penner, S. S., Harshbager, F., and Vall, V., "An Introduction to the Use of the Shock Tube for the Determination of Physico-Chemical Parameters," "Combustion Researches and Reviews," 1957, Butterworths Scientific Publications, London, 1957.

58. Courant, R. and Friedriches, "Supersonic Flow and Shock Waves," Interscience Publications, New York, 1948.

59. Rudinger, G., "Nonsteady Flow in Ducts," Van Nostrand, New York, 1955.

60. Lobb, K., "On the Length of a Shock Tube," Toronto University, UTIA Report No. 4, Toronto, 1950.

61. Lobb, K., "The Study of Supersonic Flows in a Shock Tube," Ph.D. Thesis, University of Toronto, 1950.

62. Lukasiewicz, J., "Shock Tube Theory and Applications," National Research Council (Canada) Report No. MT-10, Ottawa, 1950.

63. Geiger, F. W., Mantz, C. W., "The Shock Tube as an Instrument for the Investigation of Transonic and Supersonic Flow Patterns," Engineering Research Institute, University of Michigan.

64. Glass, I. I., Martin, W., Patterson, G. N., "A Theoretical and Experimental Study of the Shock Tube," Institute of Aerophysics, University of Toronto, UTIA Report No. 2, November, 1953.

65. Yoler, Y. A., "Hypersonic Shock Tube," California Institute of Technology, Hypersonic Wind Tunnel Memorandum No. 18, Pasadena, California, July 1954.

66. Bethe, H. A., Teller, F., "Deviations from Thermal Equilibrium in Shock Waves," Aberdeen Proving Grounds, B. R. L. Report No. 201, 1952.

67. Duff, R. E., "The Use of Real Gases in a Shock Tube," Engineering Research Institute, University of Michigan, 51-3, 1951.

68. Bureau of Ordnance Publication, "Handbook of Supersonic Aerodynamics," NAVORD Report No. 1488, Vol. 5 (1953).

69. Strehlow, R. A., "One-Dimensional Step Shock Wave Calculations for Ideal Gases," Aberdeen Proving Grounds, BRL Report No. 978, 1956.

70. Blackman, V. H., "Vibrational Relaxation in Oxygen and Nitrogen," Journal of Fluid Mechanics, Vol. 1, 11. 61-85, 1956.

71. Alpher, R. A., Greyber, H. D., "Calculations of Shock Hugoniots and Related Quantities of Nitrogen and Oxygen," General Electric Research Laboratory Report No. 58-RL-1915, April 1958.

72. Evans, J. S., "Method for Calculating Effects of Dissociation on Flow Variables in the Relaxation Zone Behind Normal Shock Waves," NACA TN 3860, 1956.

73. Squire, W., Hertzberg, A., Smith, W. E., "Real Gas Effects in a Hypersonic Shock Tunnel," A.E.D.C. - TN - 55-14, ARDC, 1955.

74. Feldman, S., "Hypersonic Gas Dynamic Charts for Equilibrium Air," AVCO Research Laboratory, 1957.

75. Emrich, R. J. Wheeler, D. B., Jr., "Wall Effects in Shock Tube Flow," The Physics of Fluids, Vol. 1, No. 1, January-February, 1958.

76. Hollyer, R. N., Jr., "A Study of Attenuation in the Shock Tube," University of Michigan, Eng. Resc., Institute, Report M720-4, 1953, also, Journal of Applied Physics, Vol. 27, No. 2, pp. 254-261, 1956.

77. Mirles, H., Braun, W. H., "Nonuniformities in Shock Tube Flow Due to Unsteady Boundary Layer Action," N.A.C.A. TN 4021, 1957.

78. Martin, W. A., "An Experimental Study of the Boundary Layer Behind a Moving Plane Shock Wave," UTIA Report No. 47, November 1957.

79. Rose, P. H., Nelson, W., "On the Effects of Attenuation on Gas Dynamic Measurements in Shock Tubes," AVCO Research Laboratory, Report No. 24, 1958.

80. Trimpini, R. L., and Cohen, N. B., "A Theory for Predicting the Flow of Real Gases in Shock Tubes with Experimental Verification," NACA-TN 3375, 1955.

81. Hall, J. G., Hertzberg, A., "Recent Advances in Transient Surface Temperature Thermometry," Jet Propulsion, Vol. 28, No. 10, p. 719, October 1958.

82. Robinowicz, J., Jessey, M. R., Bartock, C. A., "Resistance Thermometer for Heat Transfer Measurements in a Shock Tube," GALCIT Hypersonic Research Project, Mano. No. 33, July 1956.

83. Nagamatsu, H. T., Geiger, R. E., "A Fast Response Device for Measuring Heat Transfer," General Electric, Schnectady, Turbine Machinery Instrumentation, 2nd Annual Seminar, Schnectady, New York, May, 1957.

84. Vidal, R. J., Hilton, J. H., "The Construction and Application of a Rapid Response Resistance Thermometer Probe," C.A.L. Report No. 1M-1062-A-1, April, 1956.

85. Bromberg, R., "Use of the Shock Tube Wall Boundary Layer in Heat Transfer Studies," Jet Propulsion, Vol. 26; p. 737, September 1956.

86. Resler, E. L., Lin, S. C., Kantrowitz, A., "The Production of High Temperature Gases in Shock Tubes," J. Appl. Phys., Vol. 23, No. 12, 1390, December 1952.

87. Ford, C. A., Glass, I. I., "An Experimental Study of Shock Wave Refraction," University of Toronto, Institute of Aerophysics, UTIA Report No. 29.

88. Wittliff, C. E., Wilson, M. R., Hertzberg, A., "The Tailored Interface Hypersonic Shock Tunnel," Paper presented at the ASME - ARS Aviation Conference, Dallas, Texas, March 16-20, 1958. Also, see Journal of the Aero/Space Sciences, Vol. 26, No. 4, April 1959.

89. Private Communication - Paul V. Marrone, Cornell Aeronautical Lab. (November 1959).

APPENDIX A

CONDUCTIVE HEAT TRANSFER TO THE END WALL OF A SHOCK TUBE PRODUCED BY NORMAL SHOCK REFLECTION

The normal reflection of a plane shock wave from the end wall of a shock tube produces a conductive heating of the wall from the hot, stagnant, gas in the driven section of the tube, which has been doubly compressed, once by the incident shock and once by the retreating reflected shock. A knowledge of the initial temperature and pressure levels of the gas in the downstream section of the tube as well as the Mach number of the incident shock wave is sufficient to uniquely specify the state of the gas behind the reflected shock wave (Section 3). The heating of the end wall starts at the moment of shock reflection, initially from an infinitesimally thin layer of hot gas between the wall and the retreating reflected shock wave. It continues as the reflected wave moves further from the wall, leaving behind it a thickening slug of hot stagnated gas. The following analysis idealizes this transient heating from a source of varying extent to a sink of finite length by considering both the source and sink to be semi-infinite. This assumption will be examined later.

The idealized problem, therefore, will be represented as that of two semi-infinite media, initially at different uniform temperatures, instantaneously brought into surface contact. If a one-dimensional coordinate system (x) is fixed with the zero located at the interface, then the classical solutions T (x, t), describing the temperature distributions in both media at any time, to the governing non-steady one-dimensional Fourier Heat Conduction Equation,

$$\frac{\partial T}{\partial t} = \frac{\lambda}{\rho C_p}\frac{\partial^2 T}{\partial X^2} = \alpha \frac{\partial^2 T}{\partial X^2}$$

where:
ρ = density
C_p = specific heat
λ = thermal conductivity
$\frac{\lambda}{\rho C_p} \equiv \alpha$ = thermal diffusivity

are readily obtained for the case of constant density and thermal properties (References 16, 17) for the following conditions:

(i) Initial gas temperature taken as T_5

$$X > 0 \; ; \; T_g = T_5 \; @ \; t < 0$$

(ii) Initial wall temperature taken as T_1

$$X < 0 ; \; T_w = T_1 \; @ \; t < 0$$

(iii) Continuous temperature distribution at interface

$$X = 0 ; \; T_g = T_w = T_s \; @ \; t \geq 0$$

(iv) No heat accumulation at interface.

$$-\lambda_g \frac{\partial T_g}{\partial X} = \lambda_w \frac{\partial T_w}{\partial X}$$

Solutions to the equations are of the type:

$$T_g = A_g + B_g \, erf \frac{X}{2\sqrt{a_g t}} \; ; \; X > 0 ; \; t \geq 0$$

$$T_w = A_w + B_w \, erf \frac{X}{2\sqrt{a_w t}} \; ; \; X < 0 ; \; t \geq 0$$

Apply boundary conditions to determine arbitrary constants

(i) $T_g = A_g + B_g = T_5$

(ii) $T_w = A_w + B_w = T_1$

(iii) $A_g = A_w = T_s$

(iv) $(\lambda \rho C_p)_g^{1/2} B_g = (\lambda \rho C_p)_w^{1/2} B_w$

therefore,

$$T_s - T_1 = \frac{(\lambda \rho C_p)_g^{1/2}}{(\lambda \rho C_p)_g^{1/2} + (\lambda \rho C_p)_w^{1/2}} \times (T_5 - T_1)$$

and

$$\dot{q}_w = \frac{(\lambda \rho C_p)_w^{1/2}}{(\pi t)^{1/2}} \times (T_s - T_1)$$

also,

$$T_g = T_s + (T_5 - T_s) \, erf \frac{X}{2\sqrt{a_g t}} \; ; \; T_w = T_s + (T_s - T_1) \, erf \frac{X}{2\sqrt{a_w t}}$$

It is convenient to define $\bar{T}_s = T_s - T_1$ and $\bar{T}_5 = T_6 - T_1$ so that:

$$\bar{T}_s = \frac{(\lambda\rho C_p)_g^{1/2}}{(\lambda\rho C_p)_g^{1/2} + (\lambda\rho C_p)_w^{1/2}} \times \bar{T}_5$$

and

$$\dot{q}_w = \frac{(\lambda\rho C_p)_w^{1/2}}{(\pi t)^{1/2}} \times \bar{T}_5$$

Temperature distributions in both the gas and wall are qualitatively indicated in (Figure 43).

Notice that the interfacial temperature remains at a constant value, after the heating starts. It immediately jumps to this value at the instant of reflection. The infinite rate of change necessary to accomplish this is a consequence of the infinite heat transfer rate, which acts only for this instant. That is, the singular behavior has an infinitesimal duration and it can be readily demonstrated that the singularity is integrable, yielding a parabolic variation of total heat transferred with time.

The solution would obviously be a poor approximation to the real situation for a thin end wall and/or for short times after reflection since the semi-infinite assumption would then be violated. A criterion for evaluation of the validity of the theoretical solution will now be established. It is based on the notion that as long as the distance of "thermal wave" penetration is small compared to the medium's depth, then the medium can be taken as being semi-infinite in extent for the purpose of heat transfer calculations.

The "thermal wave" is, of course, not really a wave, but rather a conceptual device used to interpret the diffusion equation solution. The exact solution implies that a perturbation at any position instantaneously affects the entire field (i.e., has an infinite propagation velocity) (Reference 31). However, since the strength of the perturbation attenuates with distance, it is convenient to define an artificial "thermal wave front" or "thermal layer thickness" representing a distance into which the thermal effect may be considered to be compressed. Let,

δ_T be the "thermal layer thickness"

so that $\delta_{T_g}(T_5 - T_s)$ - characterizes the thermal effect, "cooling wave", in the gas,

and $\delta_{T_w}(T_s - T_1)$ - characterizes the thermal effect, "heating wave", in the solid.

First, for the gas phase; this quantity can be determined simply by placing it equal to the integral of the difference between the local gas temperature, T_g, and the uncooled temperature behind the reflected shock wave, T_5.

$$\delta_{T_g}(T_5 - T_s) = \int_0^\infty (T_5 - T_g)\, dx$$

but

$$T_g = T_s + (T_5 - T_s)\, \mathrm{erf}\, \frac{x}{2\sqrt{\alpha_g t}}$$

so

$$\delta_{T_g}(T_5 - T_s) = (T_5 - T_s) \int_0^\infty \left(1 - \mathrm{erf}\, \frac{x}{2\sqrt{\alpha_g t}}\right) dx$$

or,

$$\delta_{T_g} = \int_0^\infty \mathrm{erfc}\, \frac{x}{2\sqrt{\alpha_g t}}\, dx = 2\sqrt{\alpha_g t} \int_0^\infty \mathrm{erfc}\, \frac{x}{2\sqrt{\alpha_g t}}\, \frac{dx}{2\sqrt{\alpha_g t}}$$

Let

$$\phi \equiv \frac{x}{2\sqrt{\alpha_g t}}, \quad \text{so} \quad \delta_{T_g} = 2\sqrt{\alpha_g t} \int_0^\infty \frac{2}{\pi} \int_\phi^\infty \varepsilon^{-\omega^2}\, d\omega\, d\phi$$

which can be evaluated by reversing the order of integration to find,

$$\delta_{T_g} = \frac{2}{\sqrt{\pi}} \sqrt{\alpha_g t}$$

Then, following the same procedure to evaluate the temperature effect in the end wall.

$$\delta_{T_w}(T_s - T_1) = \int_0^\infty (T_w - T_1)\, dx$$

with

$$T_w = T_s - (T_s - T_1)\, \mathrm{erf}\, \frac{x}{2\sqrt{\alpha_g t}}$$

to find that

$$\delta_{T_w} = \frac{2}{\sqrt{\pi}} \sqrt{\alpha_w t}$$

For the slug of hot gas to be effectively semi-infinite, the penetration of the cooling wave must be small compared to the total depth of the hot stagnant gas, given by the reflected shock wave position. That is,

$$U_{rs}\, t \gg \frac{2}{\pi}\sqrt{\alpha_g t}$$

where, U_{rs} is the velocity of the reflected shock wave. Therefore, the solution is valid for $t \gg \alpha_g / U_{rs}^2$. Also, the solid end wall will be effectively semi-infinite if its thickness is very much greater than $\sqrt{\alpha_w t}$.

It is interesting to note that the temperature jump experienced by the end wall will only be a few percent of the temperature jump of the shocked gas, since the quantity $(\lambda \rho C_p)$ for the gas is only a few percent of that for the solid. This is due, primarily, to the thousand-fold difference in their densities. The following example illustrates the magnitudes of the various quantities for a typical end wall heating situation.

Propellant sample - a $\frac{77\text{-}1/2}{22\text{-}1/2}$ weight ratio of ammonium perchlorate oxidizer and Paraplex P-13 binder

Shock tube operating conditions:

$$P_4 = 980 \text{ psi He};\ P_1 = 14.7 \text{ psi air};\ T_1 = 300^{\circ}\text{K}$$

Actual $M_S = 3.1$ for actual pressure ratio (P_4/P_1) of 67 (Figure 9). Actual $P_5/P_4 = 0.75$ (Figure 14). Therefore, $P_5 = 51$ atm. For $M_S = 3.1$, $T_5 = 1070^{\circ}\text{C}$ (Figure 42), so $T_5 = 1070 + 300 = 1370$. At 1370°K and 1 atmos pressure

$(\lambda \rho C_p)_g^{1/2} = 1.25 \times 10^{-4} \left(\frac{\text{cal}}{\text{cm}^2 \text{ sec}^{1/2} {}^{\circ}\text{C}}\right)$ (Table III)

Correcting for pressure $(\lambda \rho C_p)_g^{1/2} = 8.95 \times 10^{-4} \left(\frac{\text{cal}}{\text{cm}^2 \text{ sec}^{1/2} {}^{\circ}\text{C}}\right)$ (Table III)

for P-13, $(\lambda \rho C_p)_w^{1/2} = 1.36 \times 10^{-2} \left(\frac{\text{cal}}{\text{cm}^2 \text{ sec}^{1/2} {}^{\circ}\text{C}}\right)$ (Table III)

The jump of the surface temperature is given by

$$\overline{T_s} = \frac{\sqrt{(\lambda \rho C_p)_g}}{\sqrt{(\lambda \rho C_p)_w} + \sqrt{(\lambda \rho C_p)_g}} \times \overline{T_5}$$

Therefore, the surface temperature of the fuel will be:

$$\bar{T}_{s_{P-13}} = \frac{\frac{8.95}{1.36} \times 10^{-2}}{1 + \frac{8.96}{1.36} \times 10^{-2}} \times 1070 = 66.0\,(^{\circ}C)$$

Also, for the ammonium perchlorate $(\lambda \rho C_p)_{\omega}^{1/2} = 2.5 \times 10^{-2}$ (Table III)

So that,

$$\bar{T}_{s_{NH_4ClO_4}} = \frac{\frac{8.95}{2.5} \times 10^{-2}}{1 + \frac{8.95}{2.5} \times 10^{-2}} \times 1070 = 38.4\,(^{\circ}C)$$

Note that the perchlorate surface temperature jump is approximately half that of the fuel binder due to their different thermal properties.

The conditions for which the solution is valid are determined by employing the criteria that:

(1) The time must be much greater than $\frac{\alpha_g}{U_{rs}^2}$

$$\alpha_g \equiv \left(\frac{\lambda}{\rho C_p}\right)_g = \frac{(0.00019)}{(0.00025\,7)(51)(0.29)} = 0.050\,\left(\frac{cm^2}{sec}\right)$$

U_{rs} is the same magnitude as the initial shock velocity $\cong 10^5\,\left(\frac{cm}{sec}\right)$

Therefore,

$$U_{rs}^2 \cong 10^{10}$$

so

$$\frac{\alpha_g}{U_{rs}^2} \cong \frac{5 \times 10^{-2}}{10^{10}} \cong 5 \times 10^{-12}\ (sec)$$

Therefore, the solution is valid after a very small fraction of a microsecond.

(2) For an ignition testing of 5 msec the wall thickness must be much greater than

$$\frac{2}{\sqrt{\pi}}\sqrt{\alpha_w t}$$

for the P-13,

$$\alpha_w = \left(\frac{\lambda}{\rho C_p}\right)_w = \frac{.000433}{(1.122)(0.38)} = 1.01 \times 10^{-3}\left(\frac{cm^2}{sec}\right)$$

so,

$$\frac{2}{\sqrt{\pi}}\sqrt{\alpha_w t} = \frac{2}{\sqrt{\pi}}\sqrt{(1.01)(10^{-3})(5)(10^{-3})}$$

$$= 2.5 \times 10^{-3}(cm) = 25 \text{ microns}$$

Therefore, the solution is valid if the wall thickness is much greater than 25 microns. Both these conditions are met in the present ignition experiment.

The theoretical end wall temperature jumps for a series of reflecting shock Mach numbers, produced by holding the helium driving gas pressure constant at 980 psi while varying the downstream air pressure, are shown in Figure 28. They were calculated in the manner illustrated above. It is to be noticed that the temperature first increases with M_s (through the increase of $\overline{T}_5$) but eventually any further decrease in pressure necessary to produce a greater M_s results in a decrease in density (through P_5) sufficient to reduce the product $T_5 \rho_5^{1/2}$, the major factor to which the end wall temperature jump responds. The maximum theoretical temperature jump is therefore limited by the density of the shocked gas at the optimum M_s, a quantity directly proportional to P_4. Therefore, it is the mechanical strength of the shock tube which limits the surface temperature of an end wall heated by normal shock reflection.

APPENDIX B

MASS TRANSFER

When a shock wave is reflected from the end wall of a shock tube the stagnant column of hot gas left behind the retreating reflected shock wave conductively heats the end wall in a manner which produces a jump of its surface temperature level. Mathematically, this can be represented as a step function, that is, the level of the wall surface temperature instantaneously increases from its initial value to a higher value and there remains constant (Appendix A). The heating causes a decomposition of both the fuel binder and oxidizer crystals of a solid composite propellant, when integrally mounted flush with the end wall. The rate of thermal decomposition of each of these particular substances depends on their respective surface temperatures, in a manner usually expressed as an Arrhenius function, according to Reference 40,

$$r = A \exp\left(\frac{-E}{RT_s}\right)$$

where: r is the linear regression rate of the heated surface.

A is the pre-exponential factor.

E is the "activation energy" for decomposition.

T_s is the absolute surface temperature.

R is the universal gas constant.

Therefore, for the case of interest (T_s = const.),the surface decomposition will take place at a constant rate.

The propagation of these decomposition products into the stagnant gas will be analyzed in this section.

The mechanism of propagation is by gaseous diffusion. Mathematically the process can be represented by the Fourier Equation as demonstrated by Fick (Reference 41). That is, for the one-dimensional case,

$$\frac{\partial C}{\partial t} = D \frac{\partial^2 C}{\partial X^2}$$

APPENDIX B

MASS TRANSFER

When a shock wave is reflected from the end wall of a shock tube the stagnant column of hot gas left behind the retreating reflected shock wave conductively heats the end wall in a manner which produces a jump of its surface temperature level. Mathematically, this can be represented as a step function, that is, the level of the wall surface temperature instantaneously increases from its initial value to a higher value and there remains constant (Appendix A). The heating causes a decomposition of both the fuel binder and oxidizer crystals of a solid composite propellant, when integrally mounted flush with the end wall. The rate of thermal decomposition of each of these particular substances depends on their respective surface temperatures, in a manner usually expressed as an Arrhenius function, according to Reference 40,

$$r = A \exp\left(\frac{-E}{RT_s}\right)$$

where: r is the linear regression rate of the heated surface.

A is the pre-exponential factor.

E is the "activation energy" for decomposition.

T_s is the absolute surface temperature.

R is the universal gas constant.

Therefore, for the case of interest (T_s = const.), the surface decomposition will take place at a constant rate.

The propagation of these decomposition products into the stagnant gas will be analyzed in this section.

The mechanism of propagation is by gaseous diffusion. Mathematically the process can be represented by the Fourier Equation as demonstrated by Fick (Reference 41). That is, for the one-dimensional case,

$$\frac{\partial C}{\partial t} = D \frac{\partial^2 C}{\partial X^2}$$

where: C is the concentration of diffusing substance.

X is the space coordinate.

t is time.

D is the diffusivity of the vaporized material in the stagnant test gas.

General solutions to this equation can be obtained for a variety of initial and boundary conditions (References 16, 17). Some specific solutions containing boundary conditions peculiar to diffusional phenomena are also available. (Reference 42).

The current problem can be idealized as a mass source of constant strength instantaneously placed at the bounding surface, X = 0, of a semi-infinite gaseous medium at t = 0. The semi-infinite assumption will be justified later. As the injected mass diffuses away from the boundary its concentration can be represented, as demonstrated (Reference 42), by the relation,

$$C(X,t) = \frac{\dot{m}\, t^{1/2}}{D^{1/2}} \times 2\,\mathrm{ierfc}\,\frac{X}{2\sqrt{Dt}}$$

where: $\dot{m}$ is the mass influx per unit area.

The propellants whose experimental ignition characteristics are reported herein were formulated with fuel components which vaporize much more readily than the ammonium perchlorate oxidizer crystals (Figure 29) for surface temperatures below about 600°K. Further, when these are subjected to heating by shock reflection, the temperature of the fuel surface will be higher than that of the oxidizer crystals (Appendix A), a situation which amplifies this imbalance of vaporization rates. Therefore, it is reasonable to neglect the small quantity of the oxidizer gas which is vaporized and consider that the diffusing gas is composed of only the vaporized fuel component. The presence of the oxidizer is taken into account only as a factor which reduces the percentage of propellant surface occupied by the fuel, that is, as a "blockage" effect. This can be characterized as the volumetric fraction of fuel in the test propellant. The rate of fuel vapor injection from a shock heated propellant surface can be represented as

$$\dot{m}_f = \nu \rho_f r_f = \nu \rho_f A_f \exp\left(\frac{-E_a}{RT_{sf}}\right)$$

where: ν = Volumetric fraction of fuel in propellant.

ρ_f = Density of fuel component.

A_f = Pre-exponential factor for fuel vaporization.

E_f = "Activation energy" for fuel decomposition.

T_{sf} = Surface temperature of fuel component.

Replacing the $\dot{m}$ with $\dot{m}_f$ in the above equation results in an equation for the distribution of the fuel vapor. One obtains,

$$C_f(x,t) = \frac{\sqrt{\rho_f A_f}}{D_{fg}^{1/2}} \exp\left(\frac{-E_f}{RT_{sf}}\right) \times 2t^{1/2}\, \text{ierfc}\, \frac{x}{2\sqrt{D_{fg}t}}$$

where: $C_f(x,t)$ is the concentration of the vaporized fuel component at any position and time; D_{fg} is the diffusivity of the vaporized fuel component into the ignition gas.

Here, as in Appendix A, the semi-infinite assumption has been made in order to obtain a simple mathematical solution. Therefore, a criterion must be established, similar to that developed in Appendix A, which will indicate when the solution is a valid approximation of the actual situation. If a "concentration wave" is defined as having an average concentration equal to the fuel concentration at the lean combustion limit C_{fl} then the thickness of the wave, δ_c, will be given by

$$\delta_c = \frac{1}{C_{fl}} \int_0^\infty C_f(x,t)\, dx = \frac{1}{C_{fl}} \int_0^\infty \frac{2\dot{m}_f t^{1/2}}{D_{fg}^{1/2}}\, \text{ierfc}\, \frac{x}{2\sqrt{D_{fg}t}}\, dx$$

$$= \frac{1}{C_{fl}} \times \frac{2\dot{m}_f \times \sqrt{D_{fg}t}}{D_{fg}^{1/2}} \times 2 \times t^{1/2} \times \text{ierfc}\, \frac{x}{2\sqrt{D_{fg}t}} \Bigg|_{x=0}^{x=\infty}$$

$$= \frac{\dot{m}_f t}{C_{fl}}$$

Now, the solution based on the semi-infinite assumption is valid when the reflected shock is much farther from the end wall than the concentration wave.

$$\delta_c \ll U_{rs}\, t$$

$$\frac{\frac{\dot{m}_f}{C_{fl}}}{U_{rs}} \ll 1$$

Therefore, the solution would be valid from the instant of shock reflection, for injection rates which are not too large. Conversely, it would never be a good approximation for high rates of mass injection.

The following example will illustrate the magnitudes of the quantities to be expected for a typical end wall heating produced by normal shock reflection. The exposure condition is selected to be the same as that employed in Appendix A, [(i.e., the Batch #6 propellant (77-1/2% ammonium perchlorate) mounted in the end wall of a shock tube which reflects a $M_s = 3.1$ shock wave], Theoretically, a 66.0°C temperature rise is predicted for the surface of the binder and a 38.4°C increment for that of the perchlorate crystal. The actual temperature rise is experimentally found to be twice this value (Section II, 4). Therefore, if mounted in the actual shock tube the surface temperatures would be

$$T_{sf} = 430^{\circ}K;\ T_{so} = 376.8^{\circ}K$$

from Reference 43, which is reproduced in Figure 4.

$$r_f = 5.52 \times 10^{-5}\ \frac{cm}{sec}$$

Data presented in References (29 &40) indicate that $r_o = 5 \times 10^{-8}$ cm/sec for the ammonium perchlorate. Therefore, since the densities of the two materials are about the same ($\rho_f = 1.122\ (\frac{gm}{cm^3})$; $\rho_o = 1.96\ (\frac{gm}{cm^3})$) and the linear regression ratesof the respective surfaces differ by a factor of 1000, then the mass rate of oxidizer gas generation is only about 1/1000 the rate of fuel gas generation, and can justifiably be neglected. Its presence in the solid mixture merely reduces the percentage of surface area available for fuel vaporization. The fraction of the total propellant surface area occupied by the fuel is equivalent to the fuel's volumetric percentage in the particular propellant formulation: Thusly,

$$\nu = \frac{\dfrac{\text{fuel wt. fraction}}{\text{density of fuel}}}{\dfrac{\text{fuel wt. fraction}}{\text{density of fuel}} + \dfrac{\text{oxidizer wt. fraction}}{\text{density of oxidizer}}}$$

$$= \frac{\dfrac{0.225}{1.122}}{\dfrac{0.225}{0.122} + \dfrac{0.775}{1.96}} = 0.30$$

Unfortunately, the exact chemical nature of the decomposition vapors which emerge from the fuel surface is unknown; certainly they cannot have a molecular weight as large as the solid polymer. For the purpose of numerical illustration they will be assumed to have the molecular weight and other properties of propane.

The diffusivity of propane into air at standard conditions is given (Reference 33) as,

$$D_{fg} = 0.1 \left(\frac{cm^2}{sec}\right)$$

When corrected (Reference 34) for the conditions behind the reflected shock wave employed in the illustrative example ($M_s = 3.1$; $P_1 = 1$ atmos) it becomes,

$$D_{fg} = (0.1)\left(\frac{T_s}{T_1}\right)^{1.75}\left(\frac{\rho_1}{\rho_s}\right)$$

$$= (0.1)\left(\frac{1370}{300}\right)^{1.75}\left(\frac{1.23 \times 10^{-3}}{1.31 \times 10^{-2}}\right) = 0.133\left(\frac{cm^2}{sec}\right)$$

Now, evaluating the above criterion,

$$\frac{\frac{\dot{m}_f}{C_{fl}}}{U_{rs}} \ll 1$$

$$\frac{\frac{1.86 \times 10^{-5}}{3.12 \times 10^{-7}}}{10^{10}} = \frac{0.6 \times 10^2}{10^{10}} \cong 10^{-8} \ll 1$$

Therefore, the mathematical solution is valid for this case.

TABLE I

Flow Quantities on the High Pressure Side of Shock Waves in Air with Temperature Dependent Specific Heat

M_s	$\frac{\rho_2}{\rho_1}$	T_2	$\frac{P_2}{P_1}$
1.523	1.907	400	2.54
1.984	2.659	500	4.43
2.377	3.225	600	6.45
2.725	3.663	700	8.55
3.041	4.015	800	10.71
3.331	4.314	900	12.94
3.611	4.540	1000	15.23
4.235	5.069	1250	21.12
4.797	5.454	1500	27.27
5.307	5.746	1750	33.52
5.778	5.978	2000	39.85
6.643	6.359	2500	53.00
7.453	6.685	3000	67.00
8.315	7.122	3500	84.10
9.297	7.697	4000	106.00
10.410	8.385	4500	134.40
11.595	9.136	5000	168.40

TABLE II

Propellant, Fuel and Inhibitor Compositions

All formulations were manufactured in the solid propellant facilities of the Aeronautical Engineering Department, Princeton University.

Batch No. 6 Propellant	
Ammonium Perchlorate (bimodal mix)	77.50%
Polystyrene Resin (Rohm and Haas P-13)	22.20%
Nuodex Cobalt	0.12%
Lecithin B-60	0.12%
Lupersol D.D.M.	0.06%
(cure for 24 hr. at 185°F)	
Batch No. 23 Propellant	
Ammonium Perchlorate (bimodal mix)	78.70%
Epoxy Resin (Shell Epon 562)	19.65%
Triethylene Tetramine	0.18%
Ferric Oxide	1.47%
(cure for 24 hr. at 185°F)	
Batch No. 33 Propellant	
Ammonium Perchlorate (bimodal mix)	79.7 %
Epoxy Resin (Shell Epon 562)	20.0 %
Triethylene Tetramine	0.3 %
(cure for 24 hr. at 180°F)	
P-13 Fuel Sample used for Pyrolysis Measurements	
Polystyrene Resin (Rohm and Haas P-13)	98.50%
Nuodex Cobalt	0.25%
Lupersol D.D.M.	1.25%
(cure for 1 wk. at 185°F)	
Epoxy Fuel Sample used for Pyrolysis Measurements	
Epoxy Resin (Shell Epon 562)	95.00%
Triethylene Tetramine	5.00%
(cure for 1wk. at 185°F)	

The inhibitor which was used to pot the end wall samples contained the following ingredients.

Polystyrene Resin (Rohm & Haas, P-13)	63.900%
Asbestos	5.650%
Talc	28.210%
Lupersol D.D.M.	1.875%
Nuodex Cobalt	0.375%

TABLE III

THERMAL PROPERTIES OF SELECTED MATERIALS

MATERIAL	λ $\left(\frac{cal}{cm\,sec\,^{\circ}C}\right)$	ρ $\left(\frac{gm}{cm^3}\right)$	C_p $\left(\frac{cal}{gm\,^{\circ}C}\right)$	$(\lambda \rho C_p)^{1/2}$ $\left(\frac{cal}{cm^2\,sec^{1/2}\,^{\circ}C}\right)$
Plexiglas II U.V.A. at 25°C (Ref. 35)	0.00446	1.19	0.35	1.36×10^{-2}
Paraplex P-13 Type Polymer at 25°C (Ref. 36)	0.00433	1.122	0.38	1.36×10^{-2}
Binder (A) at 25°C (Ref. 37)	0.00456	1.23	0.40	1.50×10^{-2}
NH_4CLO_4 at 25°C (Ref. 37)	0.00134	1.96	0.24	2.50×10^{-2}
Pyrex Type 7740 Borosilicate at 25°C (Ref. 38)	0.00230	2.35	0.20	3.28×10^{-2}
Air 14.7 psi at 1370°K (Ref. 32, 39)	0.00019	0.000257	.290	1.25×10^{-4}* at 1400°K

*This value is constant (within ± 2%) between 400°K and 2000°K

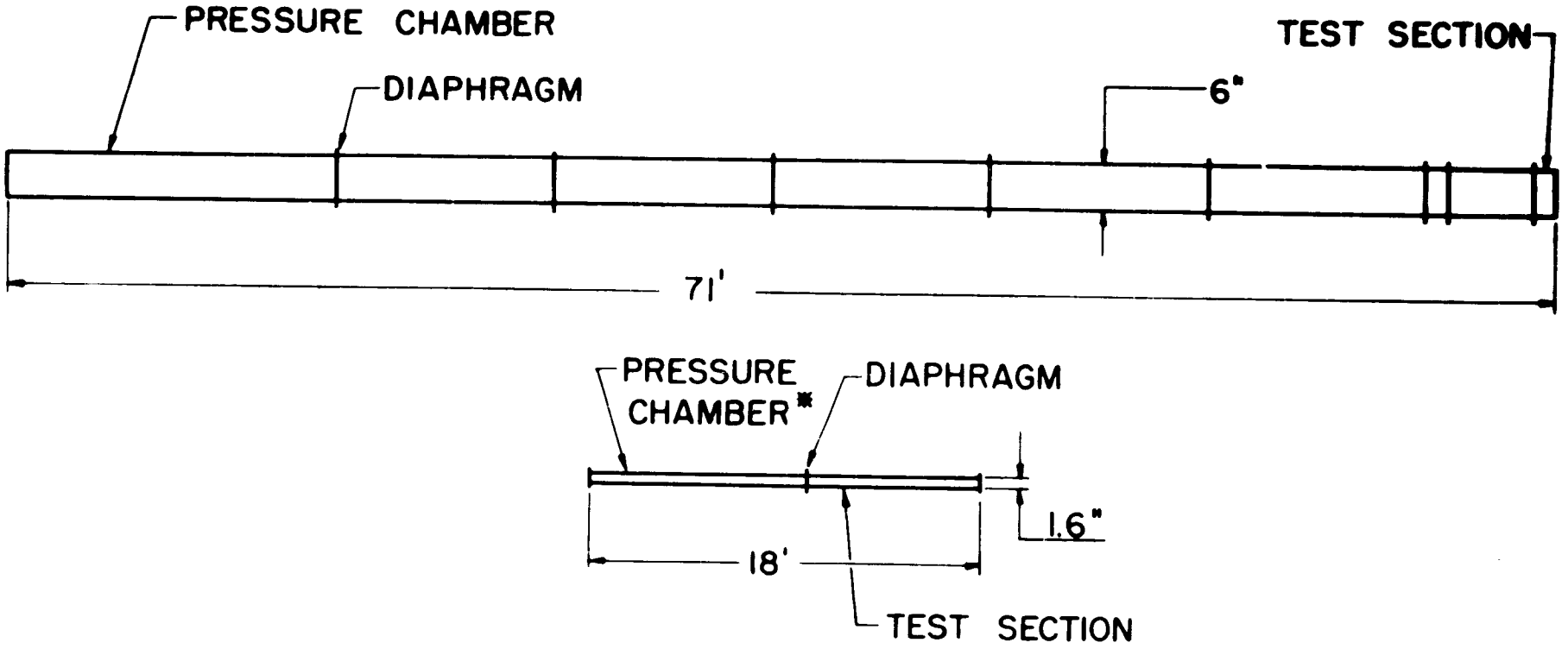

*TUBE IS DESIGNED TO PERMIT INTERCHANGE OF PRESSURE AND TEST SECTION

DRAWN TO SCALE AS FOLLOWS
LENGTH - 80:1
DIAMETER - 20:1

FIG. 1 COMPARISON OF SHOCK TUBES

FIGURE 2
TYPICAL WAVE DIAGRAM AND PRESSURE PROFILES FOR IGNITION SHOCK TUBE OPERATION

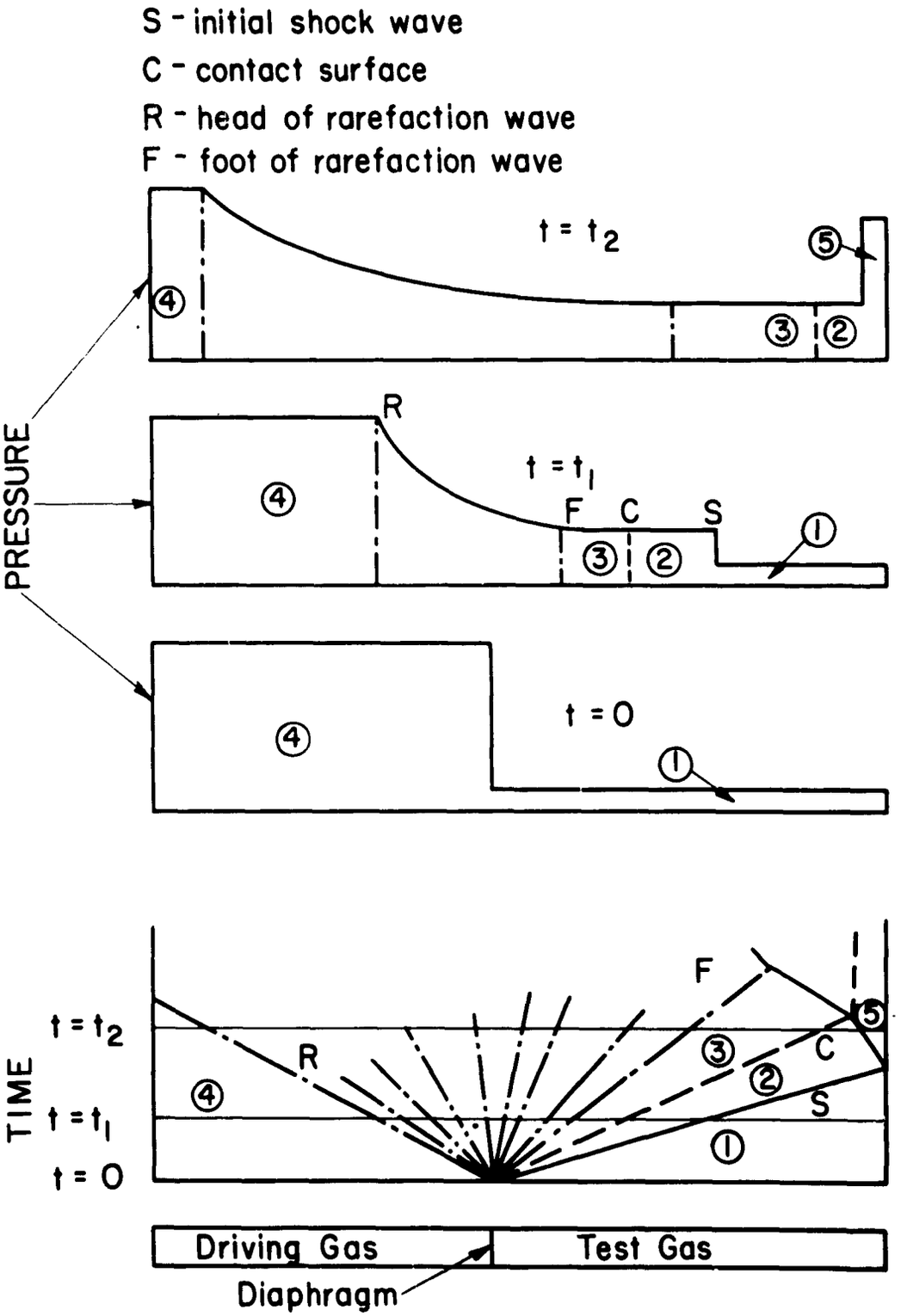

JPR 530

FIGURE 3
VARIATION OF INITIAL SHOCK WAVE PRESSURE RATIO WITH DIAPHRAGM PRESSURE RATIO FOR AIR/AIR AND HELIUM/AIR

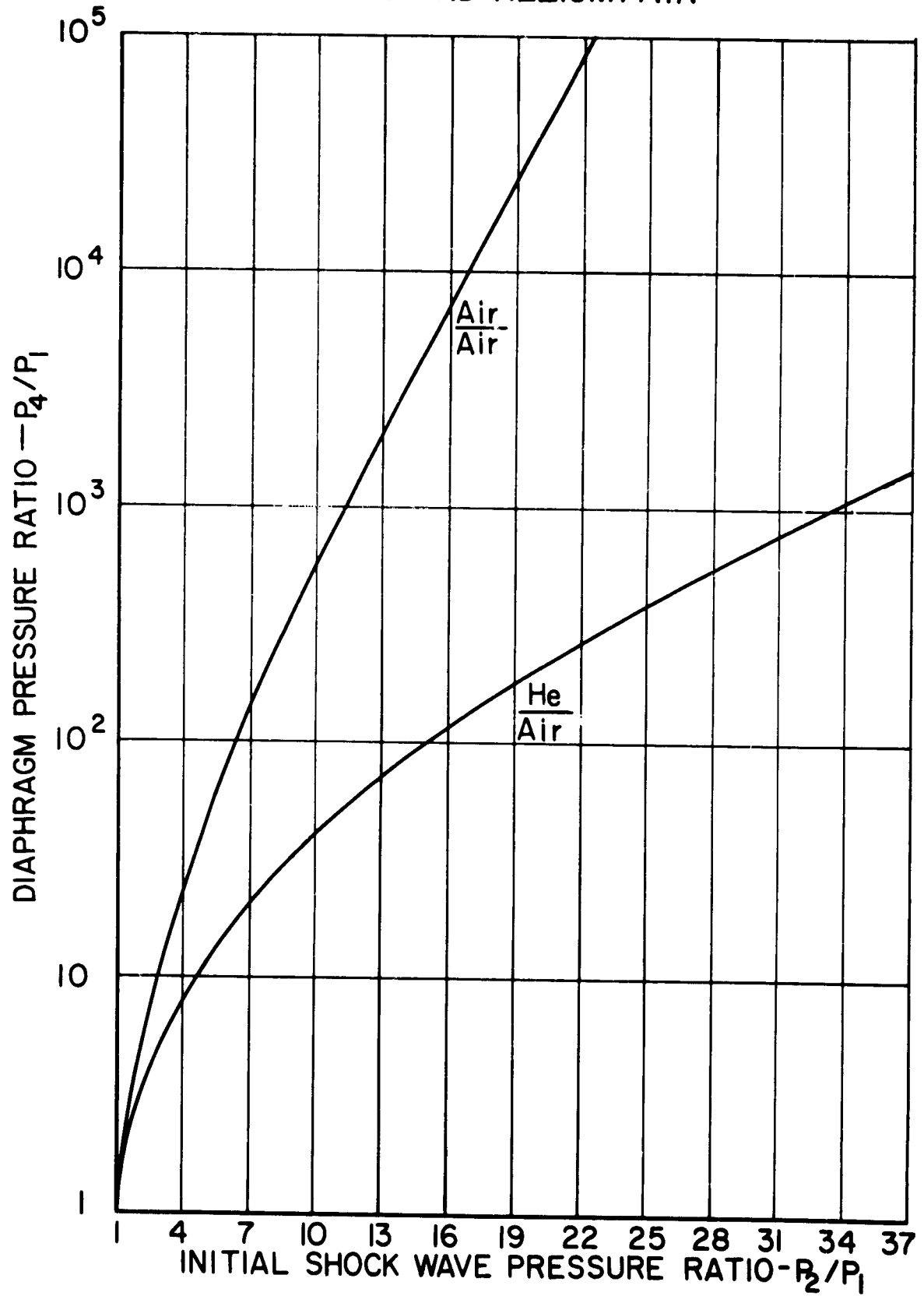

JPR 529

FIGURE 4
VARIATIONS OF THE FLOW PARAMETERS IN AIR BEHIND A NORMAL REFLECTED SHOCK WAVE VS INCIDENT SHOCK WAVE MACH NUMBER FOR VARIABLE SPECIFIC HEAT

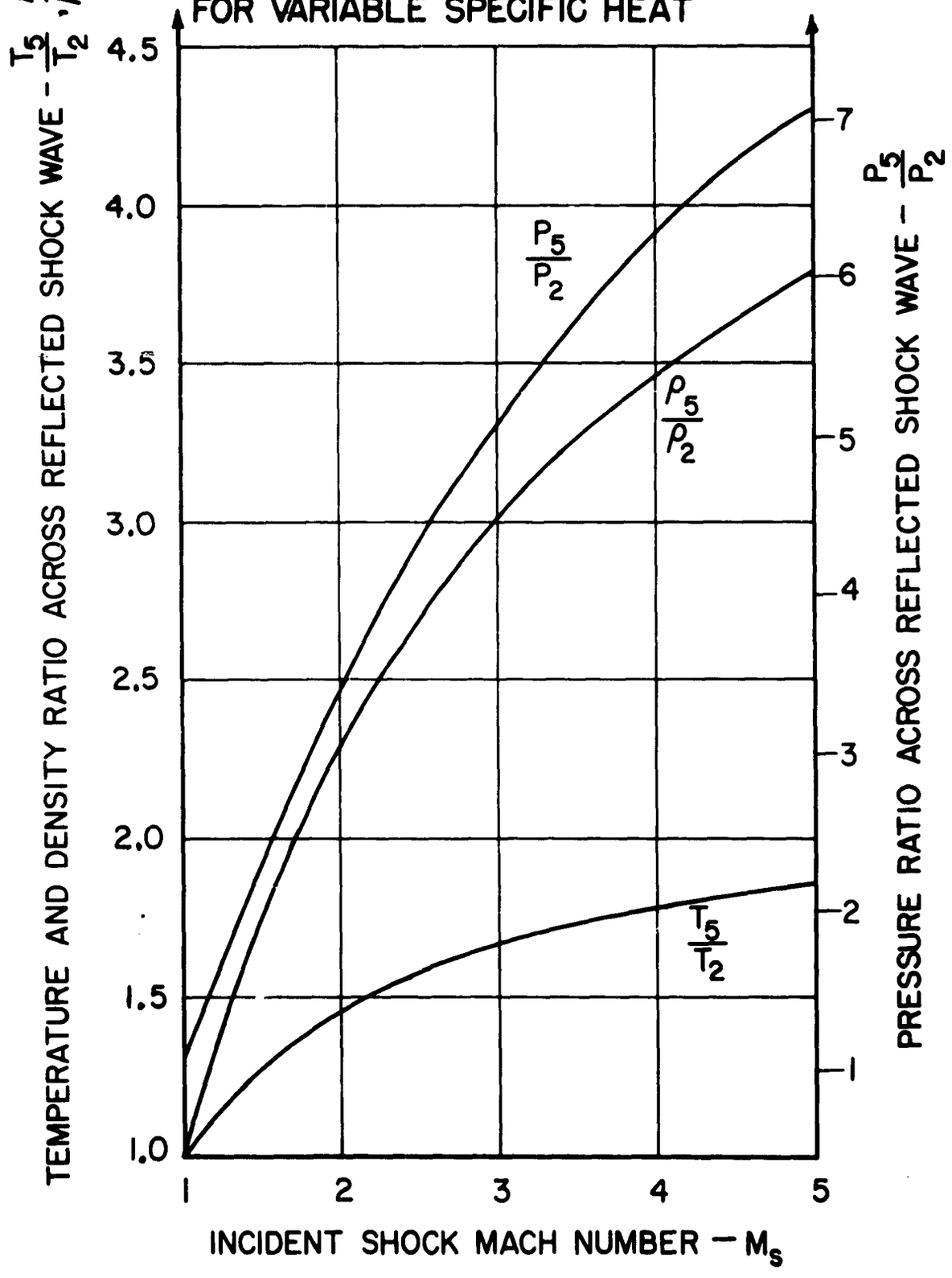

JPR 528

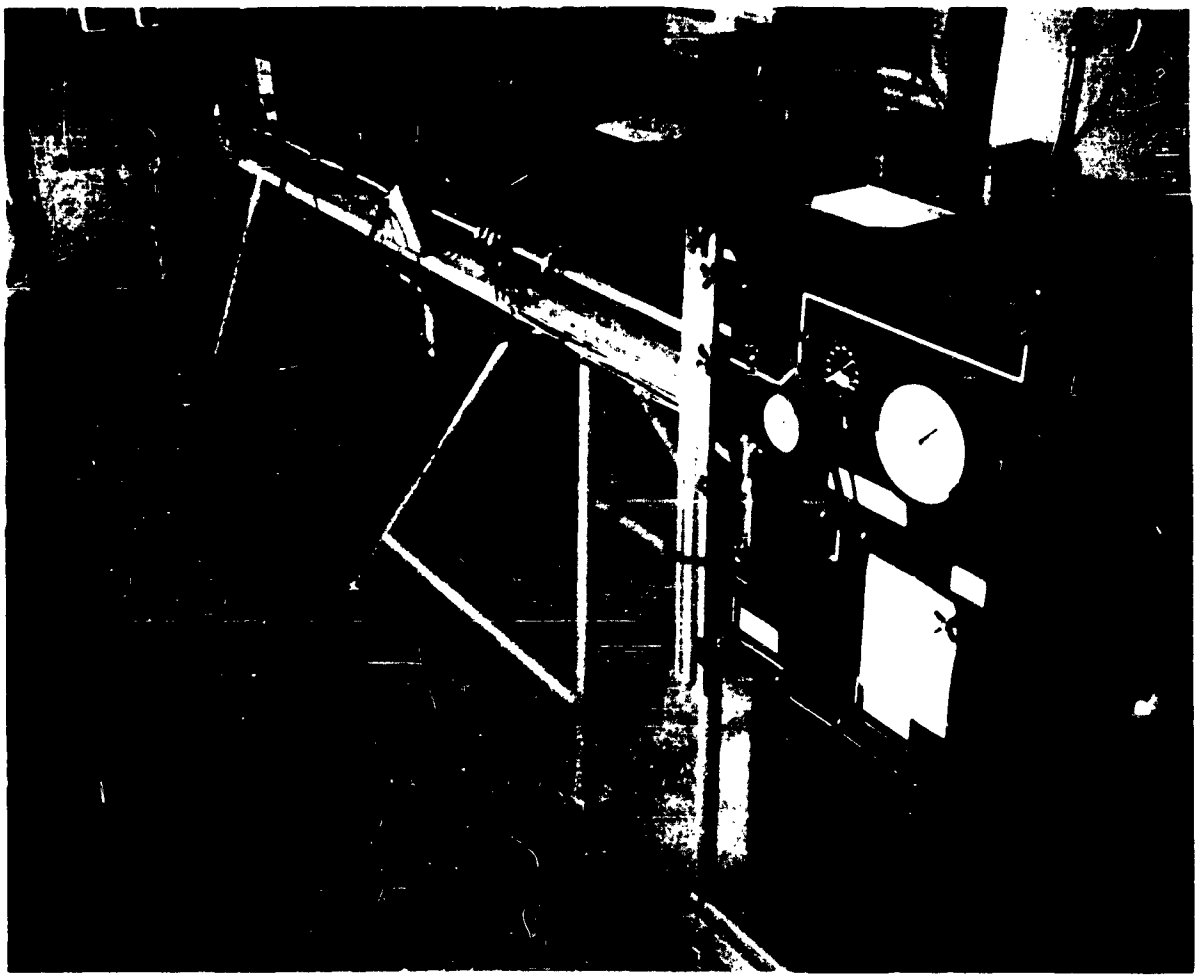

FIG. 5 1.6" I.D. SHOCK TUBE

FIGURE 6

DIAPHRAGM THICKNESS vs BURST PRESSURE IN 1.6" DIA. SHOCK TUBE FOR 3003-O AND 3003-H14 TYPE ALUMINUM

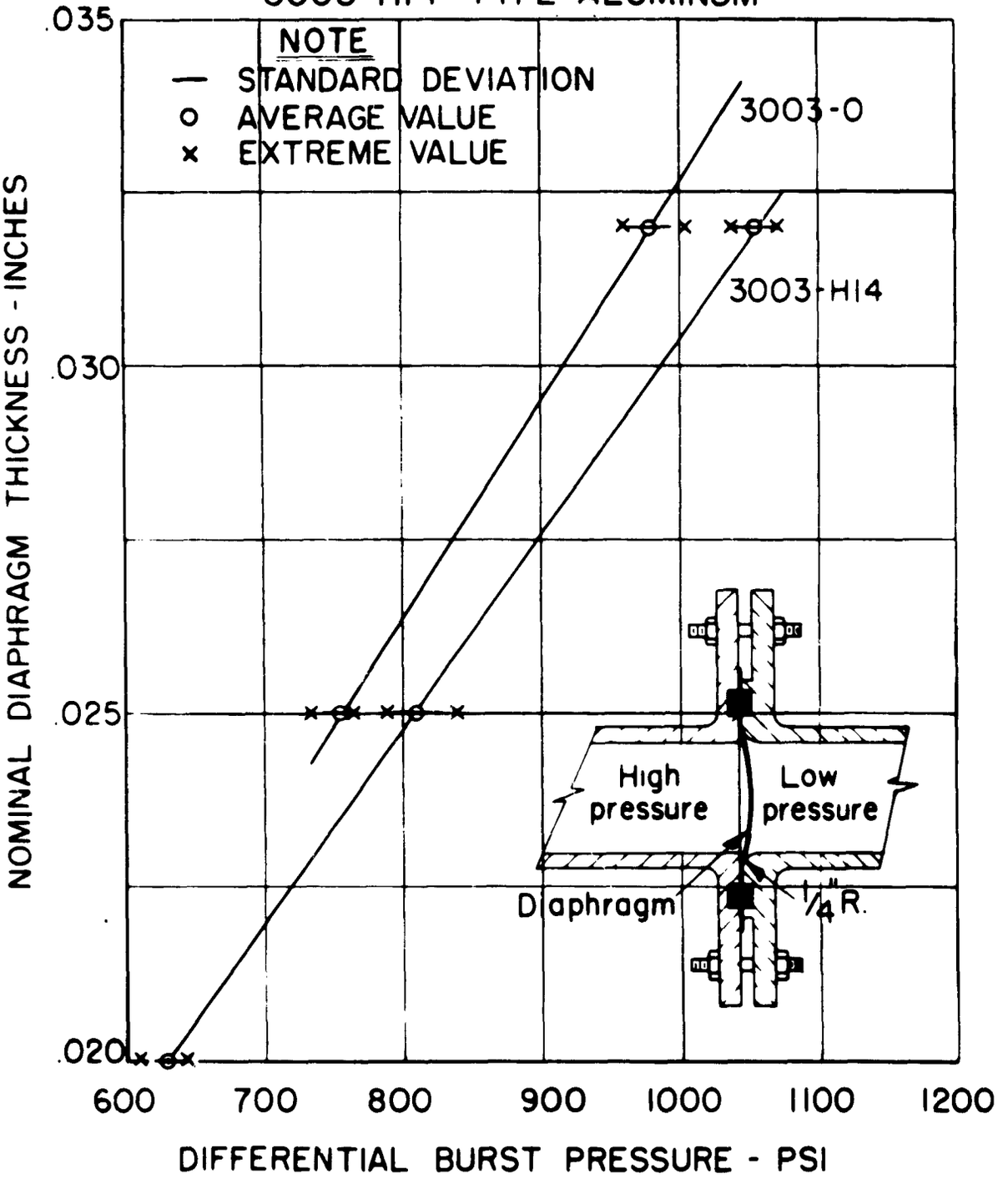

JPR 224

FIG. 7 PLATINUM FILM HEAT TRANSFER GAGE

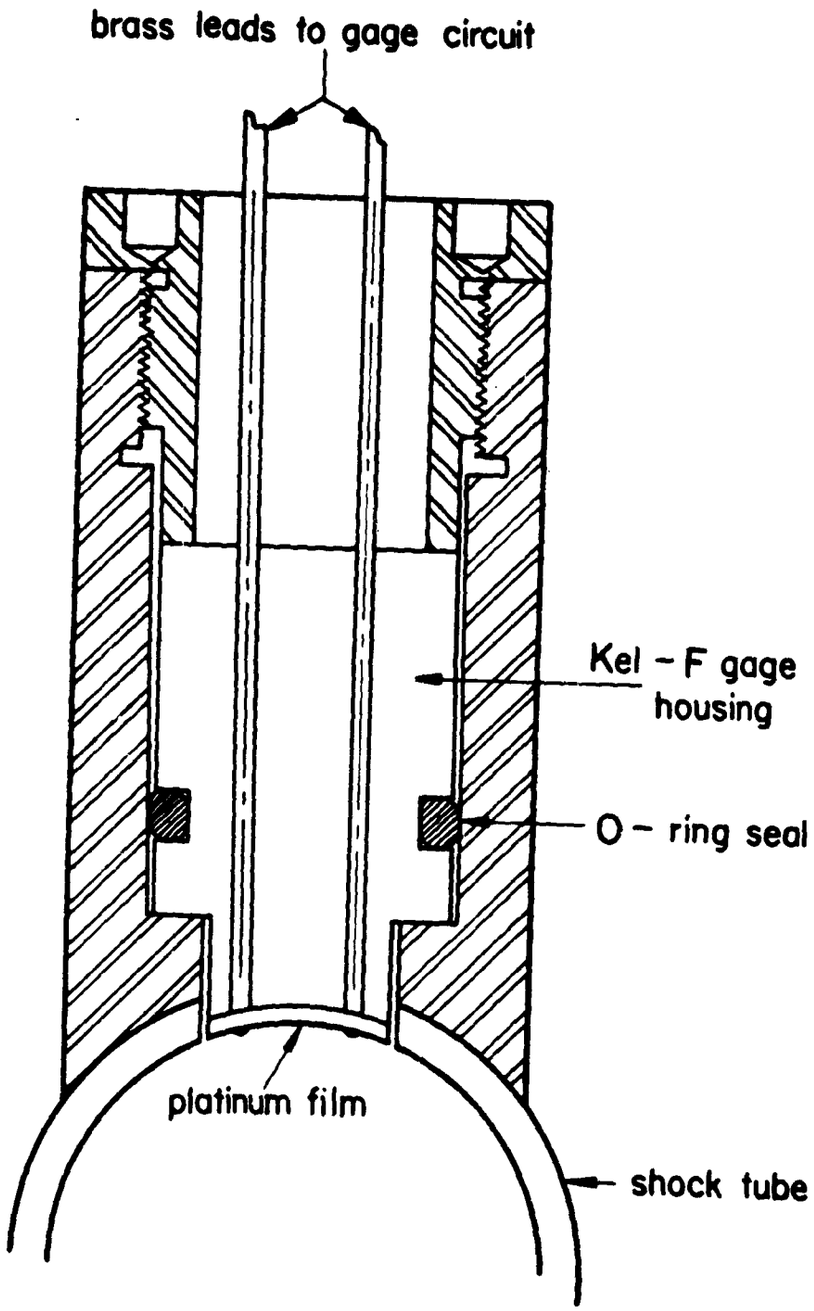

FIGURE 7a INSTRUMENTION PORT SHOWING INSTALLATION OF PLATINUM FILM HEAT TRANSFER GAUGE

JPR 482

INSTRUMENTATION SCHEMATIC FOR SHOCK TUBE VELOCITY MEASUREMENT
FIGURE 8

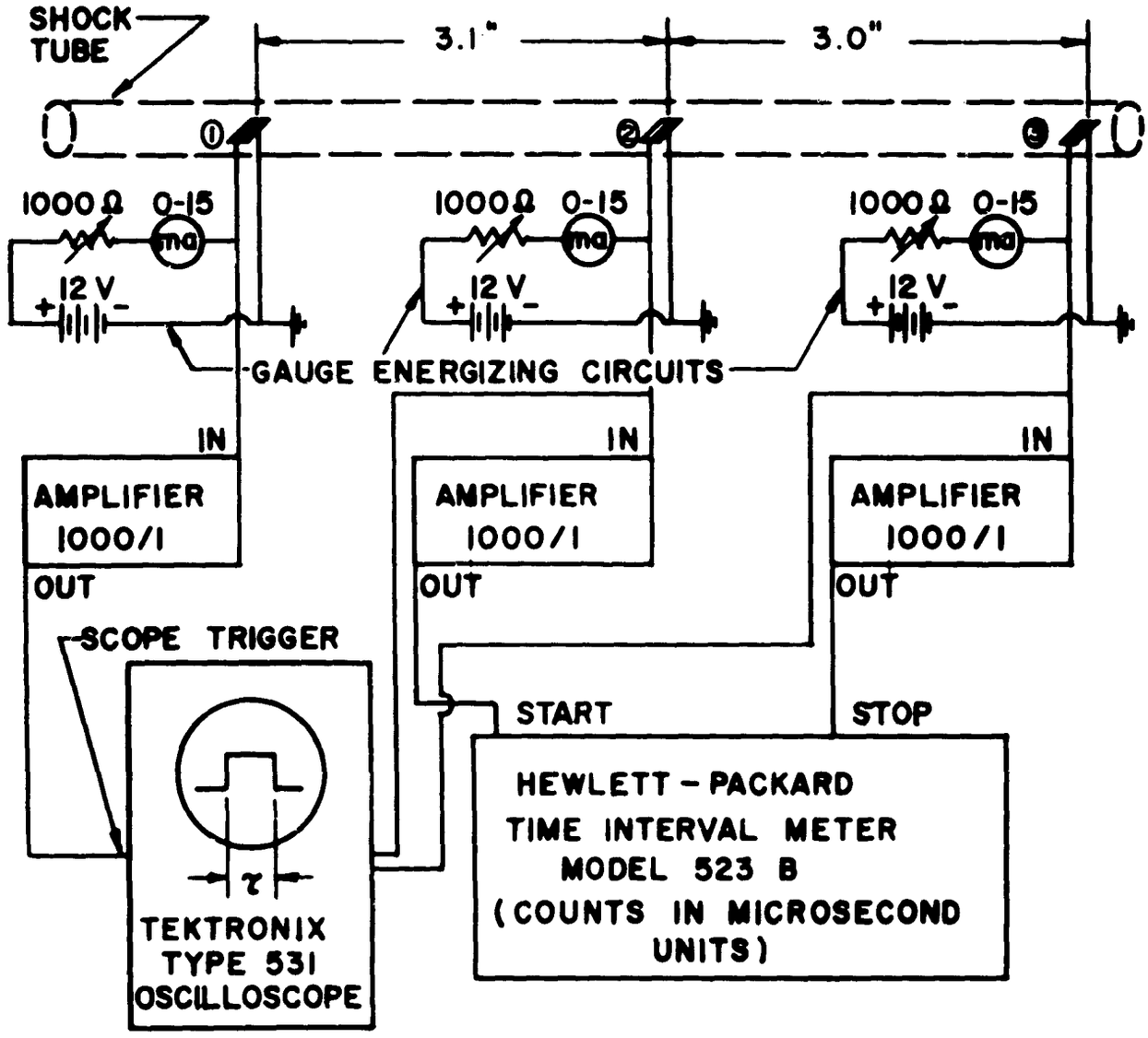

1) GAUGE ① AMPLIFIED OUTPUT TRIGGERS OSCILLOSCOPE
2) GAUGE ② AMPLIFIED OUTPUT STARTS TIME INTERVAL METER, UNAMPLIFIED OUTPUT DISPLAYED ON SCOPE
3) GAUGE ③ AMPLIFIED OUTPUT STOPS TIME INTERVAL METER, UNAMPLIFIED OUTPUT DISPLAYED ON SCOPE

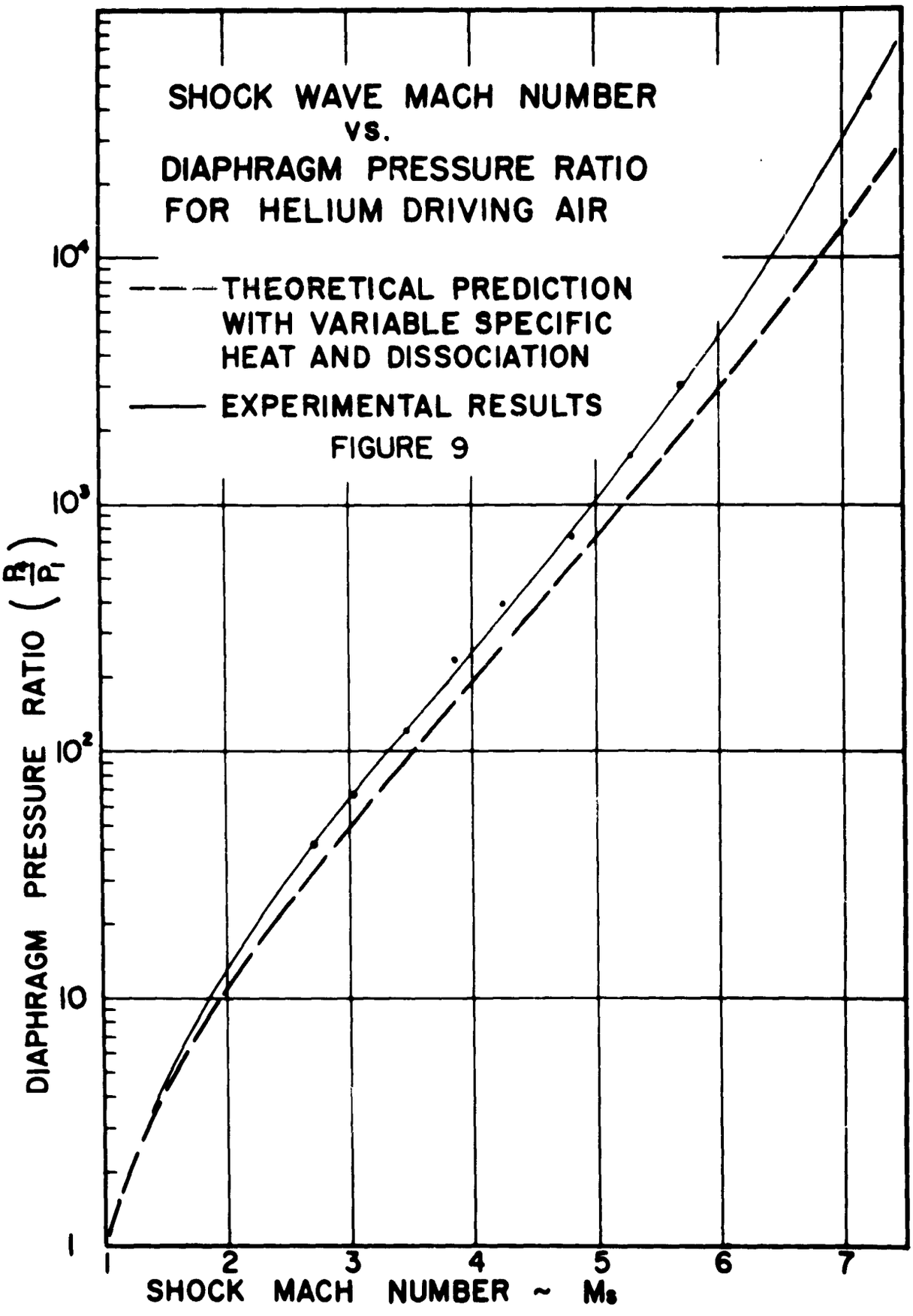
SHOCK WAVE MACH NUMBER
VS.
DIAPHRAGM PRESSURE RATIO
FOR HELIUM DRIVING AIR
THEORETICAL PREDICTION WITH VARIABLE SPECIFIC HEAT AND DISSOCIATION
EXPERIMENTAL RESULTS
FIGURE 9
DIAPHRAGM PRESSURE RATIO ($\frac{P_4}{P_1}$)
10^4
10^3
10^2
10
1
1
2
3
4
5
6
7
SHOCK MACH NUMBER ~ M_s

JPR 227

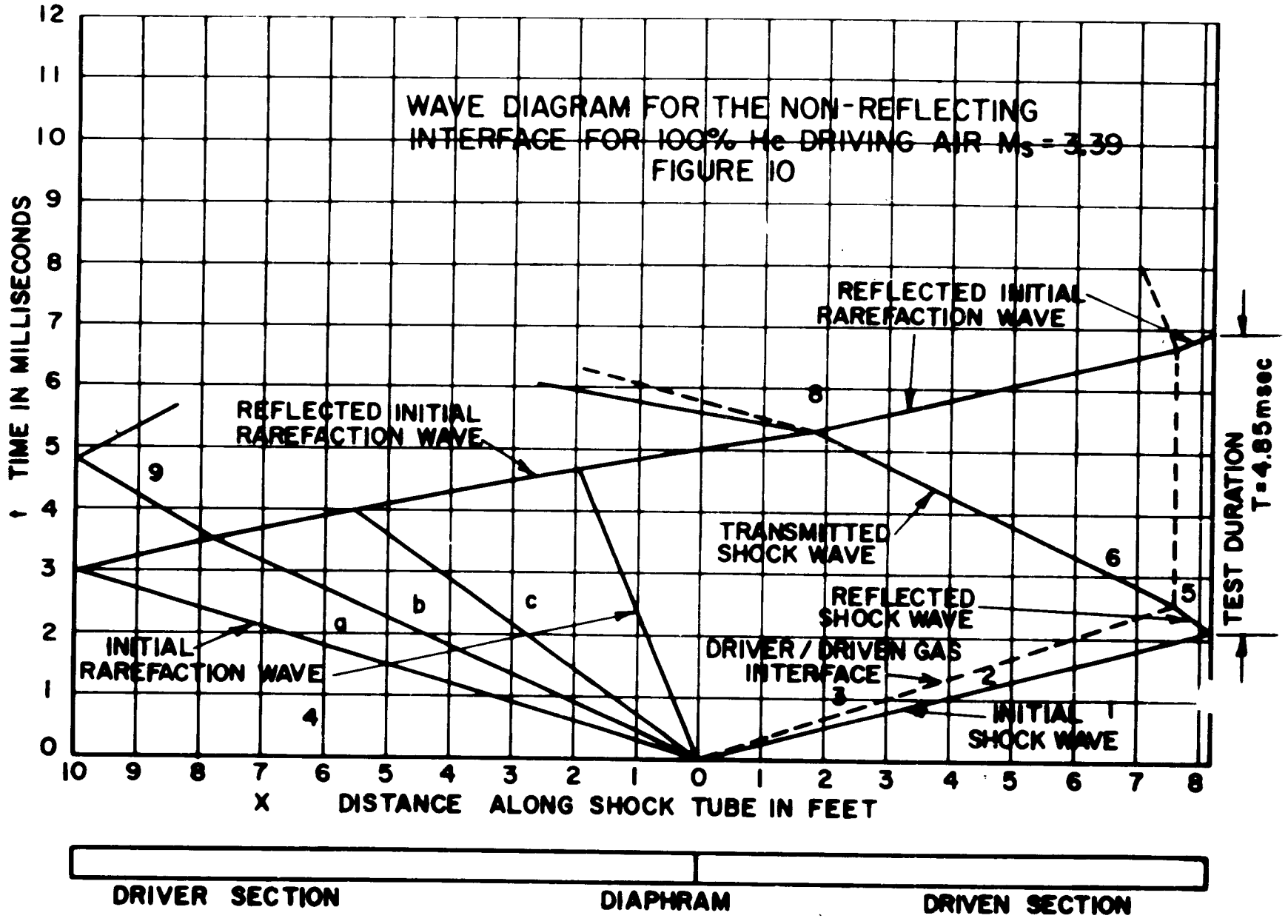
WAVE DIAGRAM FOR THE NON-REFLECTING INTERFACE FOR 100% He DRIVING AIR $M_s = 3.39$
FIGURE 10
t TIME IN MILLISECONDS
X DISTANCE ALONG SHOCK TUBE IN FEET
REFLECTED INITIAL RAREFACTION WAVE
REFLECTED INITIAL RAREFACTION WAVE
TRANSMITTED SHOCK WAVE
REFLECTED SHOCK WAVE
DRIVER / DRIVEN GAS INTERFACE
INITIAL SHOCK WAVE
INITIAL RAREFACTION WAVE
TEST DURATION T=4.85msec
DRIVER SECTION
DIAPHRAM
DRIVEN SECTION

INSTRUMENTATION SCHEMATIC FOR SHOCK TUBE PRESSURE AND RADIATION MEASUREMENT
FIGURE II

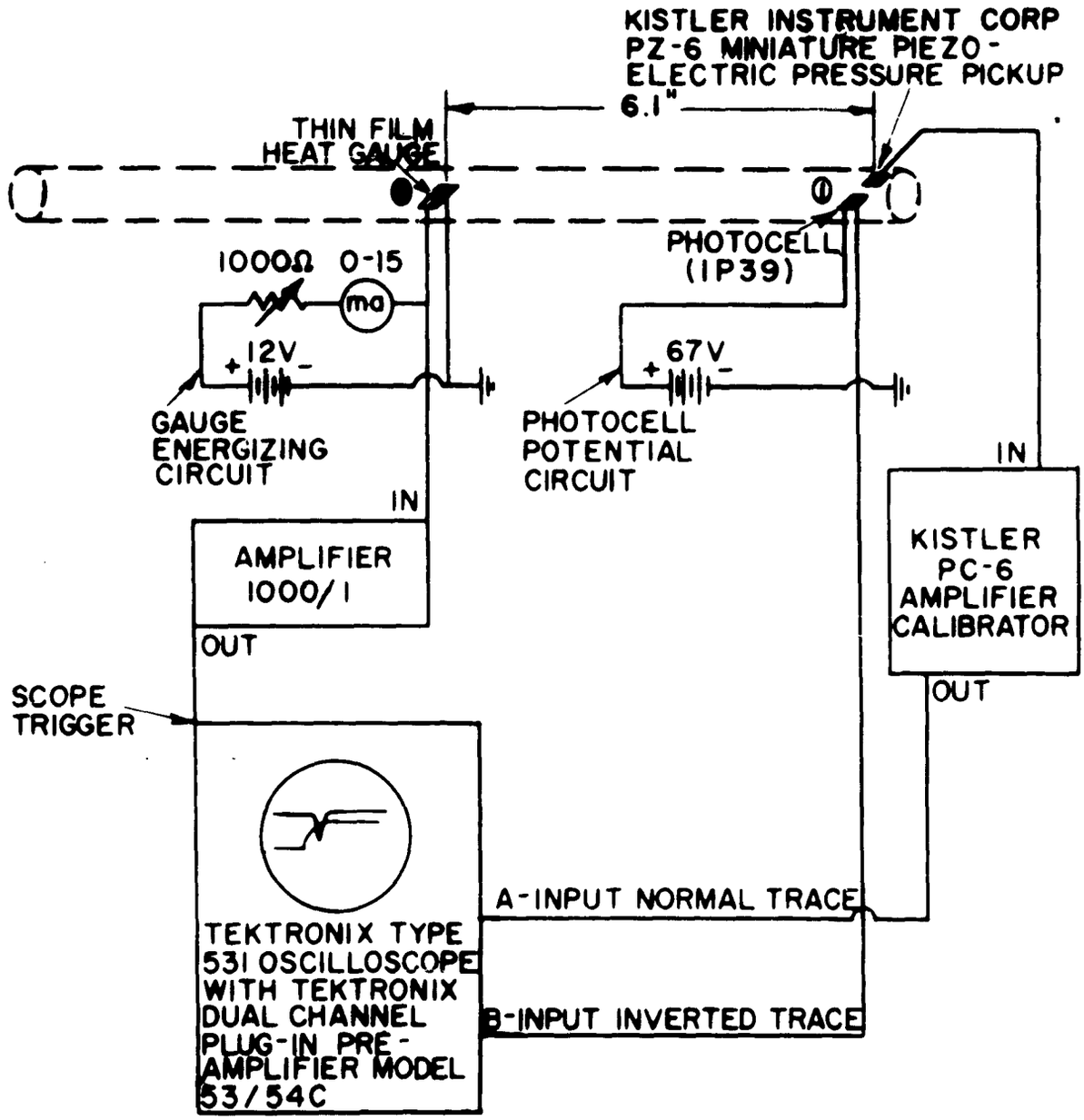

1) GAUGE ❶ AMPLIFIED OUTPUT TRIGGERS OSCILLOSCOPE

2) PHOTOCELL OUTPUT DISPLAYED ON OSCILLOSCOPE

3) PRESSURE PICKUP OUTPUT DISPLAYED ON OSCILLOSCOPE

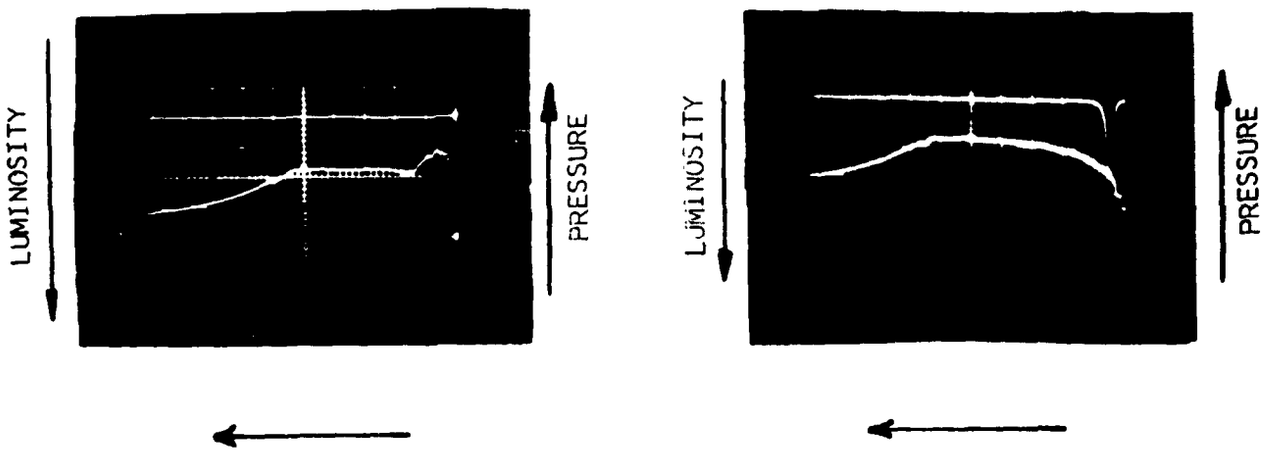

Sweeprate:	1 millisecond/division	Sweeprate:	1 millisecond/division
Vertical Deflection:	Pressure 207.7 psi/division	Vertical Deflection:	Pressure 207.7 psi/division
	Radiation 50 mv/division		Radiation 100 mv/division
$M_s = 2.7$	$P_4 = 635$ psia	$M_s = 4.76$	$P_4 = 625$ psia
$P_{4/p_1} = 42$	Helium/air	$P_{4/p_1} = 735$	Helium/air

FIGURE 12

PRESSURE-TIME AND RADIATION-TIME TRACES BEHIND THE REFLECTED SHOCK WAVE

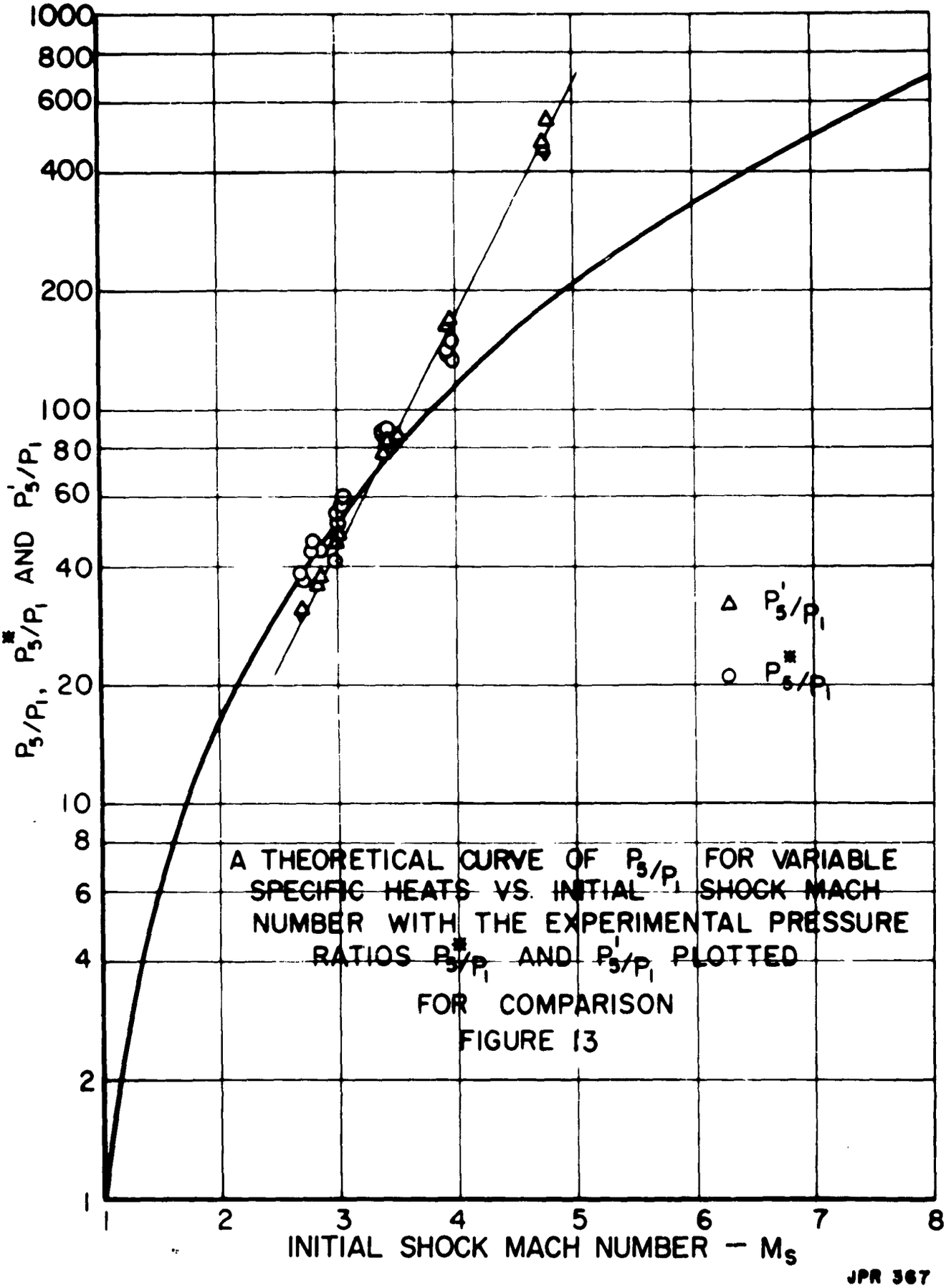

A THEORETICAL CURVE OF P_5/P_1 FOR VARIABLE SPECIFIC HEATS VS. INITIAL SHOCK MACH NUMBER WITH THE EXPERIMENTAL PRESSURE RATIOS P_5^*/P_1 AND P_5'/P_1 PLOTTED FOR COMPARISON

FIGURE 13

JPR 367

JPP 542

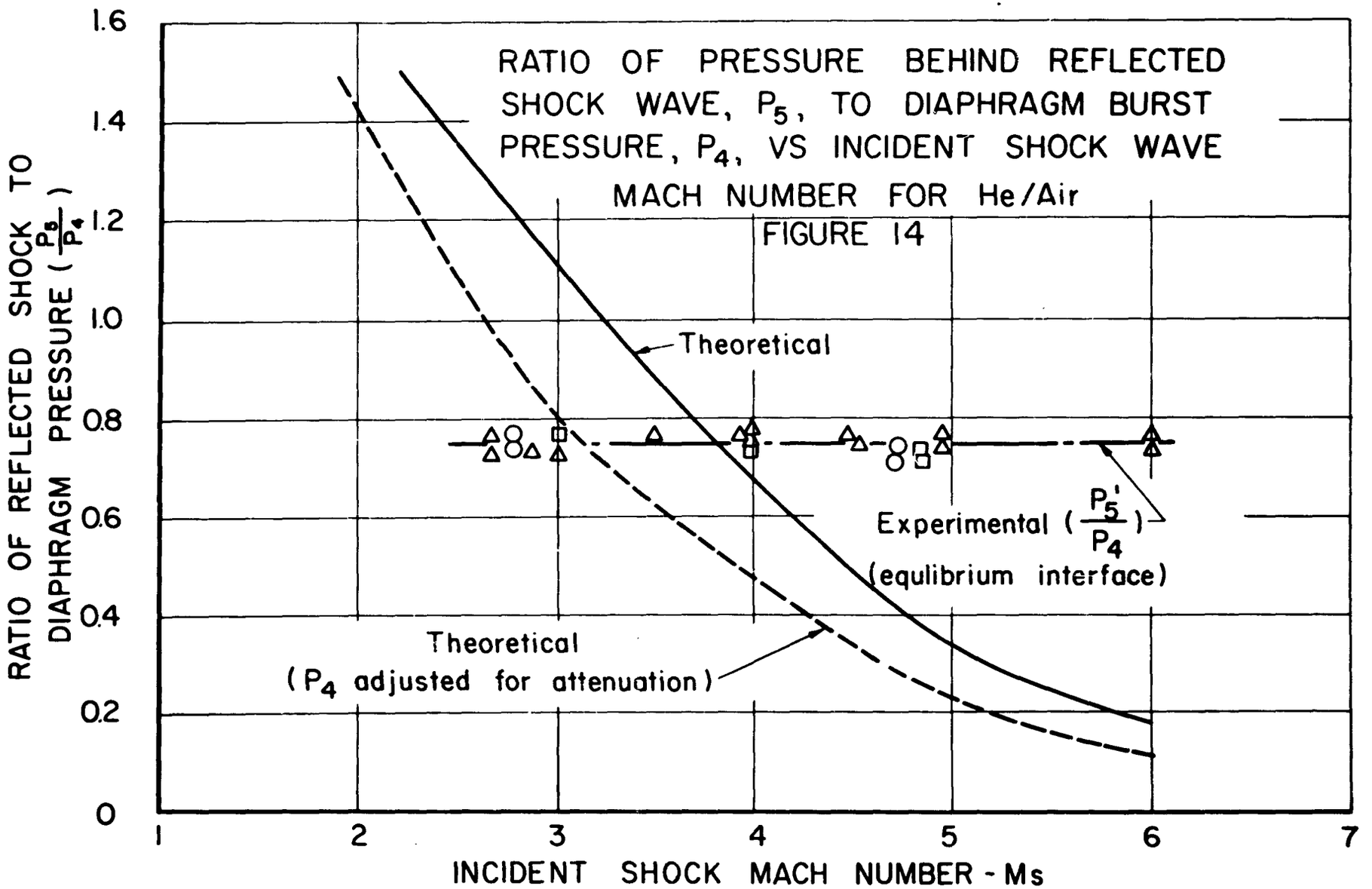
RATIO OF PRESSURE BEHIND REFLECTED SHOCK WAVE, P_5, TO DIAPHRAGM BURST PRESSURE, P_4, VS INCIDENT SHOCK WAVE MACH NUMBER FOR He/Air
FIGURE 14
RATIO OF REFLECTED SHOCK TO DIAPHRAGM PRESSURE ($\frac{P_5}{P_4}$)
1.6
1.4
1.2
1.0
0.8
0.6
0.4
0.2
0
Theoretical
Experimental ($\frac{P_5'}{P_4}$)
(equlibrium interface)
Theoretical
(P_4 adjusted for attenuation)
1
2
3
4
5
6
7
INCIDENT SHOCK MACH NUMBER - Ms

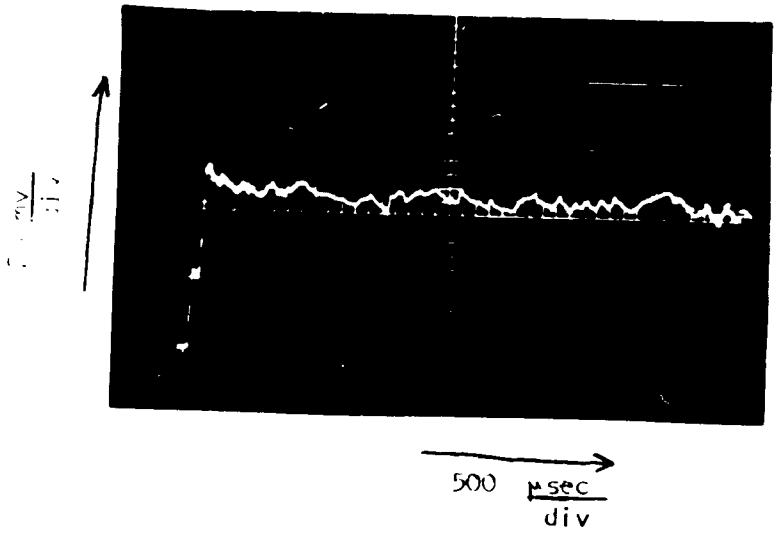

Shock Tube Operating Condition

P_4 = 980 psi He; P_1 = 1atm Air $\therefore$ M_s = 3.1 (actual)

Resistance Thermometer Response

$r_o = 49\Omega$; $\beta = 2 \times 10^{-3}$ $\frac{1}{^oC}$; $i = 16.7 \times 10^{-3}$ amps; measured $(\Delta V)_{gauge} = 45 \times 10^{-3}$ volts.

$$(\Delta T_s)_{gauge} = \frac{(\Delta V)_{gauge}}{i r_o \beta} = \frac{45 \times 10^{-3}}{(16.7 \times 10^{-3})\ (49)\ (2 \times 10^{-3})} = 27.4^oC$$

Calculated Surface Temperature of P-13 When Mounted in End Wall

$$(\Delta T_s)_{fuel} = (\Delta T_s)_{gauge} \times \frac{(\lambda \rho C_\rho)^{\frac{1}{2}}_{gauge}}{(\lambda \rho C_\rho)^{\frac{1}{2}}_{fuel}} = 27.4 \times \frac{3.28 \times 10^{-2}}{1.36 \times 10^{-2}} = 66^oC.$$

FIGURE 15 - END WALL TEMPERATURE HISTORY (M_s = 3.1)

FIGURE 16
PROPELLANT MOUNTING CONFIGURATIONS

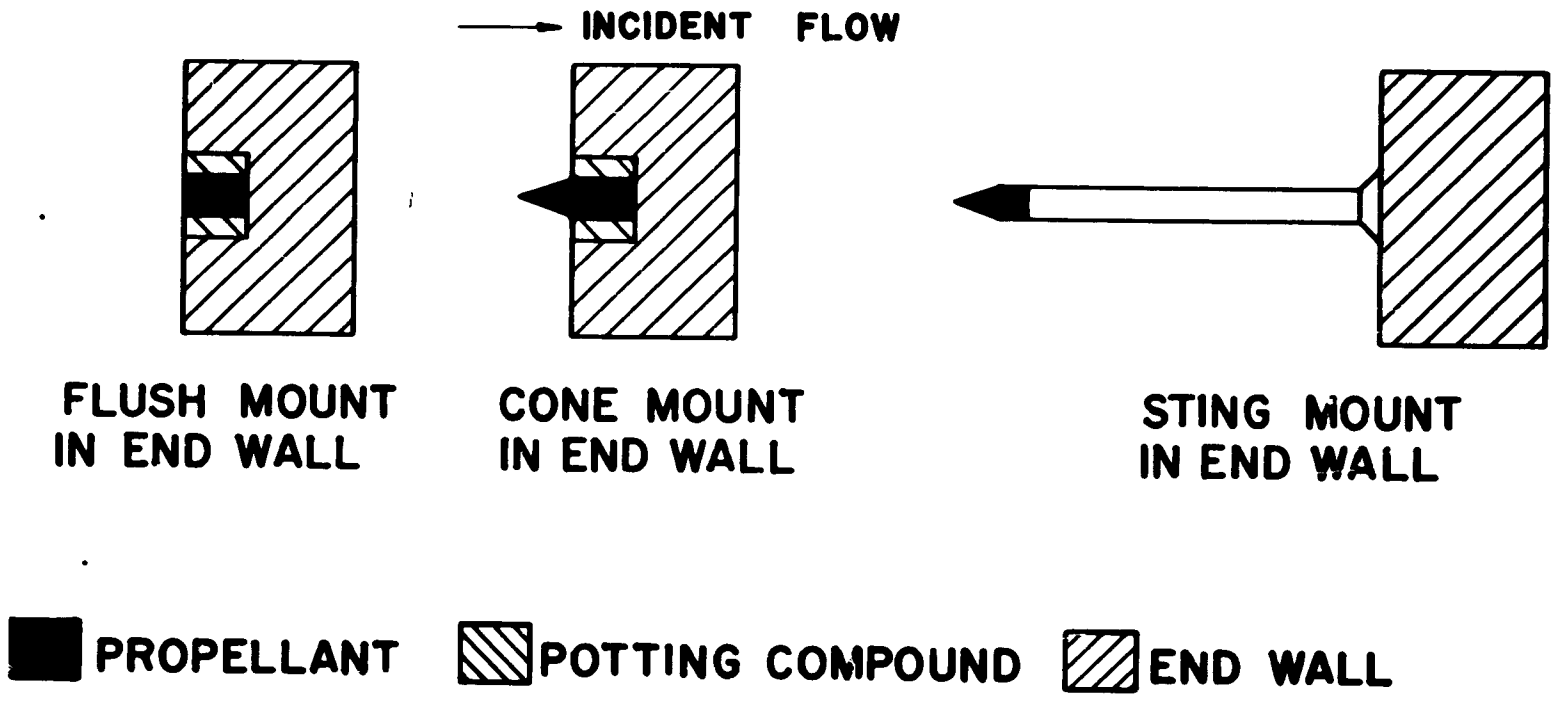

FIGURE 17
BASIC SHOCK TUBE FLOWS EMPLOYED IN STUDY
OF SOLID PROPELLANT IGNITION

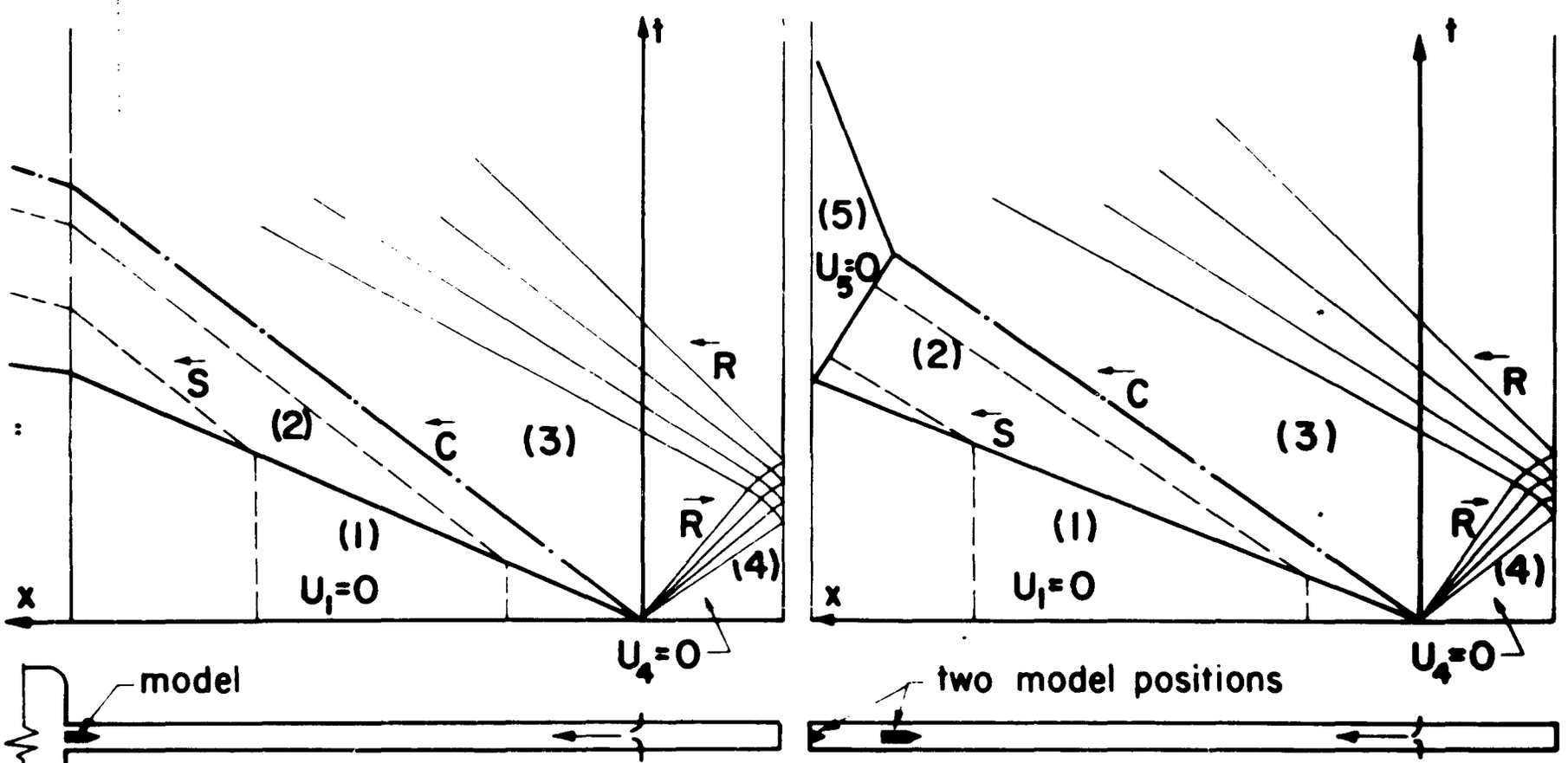

CONFIGURATION PRODUCING NO REFLECTED SHOCK WAVE

CONFIGURATION PRODUCING REFLECTED SHOCK WAVE

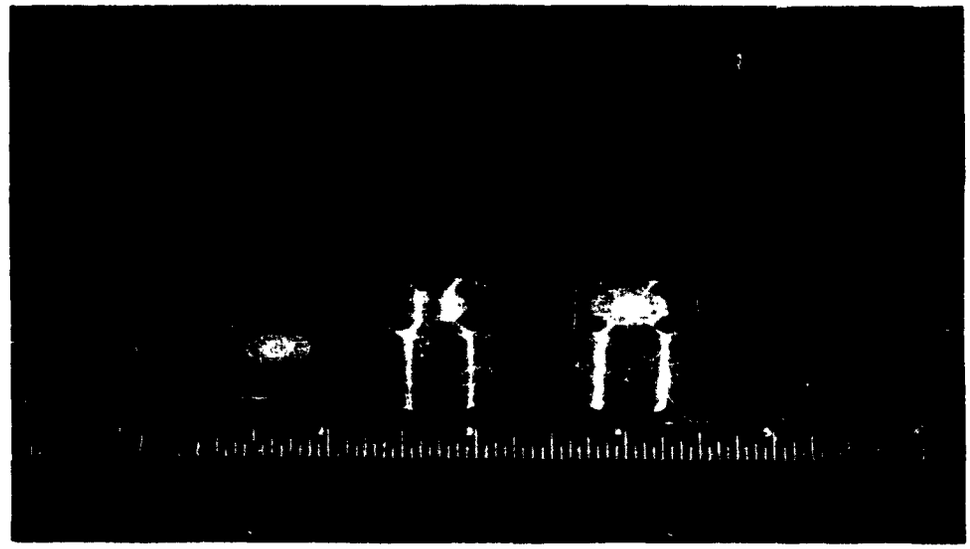

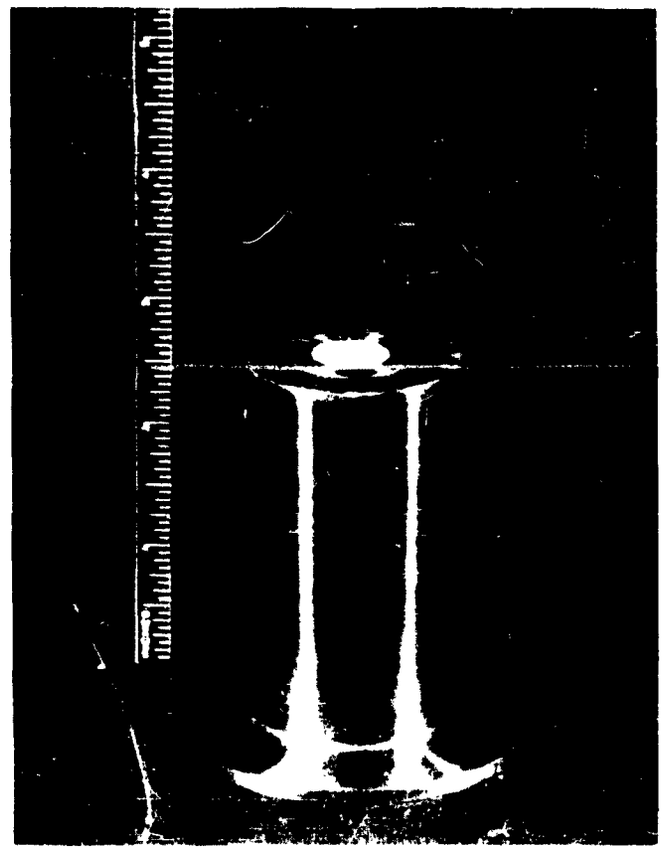

END WALL MOUNTED PROPELLANT SAMPLES

FIGURE 18

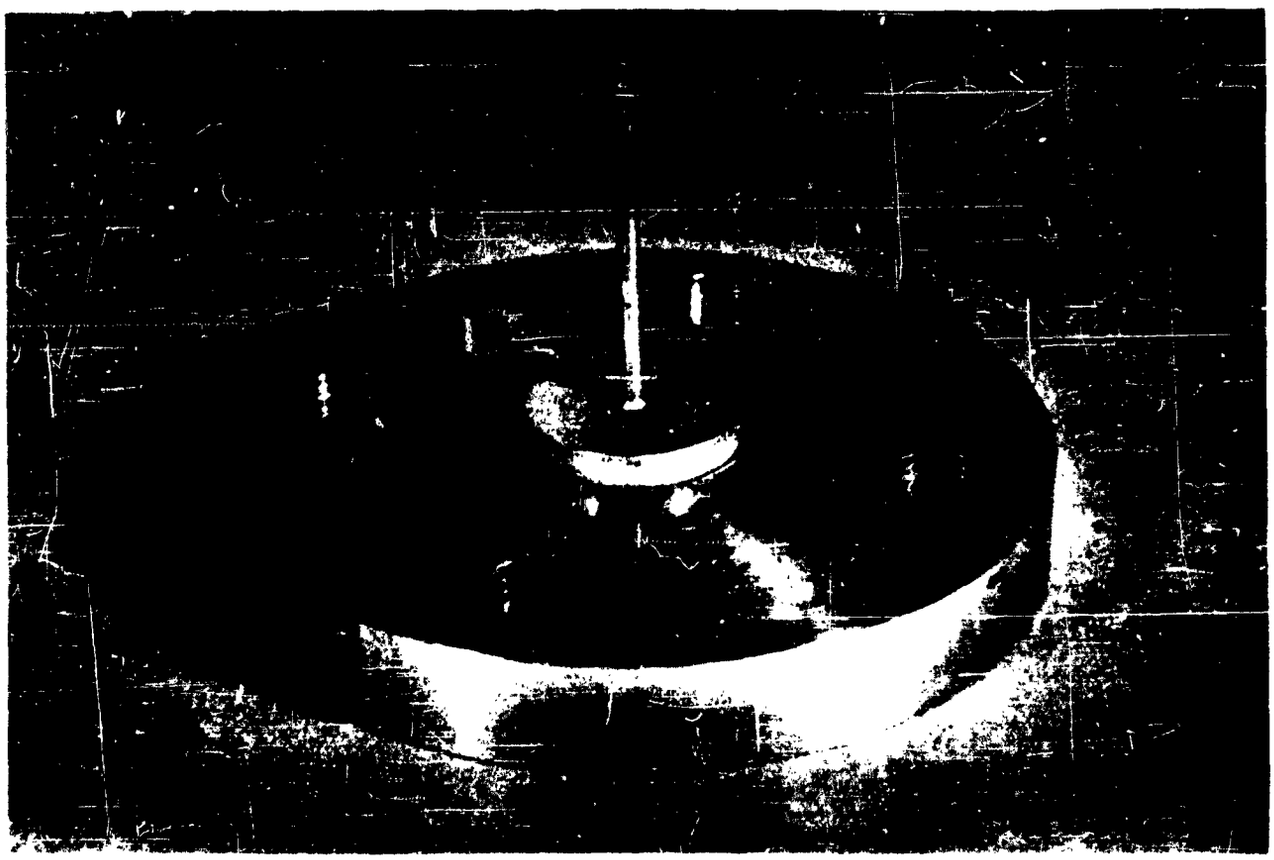

FIG. 19 STING MOUNTED PROPELLANT SAMPLES

IGNITABILITY THRESHOLD CONDITIONS FOR STING MOUNTED BATCH # 6 PROPELLANT IN 18' LONG SHOCK TUBE FOR $Z_0 = 0.50$ AND $Z_0 = 0.20$

FIGURE 20

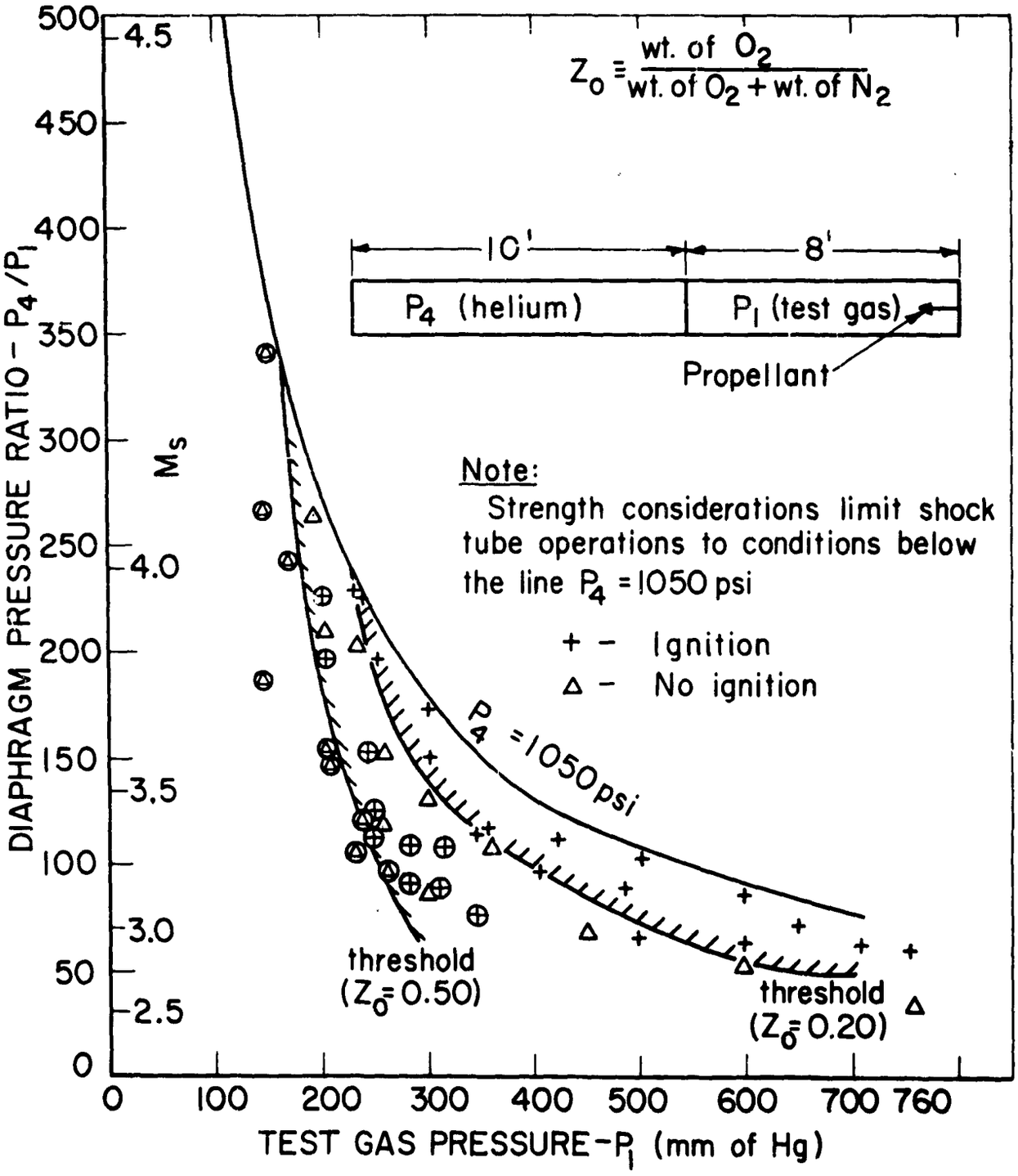

JPR 533

Passage of Reflected Shock

(a) Round Nose Propellant Sample, 75 % O_2, 3000 Frames/Sec

Passage of Reflected Shock

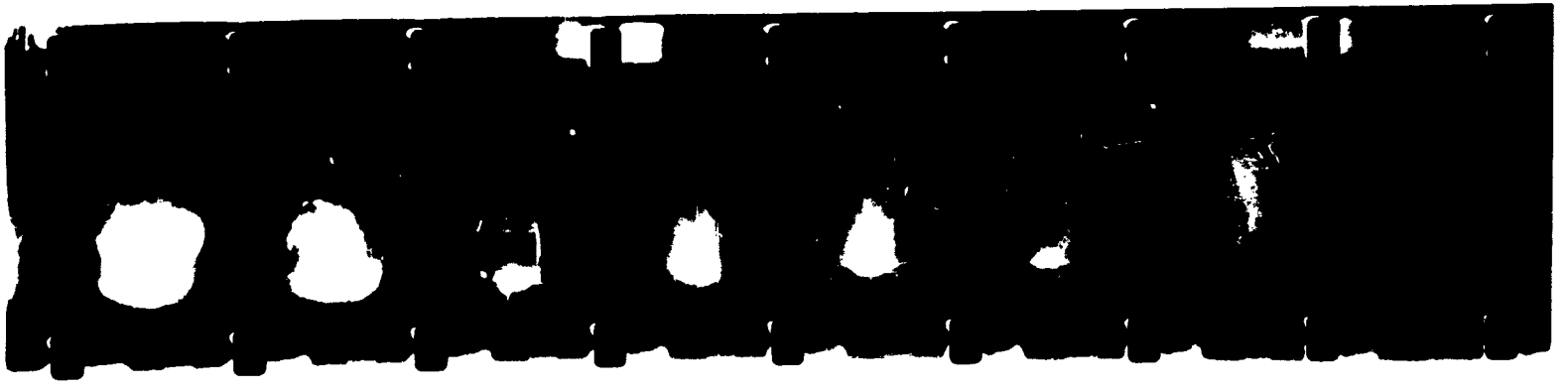

(b) Faulty Model, 46 % O_2, 4000 Frames/Sec

FIG. 21 IGNITION OF STING MOUNTED PROPELLANT SAMPLES

Passage of Reflected Shock →

(a) Polystyrene + A.P. Propellant, 53% O_2, 1000 Frames/sec

← – Time

Passage of Reflected Shock →

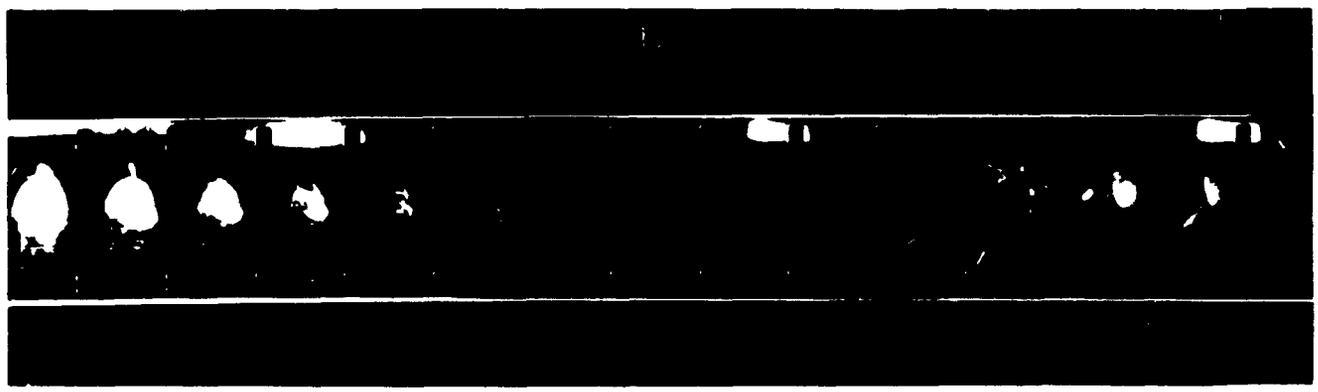

(b) Epoxy Resin + A.P. + Ferric Oxide Propellant, 46% O_2, 5000 Frames/sec

Passage of Reflected Shock →

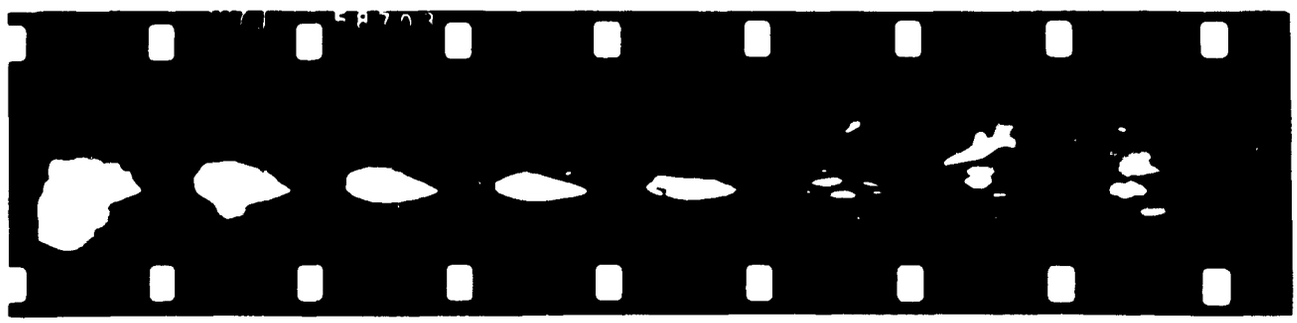

(c) Epoxy Resin + A.P. + Ferric Oxide Propellant, 75% O_2, 3000 Frames/sec

FIG. 22 IGNITION OF PROPELLANT SAMPLES IN SHOCK TUBE

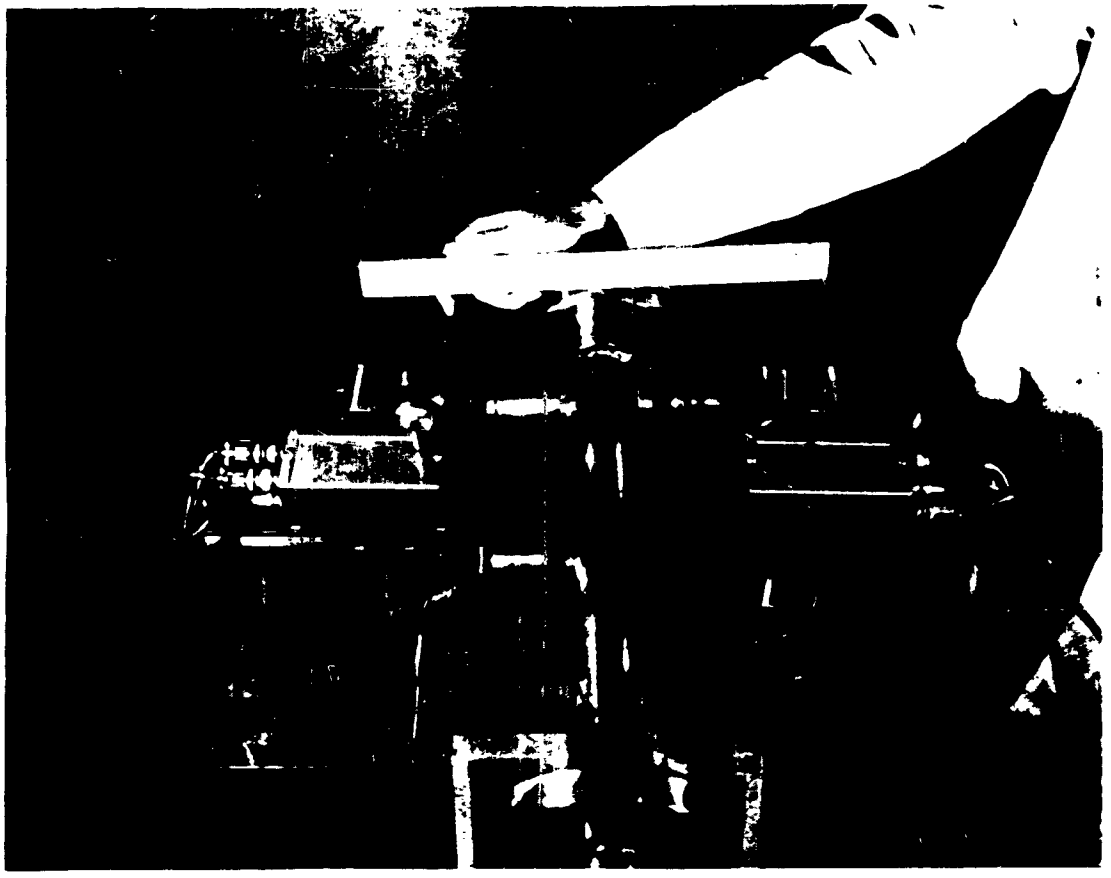

FIG. 23 INSTRUMENTATION SECTION OF 1.6" I.D. SHOCK TUBE

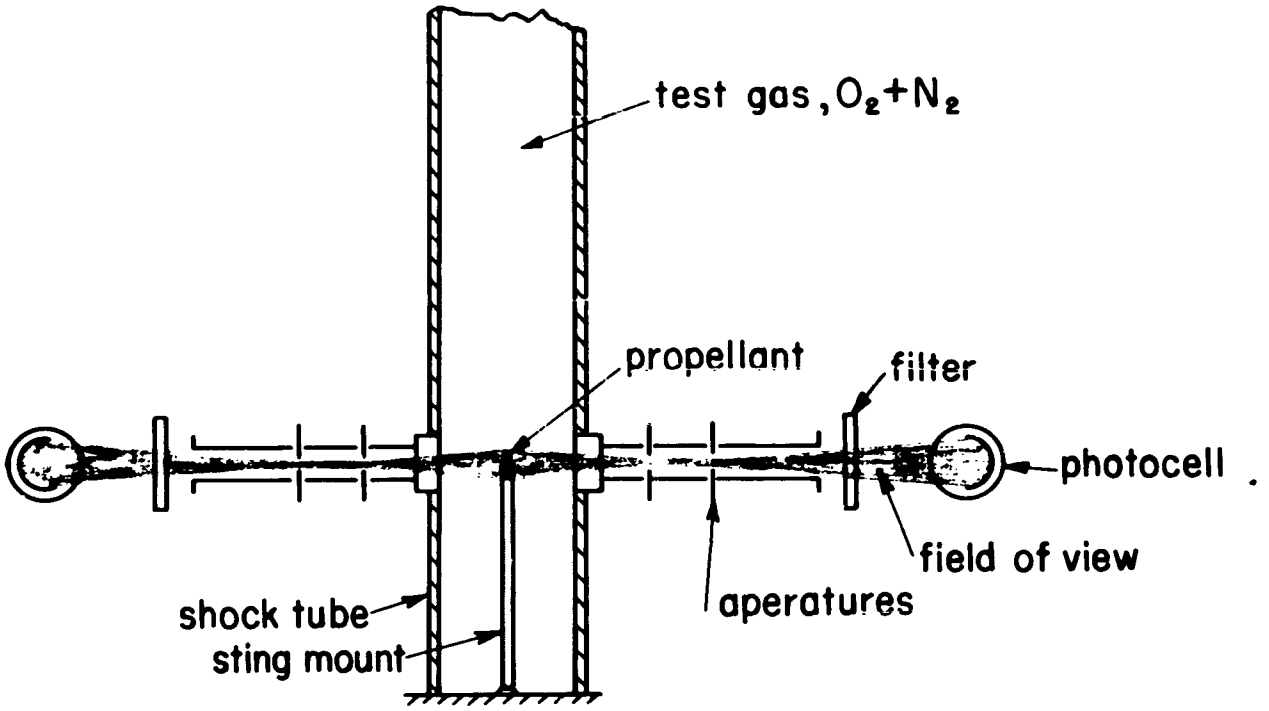

FIGURE 24 TWO PHOTOCELL OPTICAL DETECTION SYSTEM – (STING MOUNT)

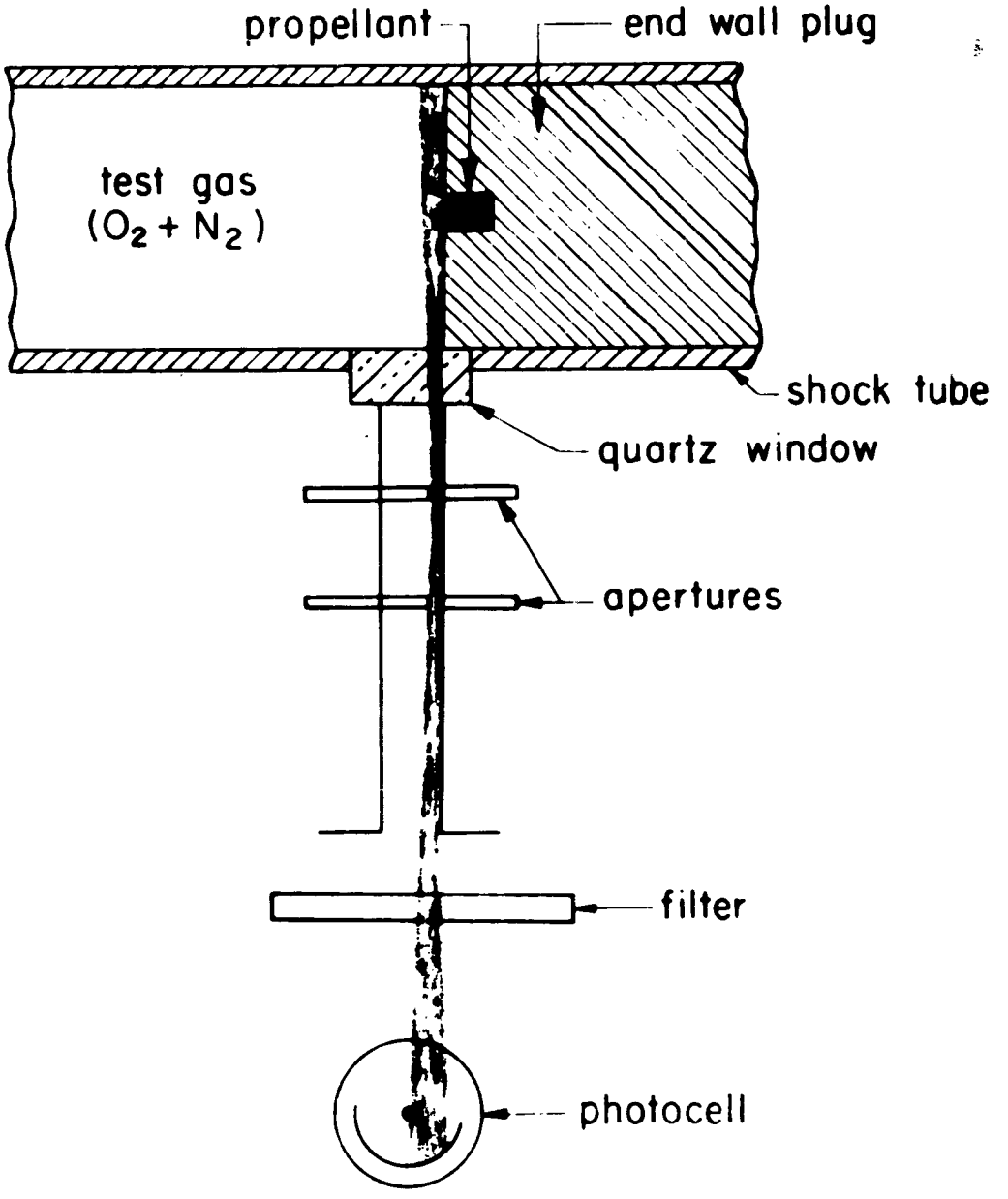

FIGURE 25 OPTICAL DETECTION SYSTEM **(END WALL MOUNT)**

INSTRUMENTATION SCHEMATIC FOR SHOCK TUBE TIME TO IGNITION MEASUREMENTS FIGURE 26

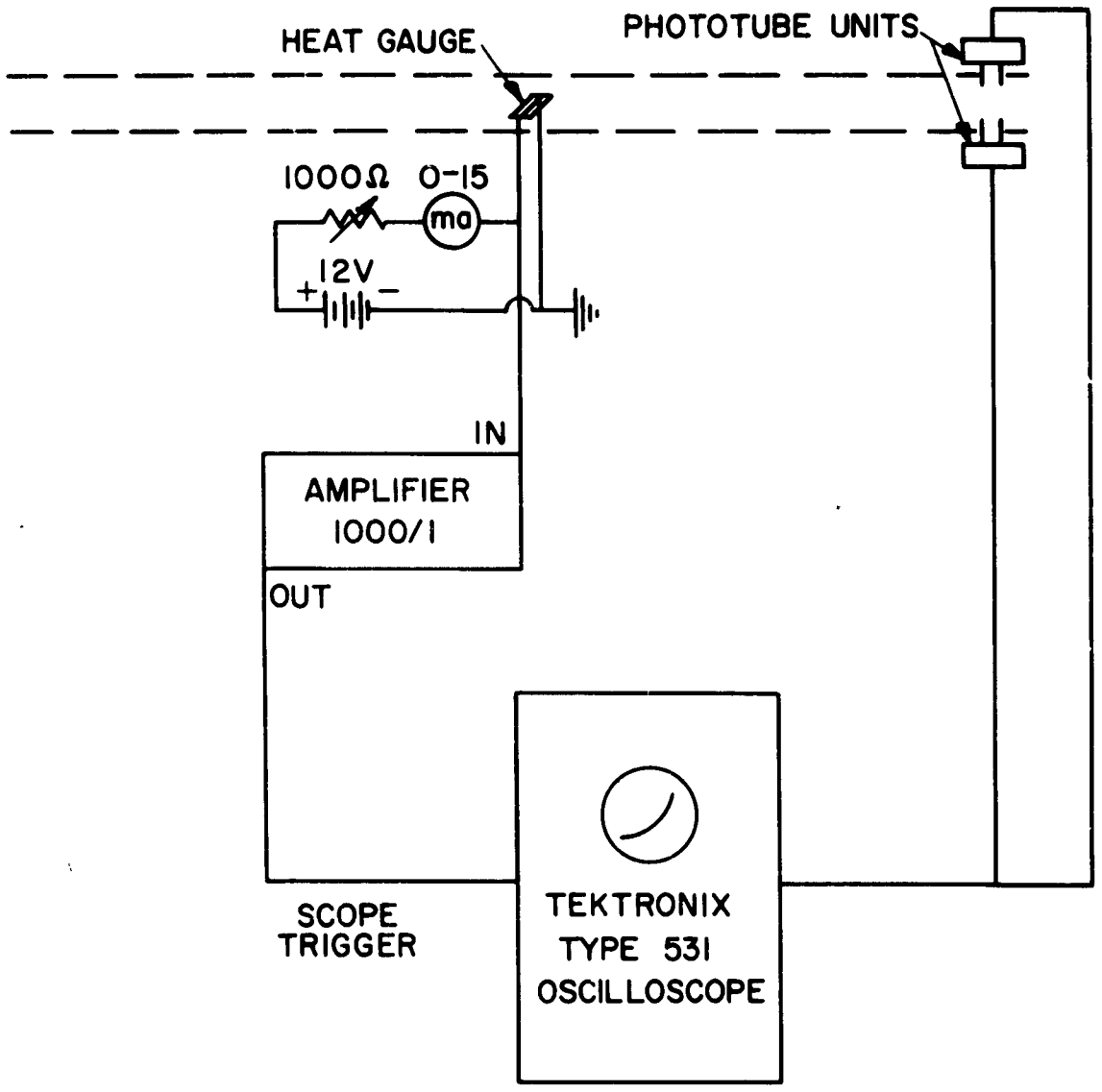

AMPLIFIED OUTPUT OF THIN FILM HEAT GAUGE TRIGGERS OSCILLOSCOPE

PHOTOTUBES DETECT LUMINOSITY AND DISPLAY OUTPUT ON OSCILLOSCOPE

JPR 526

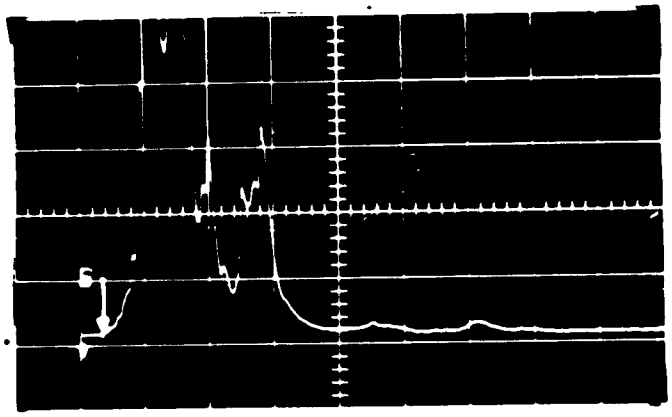

(a) Contaminated tube , no propellant

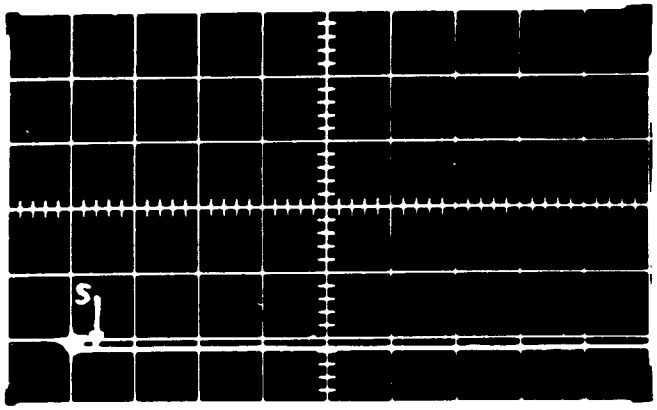

(b) Clean tube , no propellant

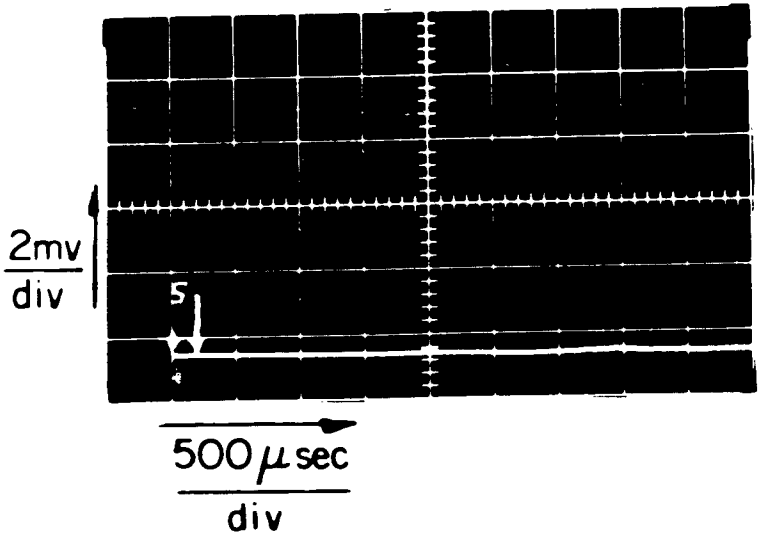

(c) Clean tube , propellant , no ignition

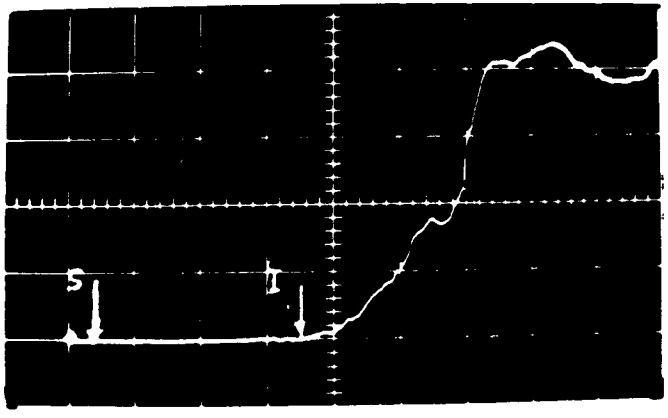

(d) Clean tube , propellant , ignition

FIG. 27 TYPICAL PHOTOTUBE TRACES $[P_4 = 980 \text{psi (He)}; P_1 = 14.7 \text{psi} (Z_0 = .78)]$

FIGURE 28
THEORETICAL INCREMENT OF END WALL SURFACE TEMPERATURE PRODUCED BY SHOCK WAVE REFLECTION
P_4 = 980 psi He ; P_1 varied to produce required M_S in air

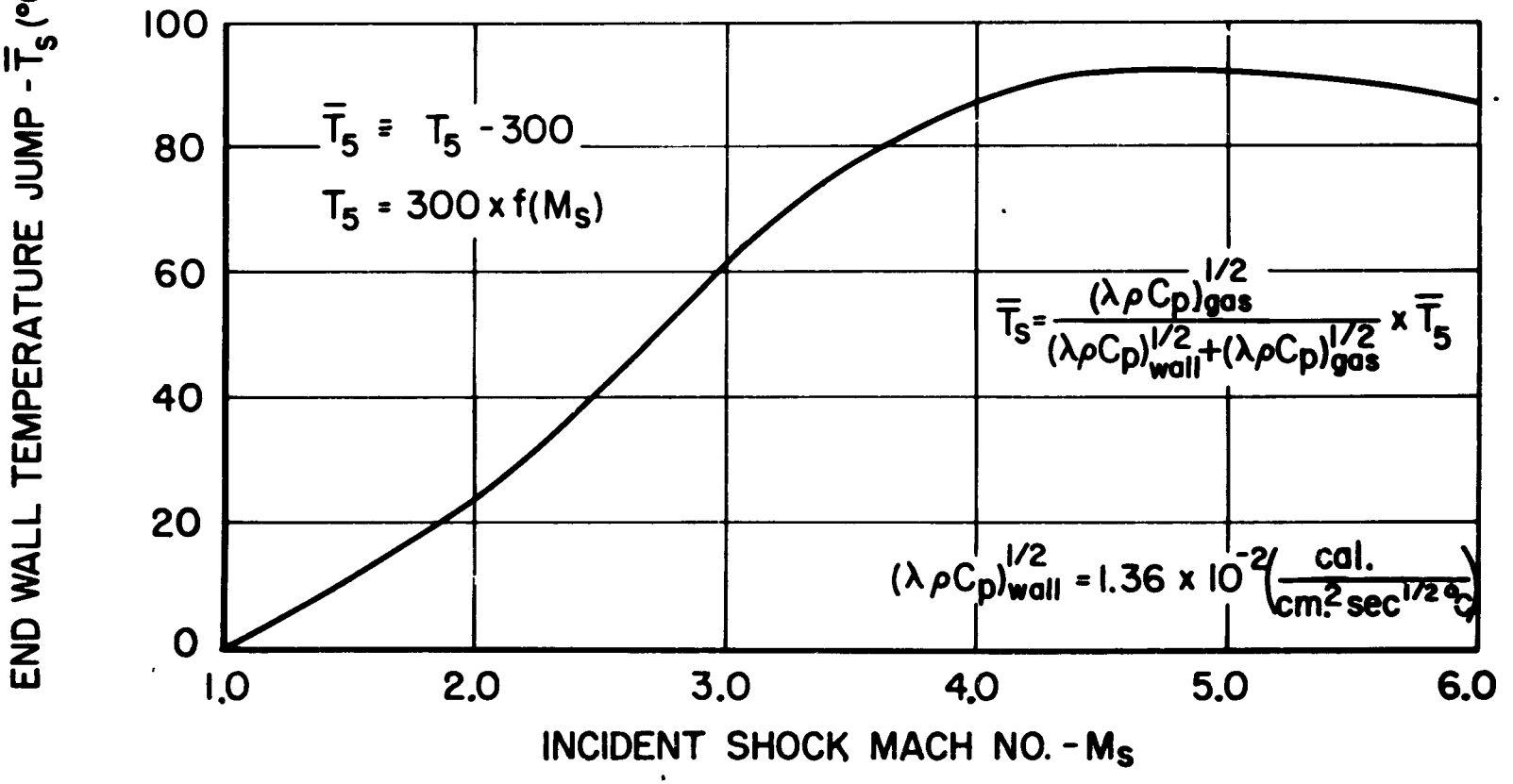

FIGURE 29

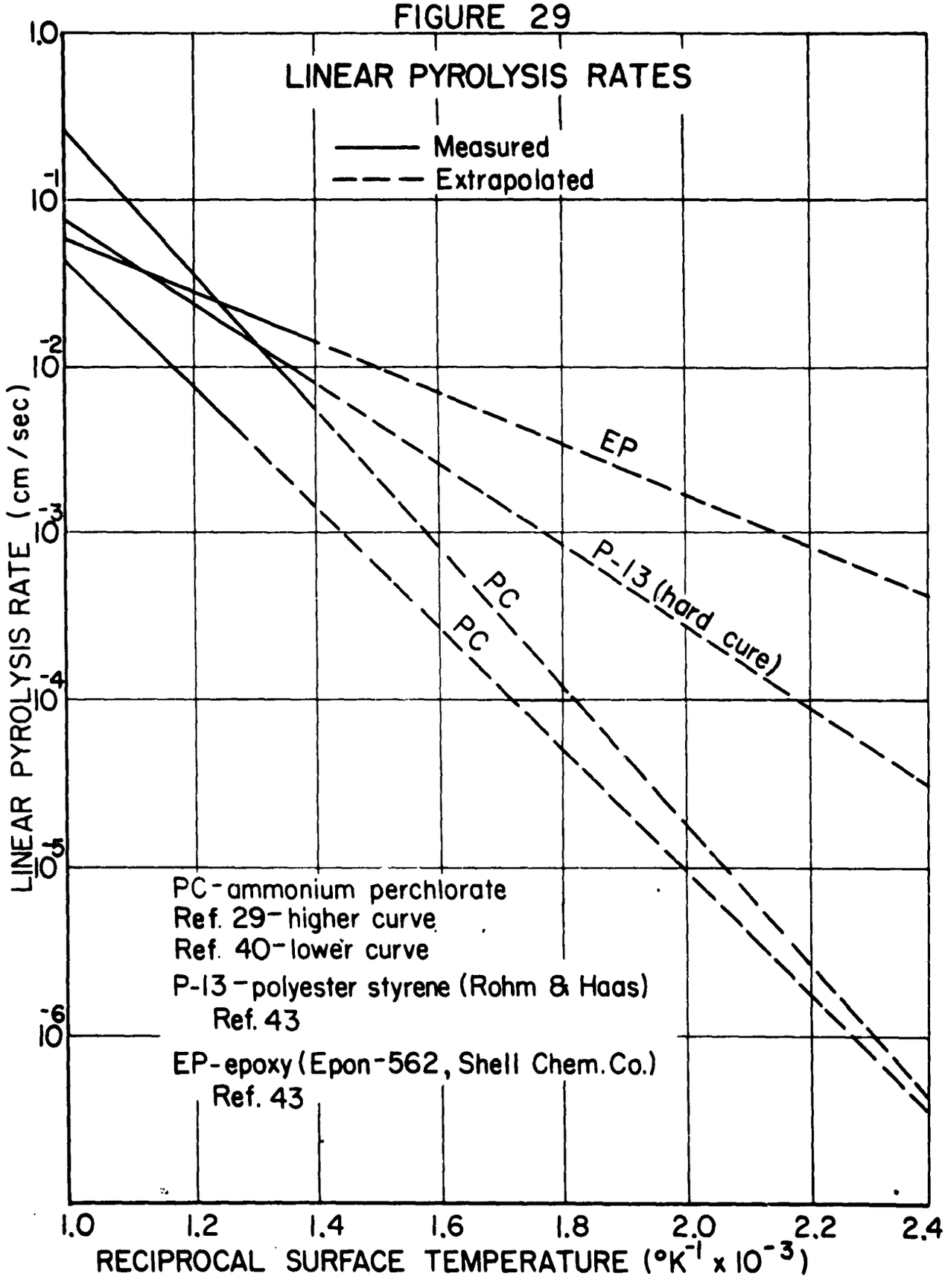

JPR 527

JPR 464

QUALITITATIVE REPRESENTATION OF FUEL VAPOR "OVERTAKING" HOT GAS "FRONT"

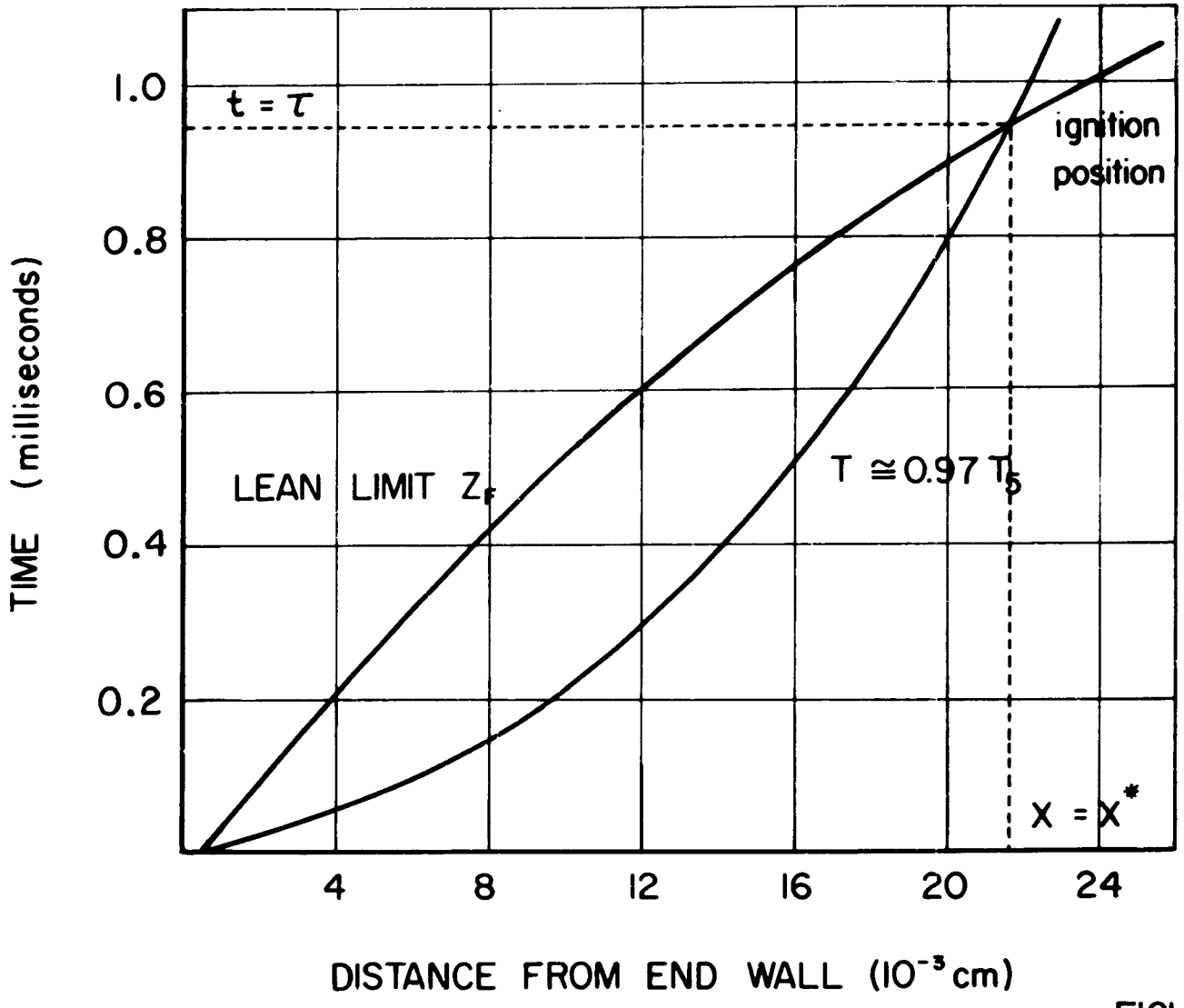

FIGURE 30

JPR 463

TEMPERATURE AND VAPORIZED FUEL DISTRIBUTIONS
AT $\frac{1}{10}$ AND 1 MILLISECOND AFTER SHOCK WAVE REFLECTION

FIGURE 31

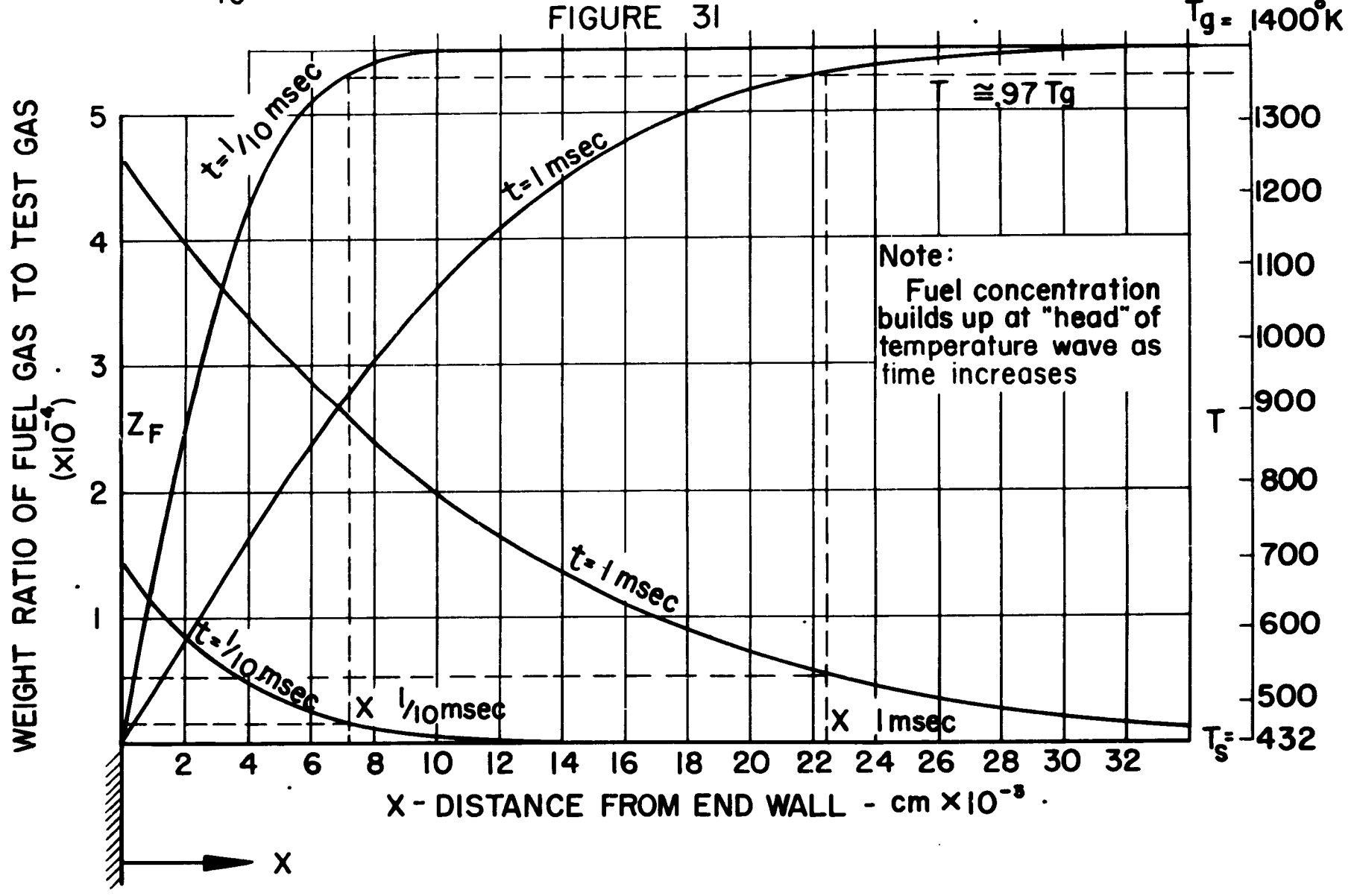

∴ JPR 461

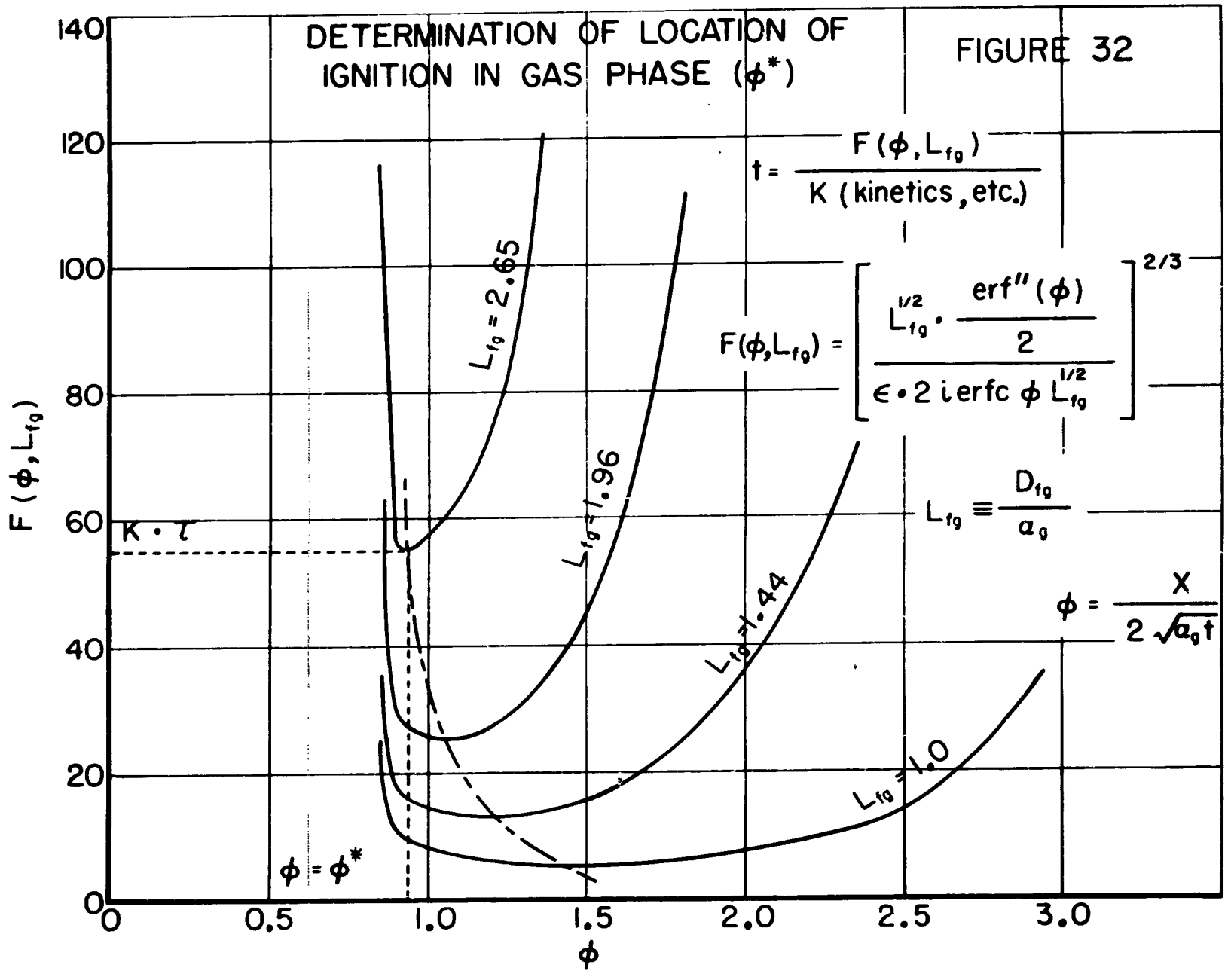
DETERMINATION OF LOCATION OF IGNITION IN GAS PHASE (ϕ^*)
FIGURE 32
$t = \frac{F(\phi, L_{fg})}{K\ (\text{kinetics, etc.})}$
$F(\phi, L_{fg}) = \left[\frac{L_{fg}^{1/2} \cdot \frac{\text{erf}''(\phi)}{2}}{\epsilon \cdot 2\ i\,\text{erfc}\ \phi\ L_{fg}^{1/2}}\right]^{2/3}$
$L_{fg} \equiv \frac{D_{fg}}{\alpha_g}$
$\phi = \frac{X}{2\sqrt{\alpha_g t}}$
$L_{fg} = 2.65$
$L_{fg} = 1.96$
$L_{fg} = 1.44$
$L_{fg} = 1.0$
$K \cdot t$
$\phi = \phi^*$
$F(\phi, L_{fg})$
ϕ
0
20
40
60
80
100
120
140
0
0.5
1.0
1.5
2.0
2.5
3.0

TIME TO IGNITION VS OXYGEN CONCENTRATION

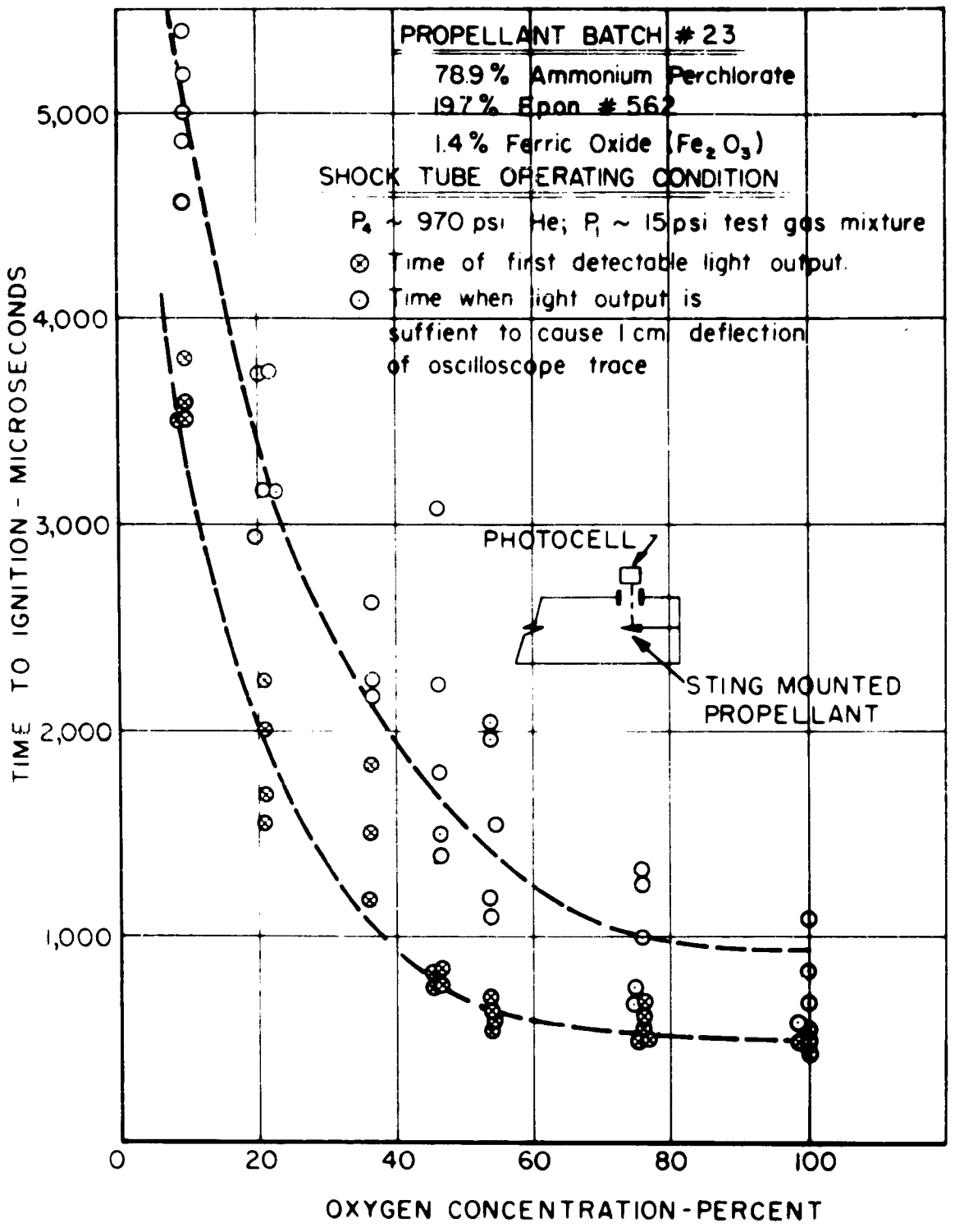

JPR 408

FIGURE 33

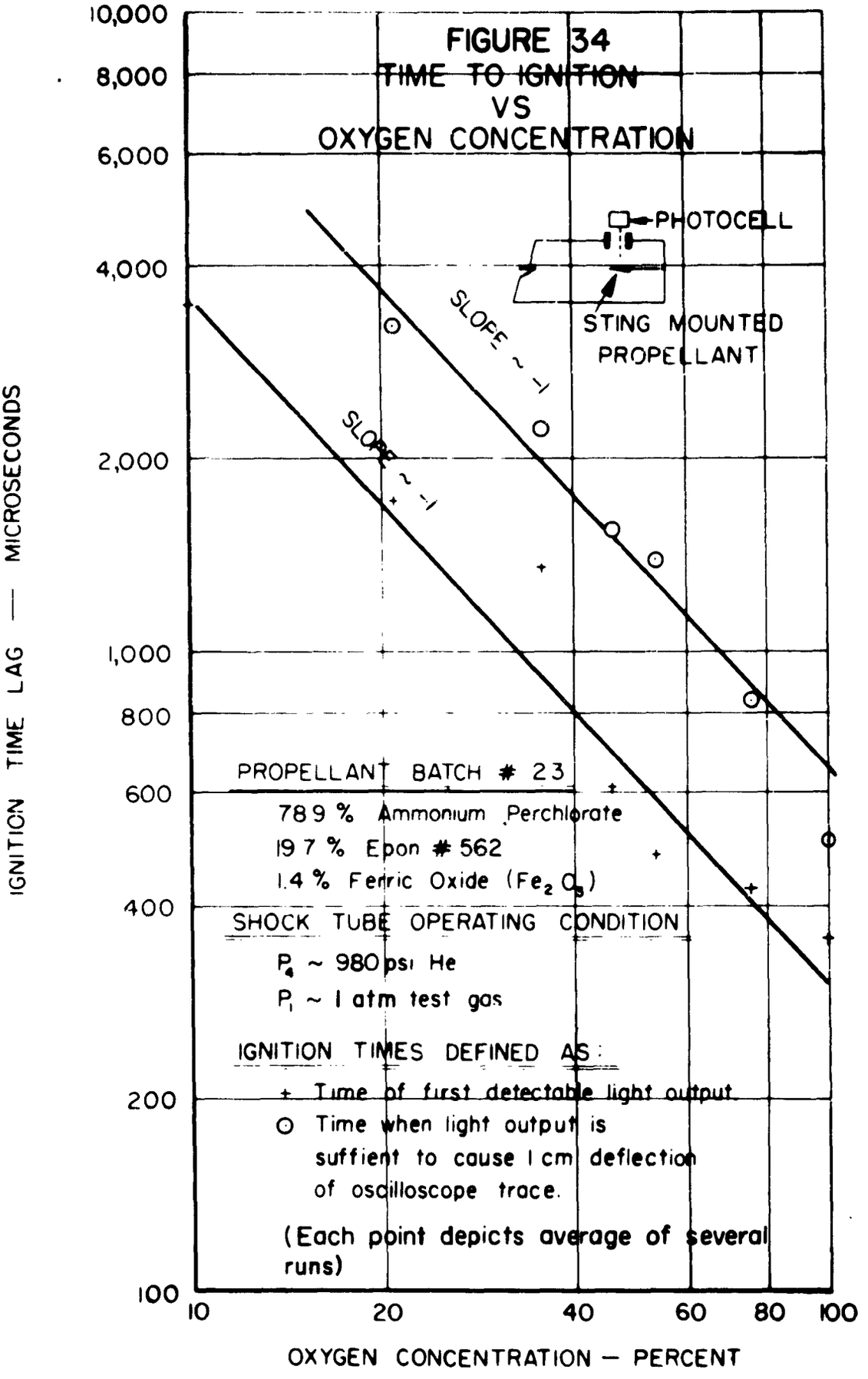
FIGURE 34
TIME TO IGNITION
VS
OXYGEN CONCENTRATION
PHOTOCELL
STING MOUNTED
PROPELLANT
SLOPE ~ -1
SLOPE ~ -1
PROPELLANT BATCH # 23
78.9 % Ammonium Perchlorate
19.7 % Epon # 562
1.4 % Ferric Oxide (Fe_2O_3)
SHOCK TUBE OPERATING CONDITION
P_4 ~ 980 psi He
P_1 ~ 1 atm test gas
IGNITION TIMES DEFINED AS:
+ Time of first detectable light output
⊙ Time when light output is suffient to cause 1 cm deflection of oscilloscope trace.
(Each point depicts average of several runs)
IGNITION TIME LAG — MICROSECONDS
10,000
8,000
6,000
4,000
2,000
1,000
800
600
400
200
100
10
20
40
60
80
100
OXYGEN CONCENTRATION — PERCENT

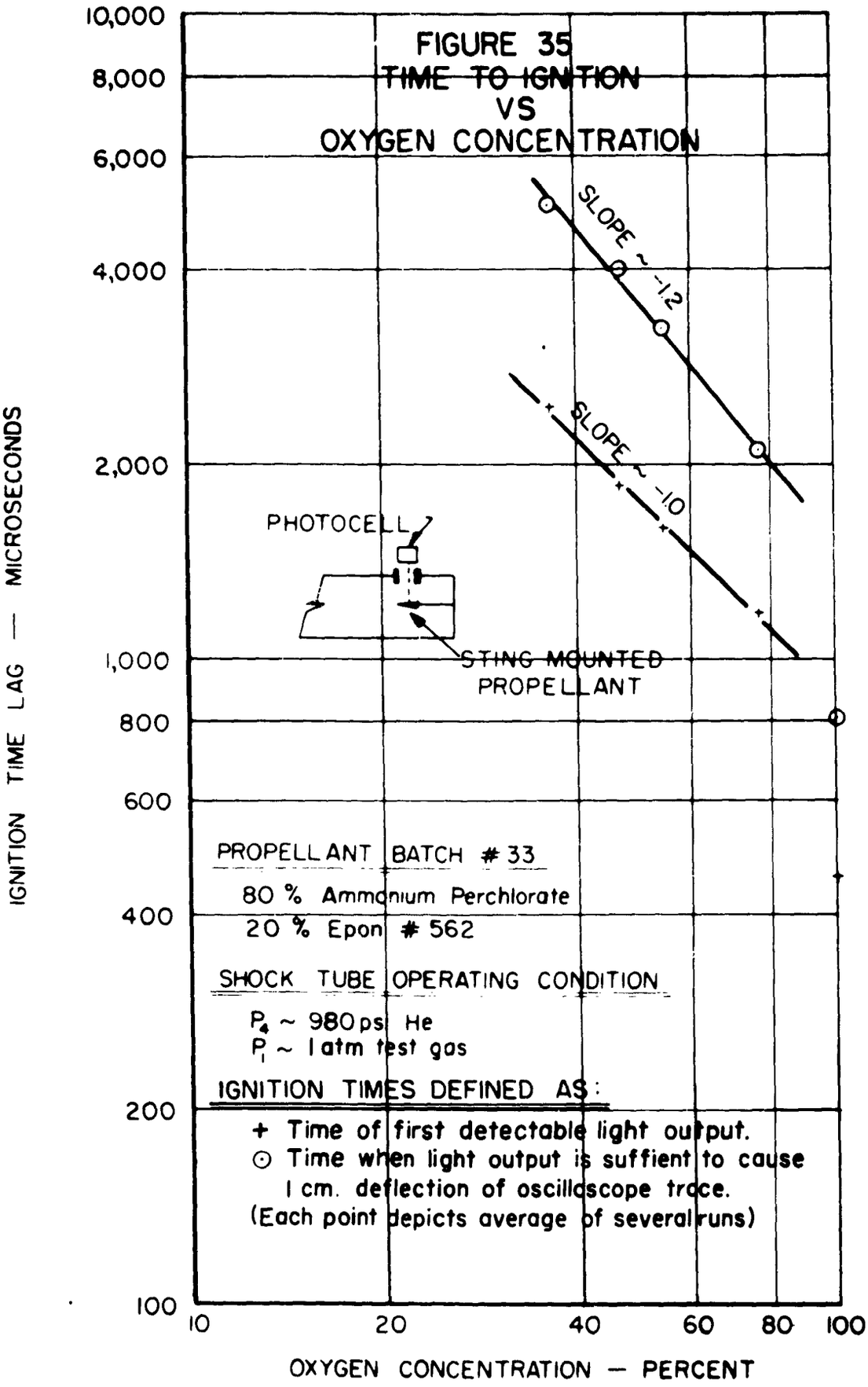
FIGURE 35
TIME TO IGNITION
VS
OXYGEN CONCENTRATION
10,000
8,000
6,000
4,000
2,000
1,000
800
600
400
200
100
SLOPE ~ -1.2
SLOPE ~ -1.0
PHOTOCELL
STING MOUNTED
PROPELLANT
PROPELLANT BATCH # 33
80 % Ammonium Perchlorate
20 % Epon # 562
SHOCK TUBE OPERATING CONDITION
P_4 ~ 980 psi He
P_1 ~ 1 atm test gas
IGNITION TIMES DEFINED AS:
+ Time of first detectable light output.
⊙ Time when light output is suffient to cause
1 cm. deflection of oscilloscope trace.
(Each point depicts average of several runs)
IGNITION TIME LAG — MICROSECONDS
10
20
40
60
80
100
OXYGEN CONCENTRATION — PERCENT

JPR 412

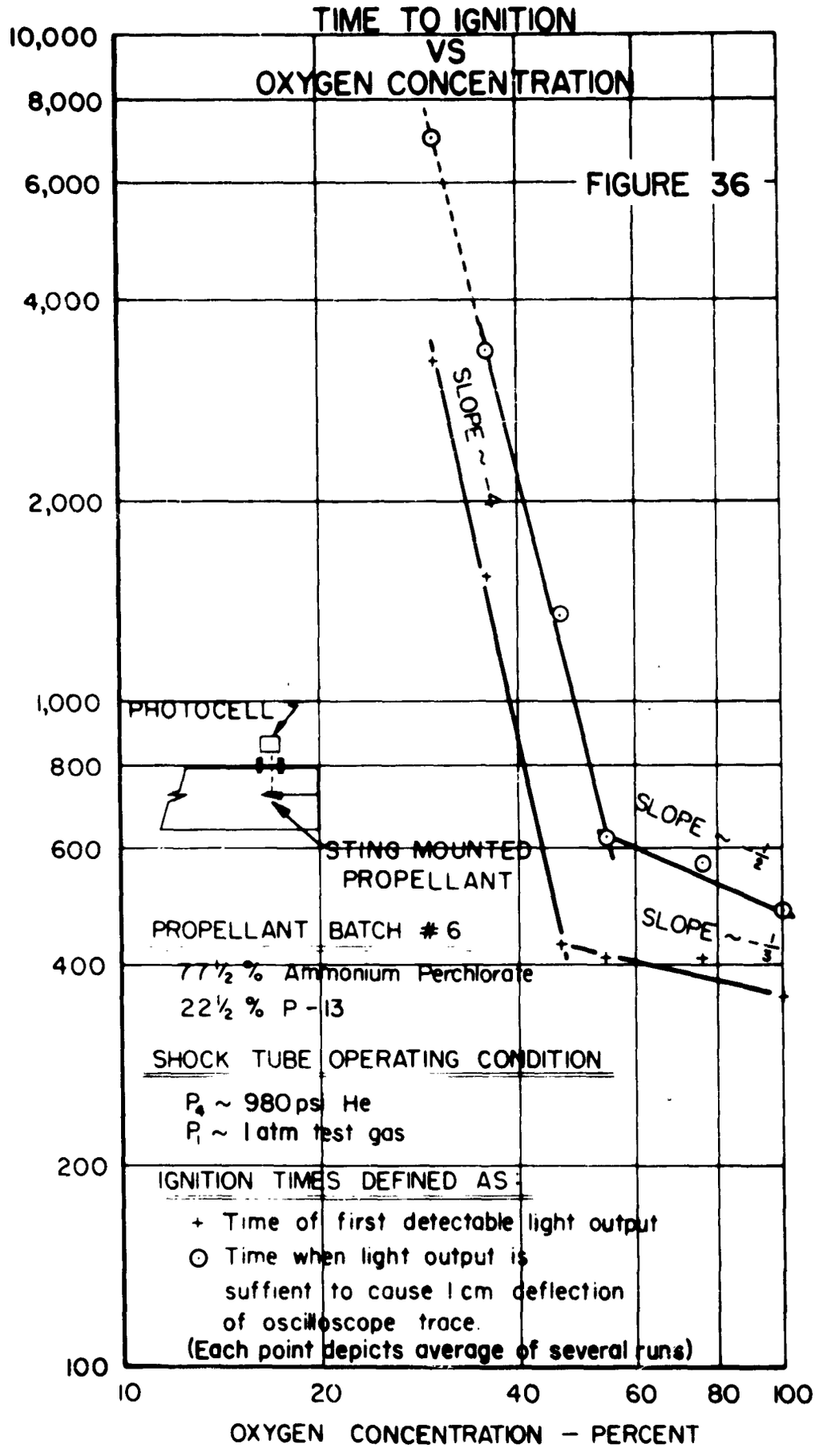
TIME TO IGNITION
VS
OXYGEN CONCENTRATION
FIGURE 36
IGNITION TIME LAG — MICROSECONDS
10,000
8,000
6,000
4,000
2,000
1,000
800
600
400
200
100
SLOPE ~ -4
SLOPE ~ -2
SLOPE ~ -1
PHOTOCELL
STING MOUNTED
PROPELLANT
PROPELLANT BATCH # 6
77½ % Ammonium Perchlorate
22½ % P-13
SHOCK TUBE OPERATING CONDITION
P4 ~ 980 psi He
P1 ~ 1 atm test gas
IGNITION TIMES DEFINED AS:
+ Time of first detectable light output
⊙ Time when light output is
suffient to cause 1 cm deflection
of oscilloscope trace.
(Each point depicts average of several runs)
10
20
40
60
80
100
OXYGEN CONCENTRATION — PERCENT

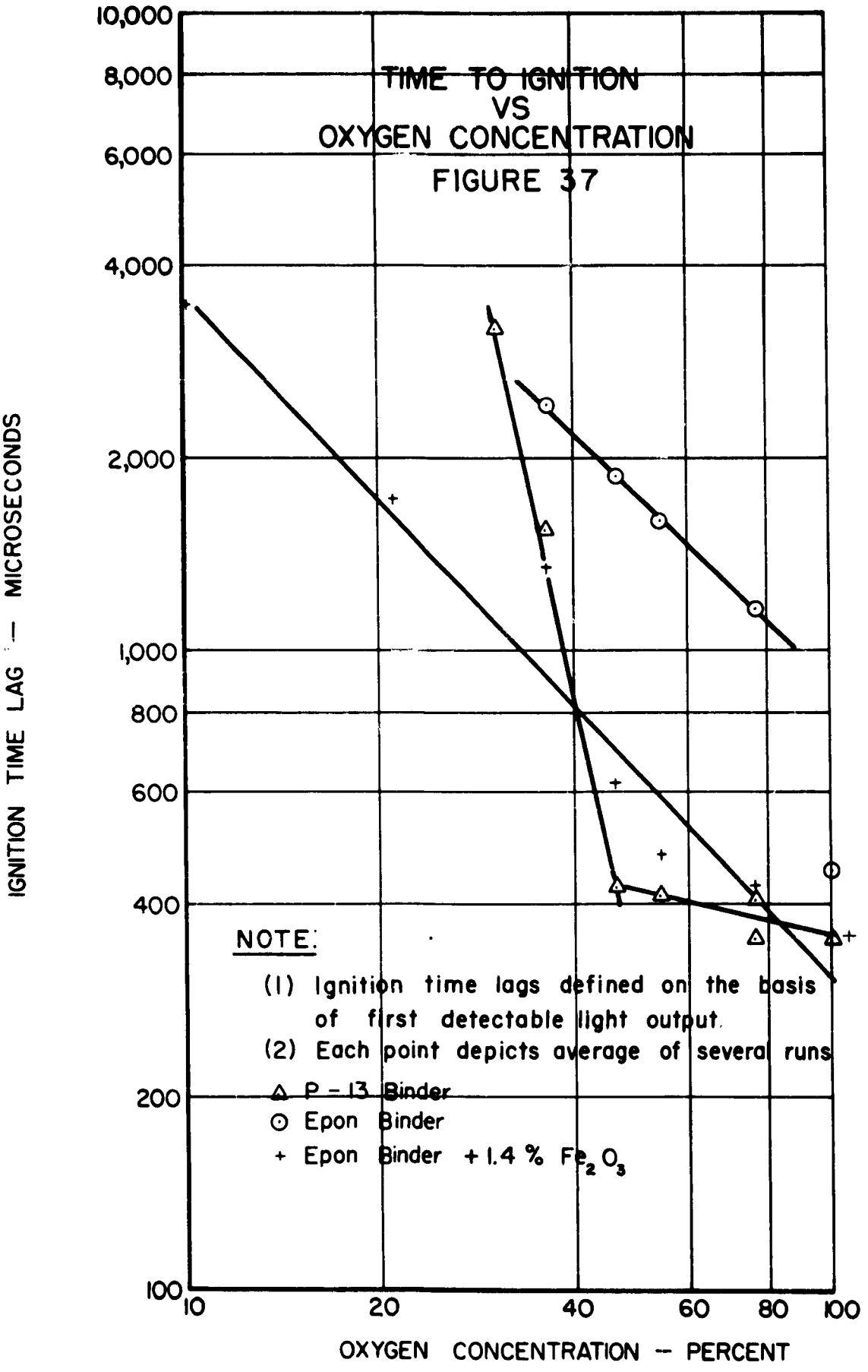
TIME TO IGNITION
VS
OXYGEN CONCENTRATION
FIGURE 37
IGNITION TIME LAG — MICROSECONDS
10,000
8,000
6,000
4,000
2,000
1,000
800
600
400
200
100
10
20
40
60
80
100
OXYGEN CONCENTRATION -- PERCENT
NOTE:
(1) Ignition time lags defined on the basis of first detectable light output.
(2) Each point depicts average of several runs
△ P - 13 Binder
⊙ Epon Binder
+ Epon Binder + 1.4 % Fe_2O_3

JPR 409

TIME TO IGNITION VS TEST GAS OXYGEN CONCENTRATION FOR BATCH #6 PROPELLANT AND P-13 FUEL MOUNTED IN END WALL SHOCK TUBE OPERATING CONDITION

P_4 = 980psi He ; P_1 = 1 atmos. test gas

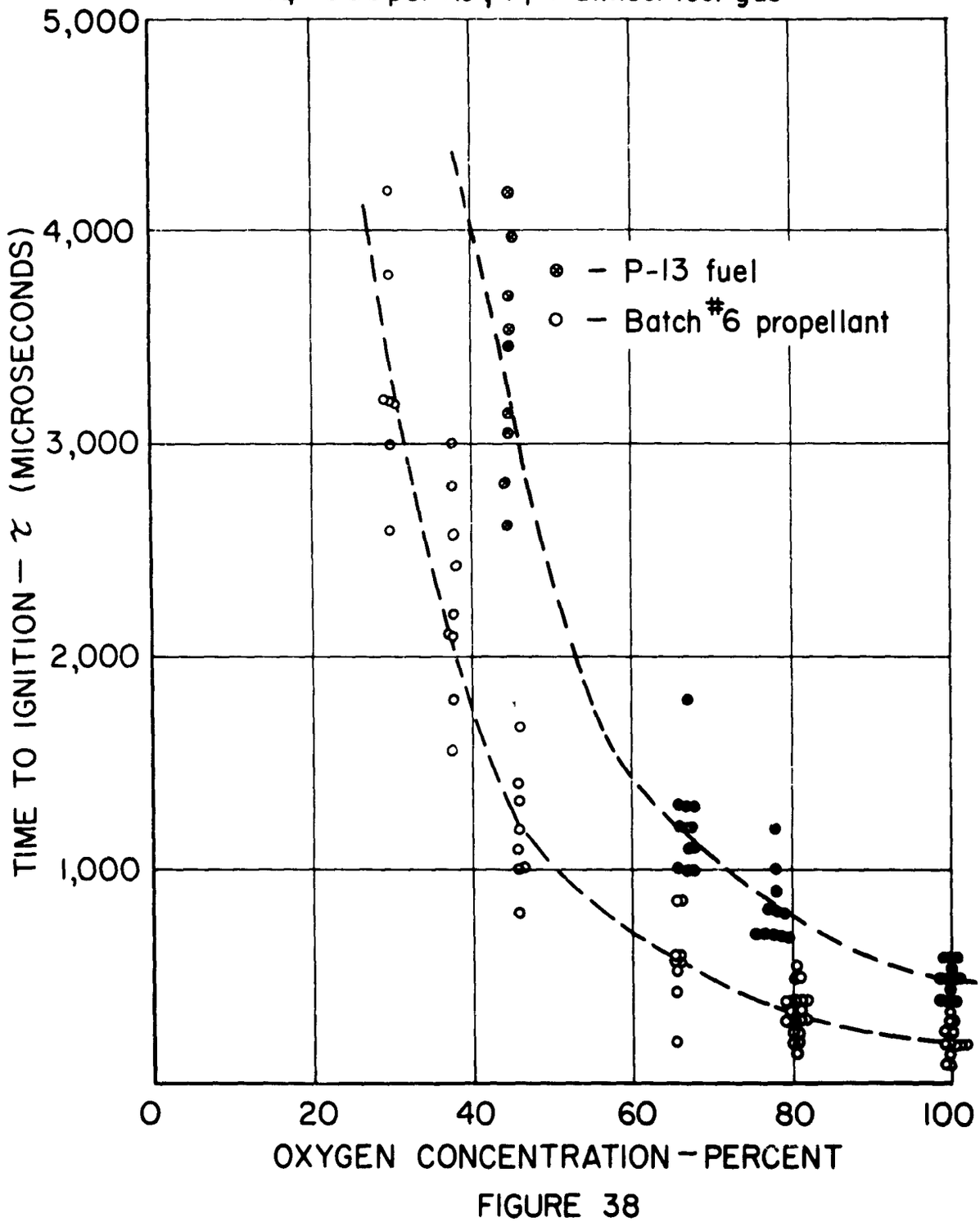

FIGURE 38

JPR 532

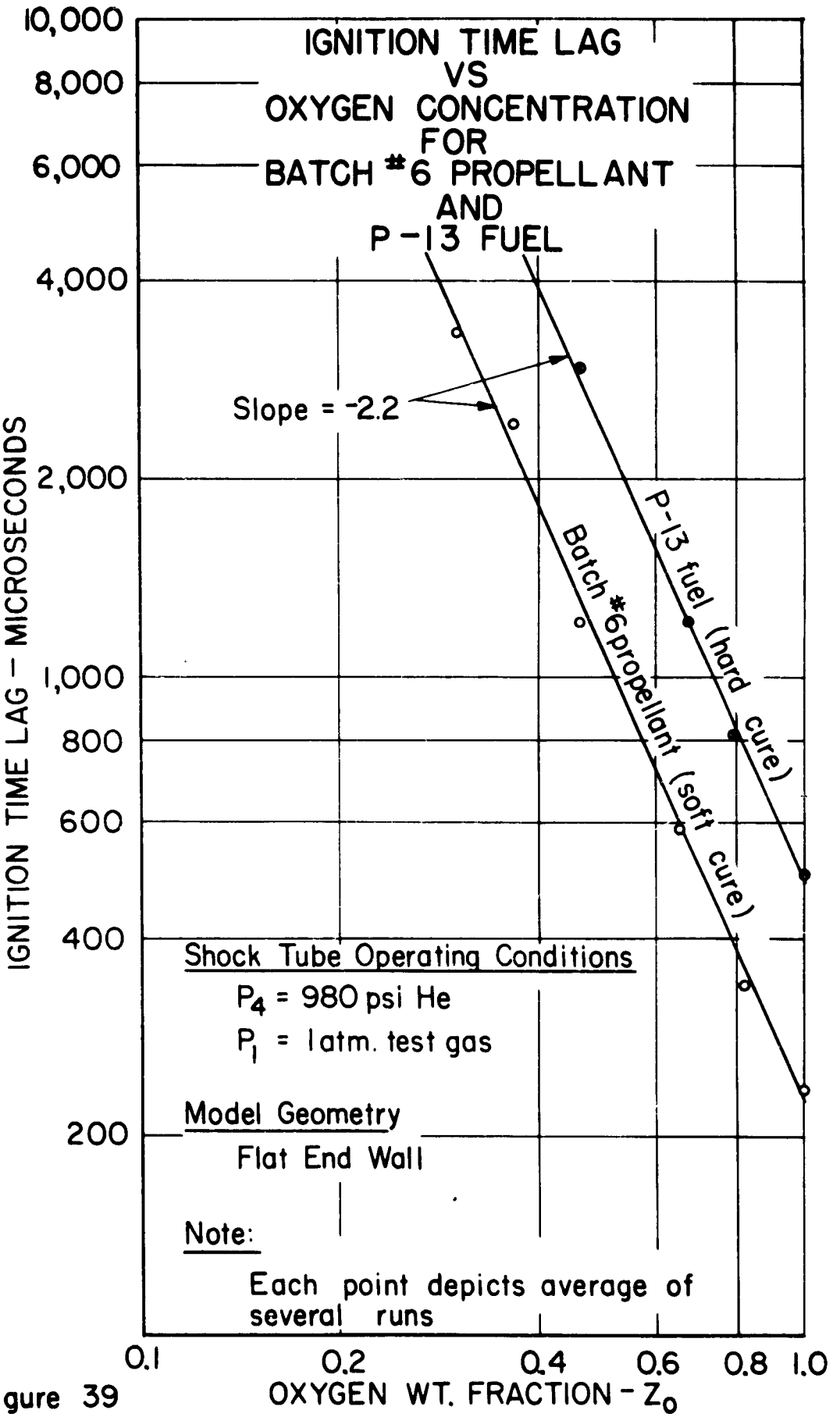

JPR 531

Figure 39

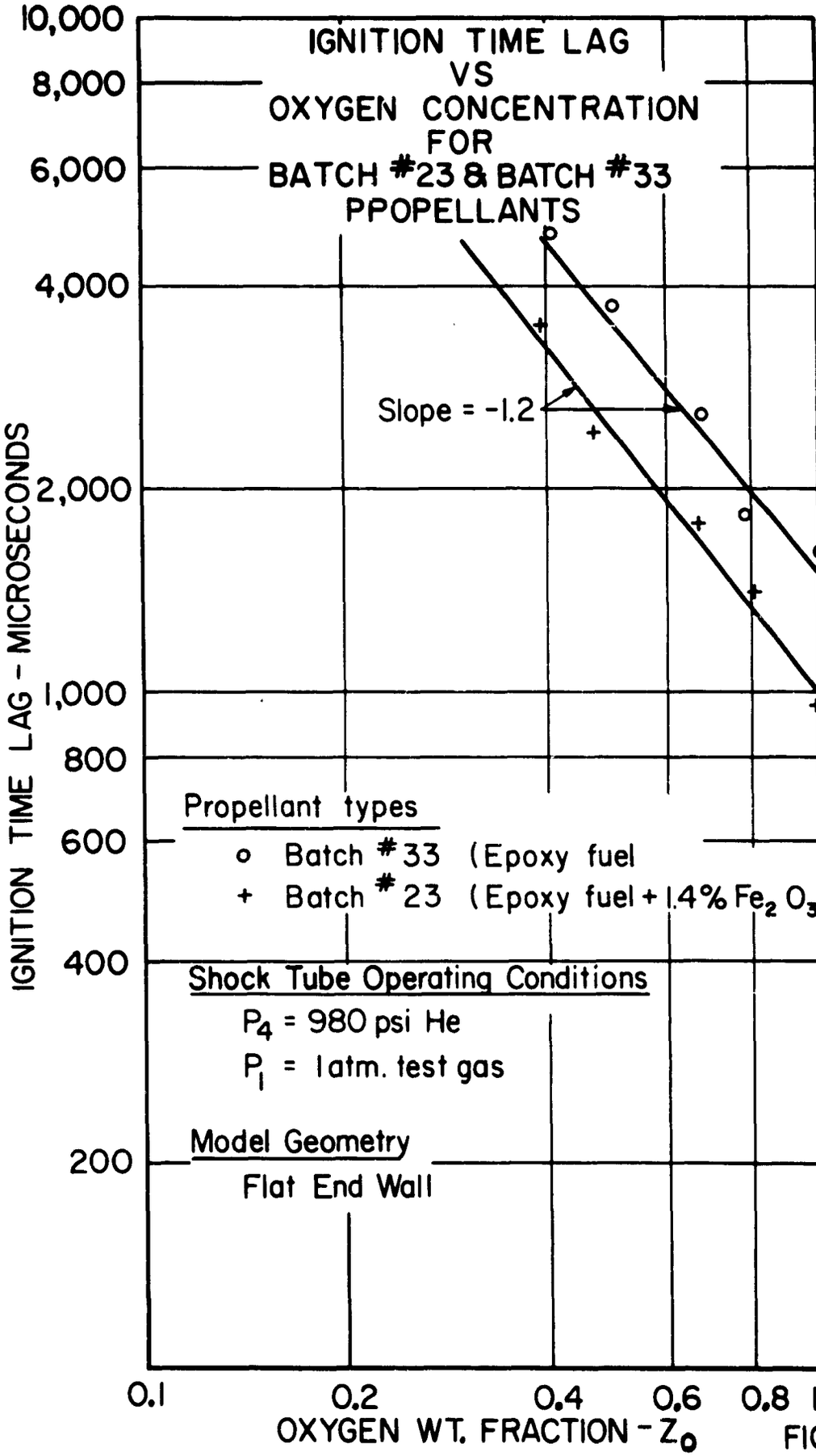

FIGURE 40

JPR 545

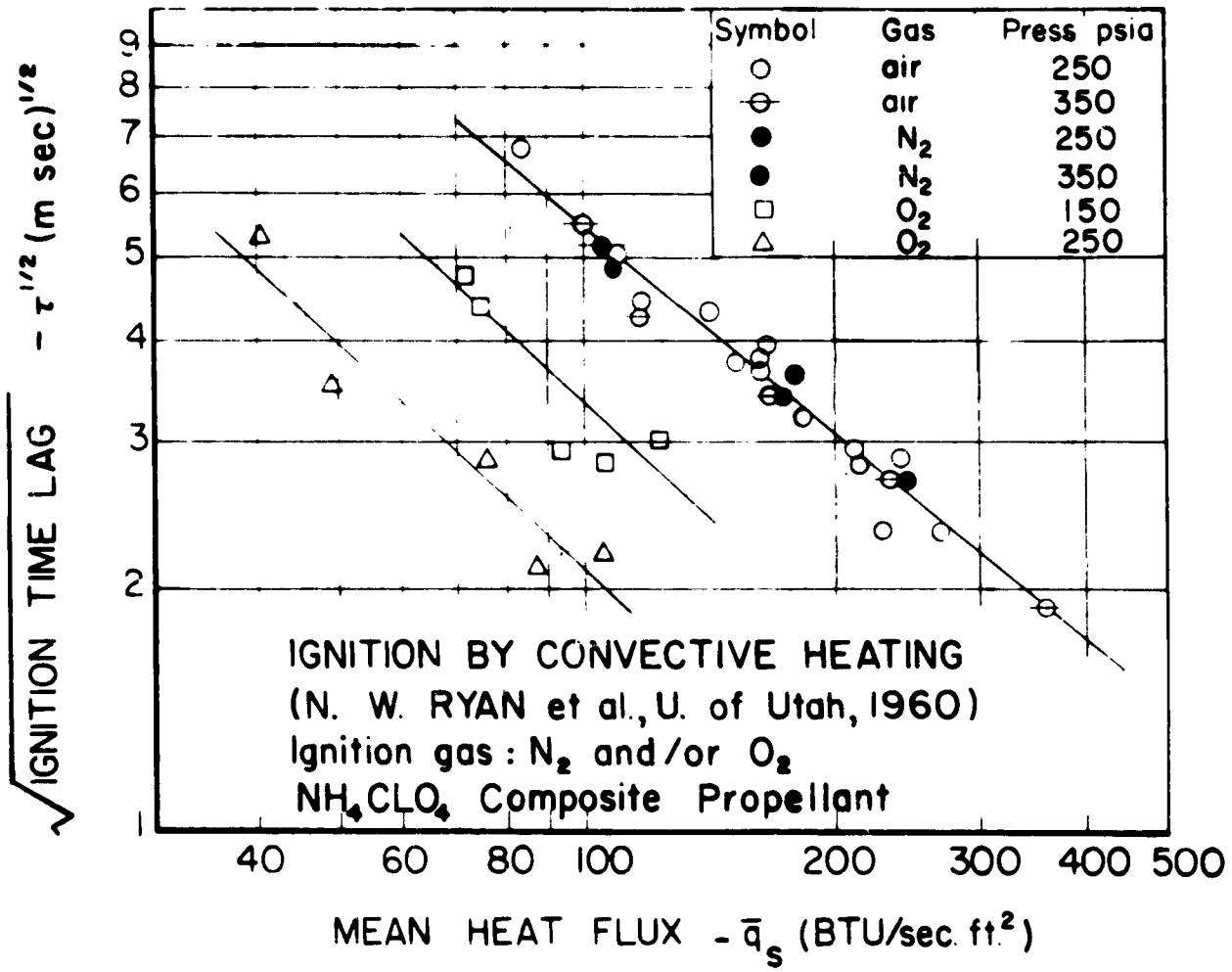

RE - PLOT OF FIGURE 5

REFERENCE 11

FIGURE 41

IGNITION TIME LAG VS. OXYGEN CONCENTRATION OF IGNITION GAS

FIGURE 42

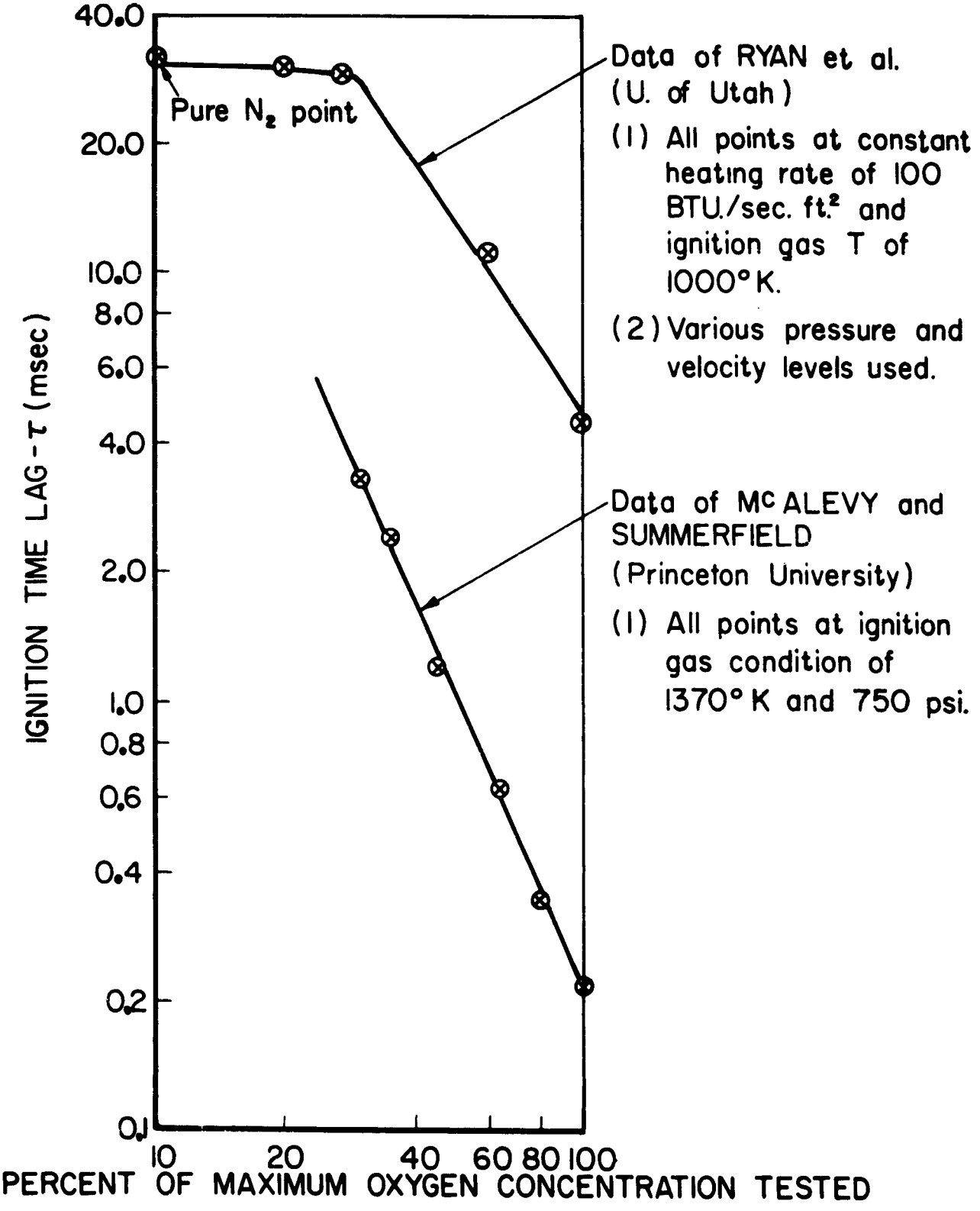

JPR 556

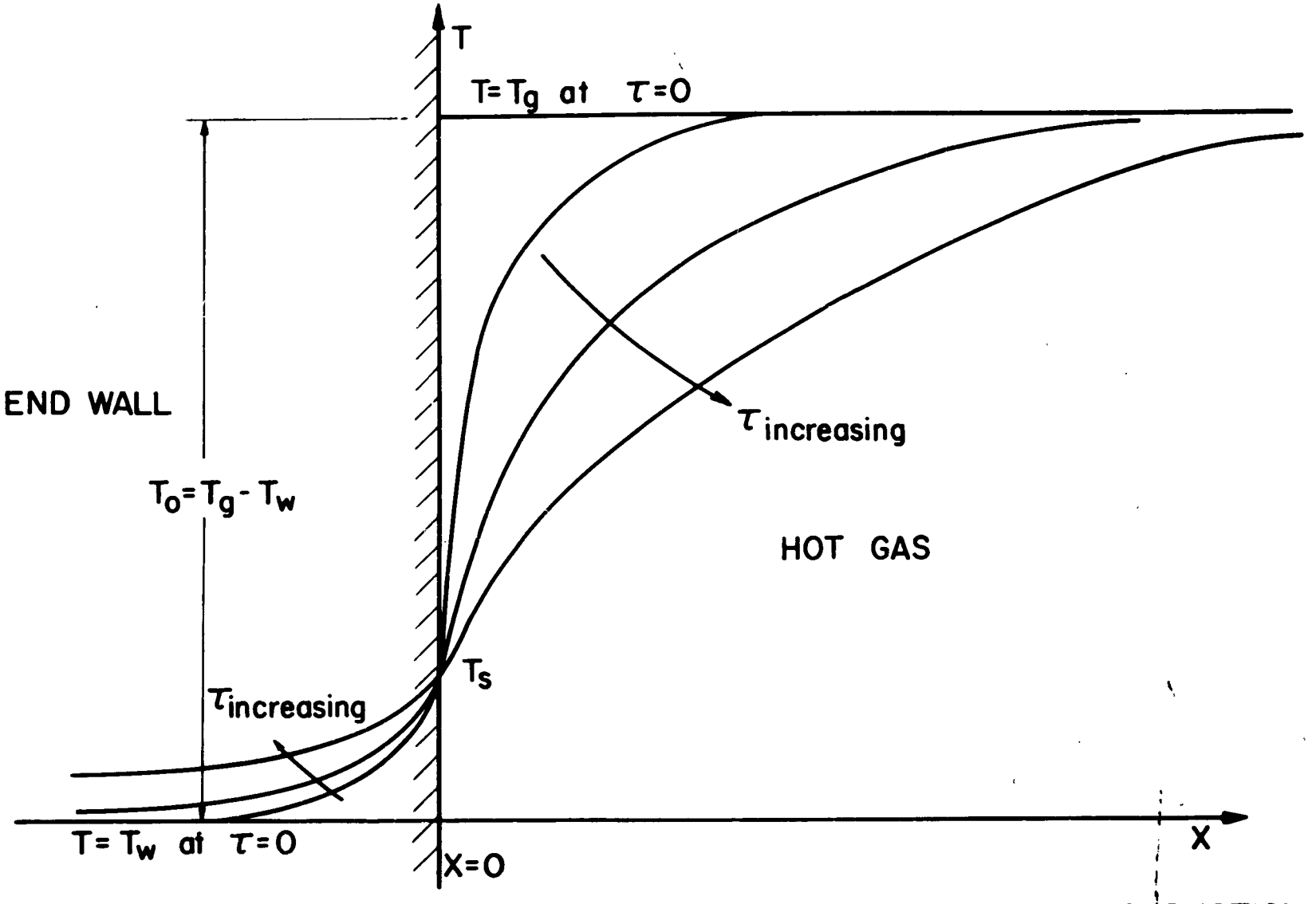

TEMPERATURE DISTRIBUTIONS AT VARIOUS TIMES DURING CONDUCTION OF HEAT FROM HOT GAS TO END WALL OF SHOCK TUBE. NOTE STEADY VALUE OF SURFACE TEMPERATURE (T_s) FIGURE 43

JPR 170

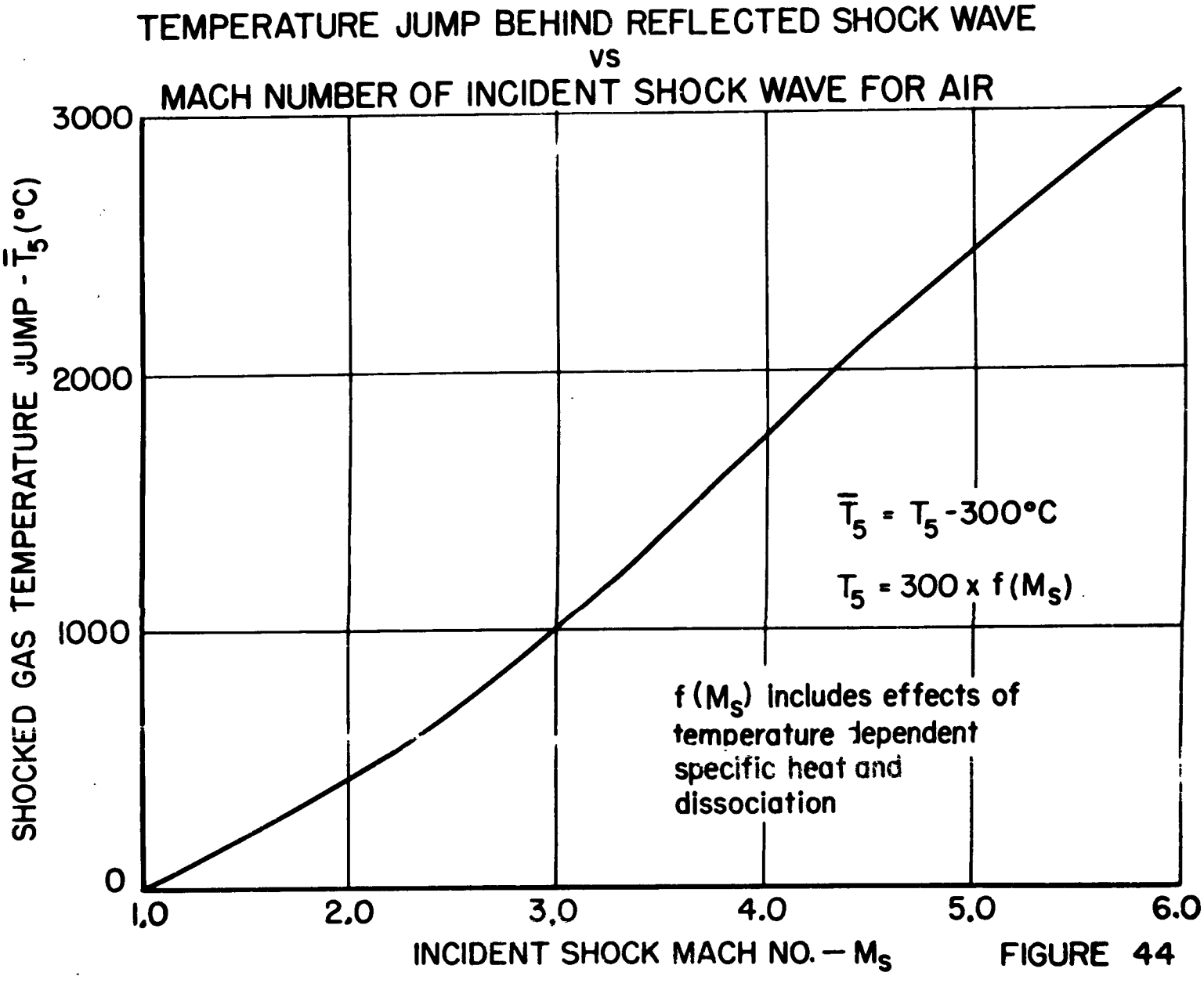
TEMPERATURE JUMP BEHIND REFLECTED SHOCK WAVE
VS
MACH NUMBER OF INCIDENT SHOCK WAVE FOR AIR
SHOCKED GAS TEMPERATURE JUMP - $\bar{T}_5$ (°C)
3000
2000
1000
0
1.0
2.0
3.0
4.0
5.0
6.0
INCIDENT SHOCK MACH NO. — M_S
$\bar{T}_5 = T_5 - 300°C$
$T_5 = 300 \times f(M_S)$
$f(M_S)$ includes effects of temperature dependent specific heat and dissociation

FIGURE 44